

NASA CONTRACTOR REPORT 165946

NASA-CR-165946
19820021846

MEDIUM ENERGY PROTON RADIATION DAMAGE TO (AlGa)As—GaAs SOLAR CELLS

R. Y. Loo, G. S. Kamath, and R. C. Knechtli

**Hughes Research Laboratories
3011 Malibu Canyon Road
Malibu, CA 90265**

**Contract NAS1-15926
July 1982**

LIBRARY COPY

AUG 31 1982

**LANGLEY RESEARCH CENTER
LIBRARY, NASA
HAMPTON, VIRGINIA**

NASA

National Aeronautics and
Space Administration

**Langley Research Center
Hampton, Virginia 23665**



NF01955

This Page Intentionally Left Blank

TABLE OF CONTENTS

SECTION		PAGE
1	INTRODUCTION AND SUMMARY	7
2	MEDIUM-ENERGY PROTON RADIATION DAMAGE	15
3	PERIODIC THERMAL ANNEALING	31
4	CONTINUOUS ANNEALING	53
5	CONCLUSION	59
	REFERENCES	61
APPENDICES		
A	MEDIUM ENERGY PROTON IRRADIATION (CALTECH)	63
B	PHOTO I-V CHARACTERISTICS OF (AlGa)As-GaAs SOLAR CELLS BEFORE AND AFTER MEDIUM-ENERGY PROTON IRRADIATION	65
C	PHOTO I-V CHARACTERISTICS OF (AlGa)As-GaAs SOLAR CELLS BEFORE AND AFTER A CONTINUOUS ANNEALING EXPERIEMNT AT 200°C	89

NS2-29722 #

This Page Intentionally Left Blank

LIST OF ILLUSTRATIONS

FIGURE		PAGE
1	(AlGa)As-GaAs solar cell structure used in proton irradiation experiments	8
2	Proton radiation damage	9
3	Integral proton fluence as a function of proton energy	11
4	Periodic Thermal Annealing at (a) 200°C, (b) 300°C, and (c) 400°C, after proton irradiation at 200 keV	13
5	GaAs solar cell 200 keV proton damage study	14
6	(AlGa)As-GaAs solar cell	27
7	Spectral response of (AlGa)As-GaAs solar cell	28
8	Spectral response of (AlGa)As-GaAs solar cell	29
9	Periodic thermal annealing flow chart	33
10	The annealing system	34
11	Isothermal annealing	35
12	Photo I-V characteristics of (AlGa)As-GaAs solar cell before and after 200 keV proton irradiation	36
13	Photo I-V characteristics of (AlGa)As-GaAs solar cell before and after 200 keV proton irradiation	37
14	Photo I-V characteristics of (AlGa)As-GaAs solar cell before and after 200 keV proton irradiation	38
15	Photo I-V characteristics of (AlGa)As-GaAs solar cell before and after 200 keV proton irradiation	39
16	Photo I-V characteristics of (AlGa)As-GaAs solar cell before and after 200 keV proton irradiation	40
17	Photo I-V characteristics of (AlGa)As-GaAs solar cell before and after 200 keV proton irradiation	41
18	Photo I-V characteristics before and after 200 keV proton irradiation	42
19	Photo I-V characteristics before and after 200 keV proton irradiation	43

FIGURE		PAGE
20	Photo I-V Characteristics of (AlGa)As-GaAs solar cell before and after 200 keV proton irradiation	44
21	Photo I-V characteristics of (AlGa)As-GaAs solar cell before and after 200 keV proton irradiation	45
22	Photo I-V characteristics of (AlGa)As-GaAs solar cell before and after 200 keV proton irradiation	46
23	Spectral response of (AlGa)As-GaAs solar cell before and after 200 keV proton irradiation and after 200°C isothermal annealing	47
24	Spectral response of (AlGa)As-GaAs solar cell before and after 200 keV proton irradiation and after 300°C isothermal annealing	48
25	Spectral response of (AlGa)As-GaAs solar cell before and after 200 keV proton irradiation and after 400°C isothermal annealing	49
26	Continuous annealing experiment	55

SECTION 1

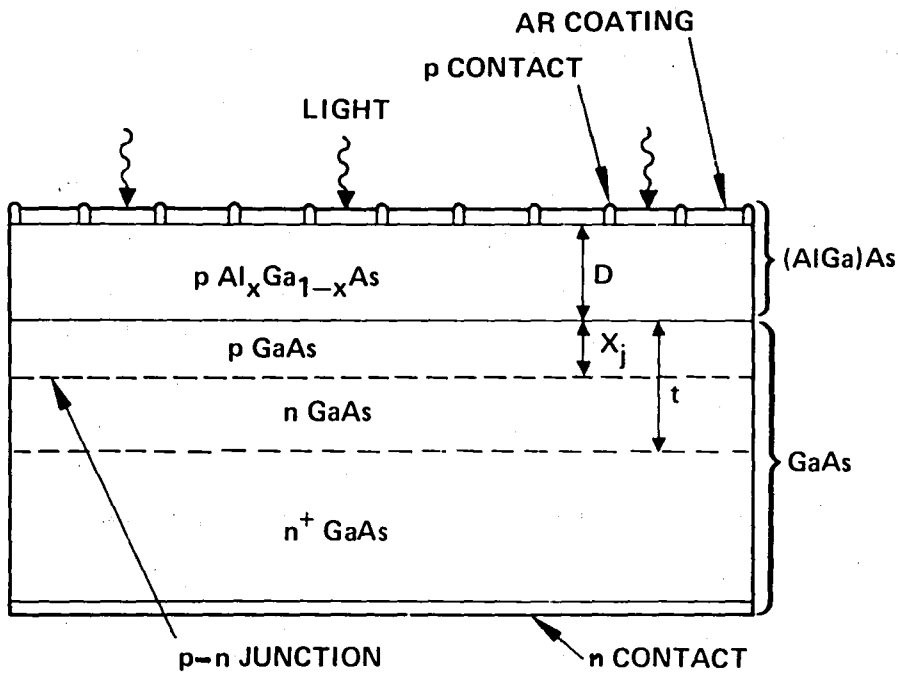
INTRODUCTION AND SUMMARY

The objective of this contract is to evaluate the performance of (AlGa)As-GaAs solar cells irradiated by medium energy protons (2, 5, and 10 MeV), and to investigate the influence of thermal annealing on radiation damage in GaAs solar cells. This study, together with our previous work on low-energy (50 to 300 keV) and high-energy (15 to 40 MeV) proton irradiation, forms a solid foundation for a thorough evaluation of the suitability of these cells for space missions. Our goal is to minimize the radiation damage to GaAs cells during these missions by incorporating appropriate low temperature (less than 200°C) annealing procedures into the solar panel design. Our results to date indicate that substantial gains in end-of-life efficiency can be made by this technique, resulting in a corresponding reduction in the panel area necessary to provide the power for the mission.

Figure 1 represents the (AlGa)As-GaAs solar cell structure used in this contract. This is the same structure used in the two preceding high- and low-energy proton irradiation damage contracts (contracts NAS1-14727 and NAS1-15443).

The medium-energy proton irradiations were performed at Caltech using their tandem accelerator. The irradiation experiment is described in Appendix A. In this experiment, both the Si (without coverglass) and a number of GaAs solar cells with 12 mil coverglass were irradiated simultaneously with our bare GaAs solar cells. We included the GaAs cells with 12 mil coverglass to verify the effectiveness of coverglass shielding of the GaAs cells. We found that this shielding provided the expected protection against the protons whose energy is ≤ 5 MeV (see Figure 2(a)).

The results of our medium-energy proton irradiation tests are summarized in Figure 2. They are also integrated with our prior measurements at low or high proton energies. Our general observation is that the radiation damage does indeed decrease monotonically with increasing proton energy, once the energy exceeds the values at which the protons are stopped within the relatively shallow active region of the GaAs solar cell (proton energies in excess



6555-2 R2
 NUMBER OF FINGERS = 24
 p CONTACT: Au-Zn-Ag
 n CONTACT: Au-Ge-Ni-Ag
 AR COATING: Ta₂O_x
 p Al_xGa_{1-x}As: $x \geq 0.85$
 CELL SIZE = 2 x 2 cm²

Figure 1. (AlGa)As-GaAs solar cell structure used in proton irradiation experiments.

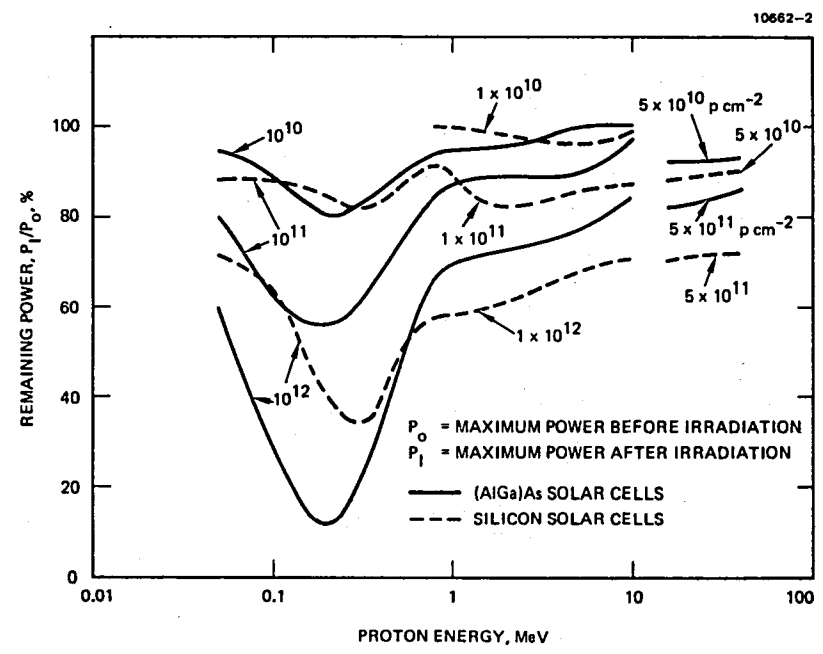
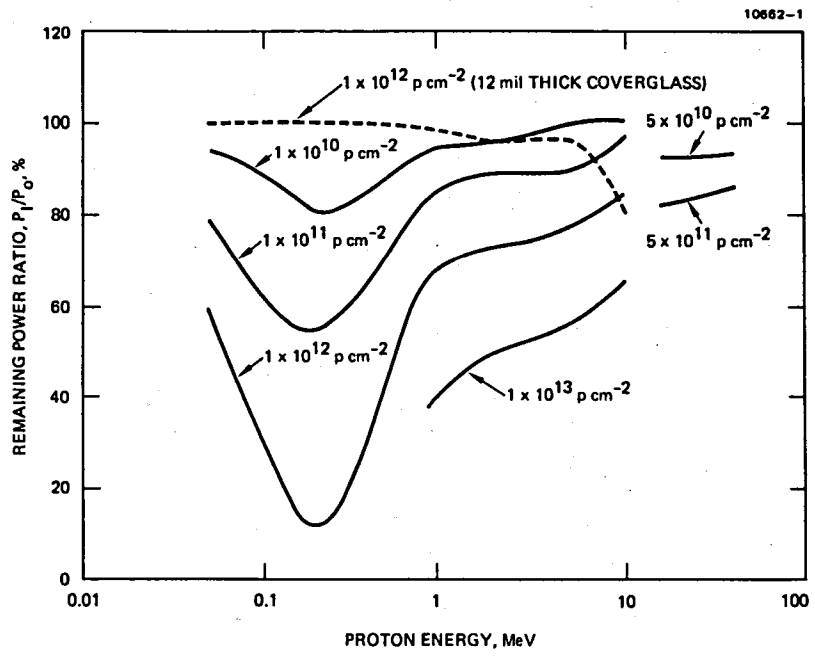


Figure 2. Proton radiation damage.

of 300 keV and active region thicknesses on the order of $2\mu\text{m}$). Figure 2(b) demonstrates the proton damage characteristics in GaAs solar cells; it also shows that for proton energies higher than 5 MeV, the GaAs cells have higher radiation resistance than the Si cells. In the region below 5 MeV, where GaAs cells are more susceptible to proton radiation damage, they are effectively shielded by the normal coverglass protection used with solar cells in all space missions (see Figure 2(a)). Some of the high-energy protons can also cause damage to the cell since they become low-energy protons by losing their energy while penetrating through the coverglass. However, the amount of damage depends on the total number of protons available at decreased energy.

Figure 3 shows the cumulative solar proton fluence as a function of proton energy encountered in geosynchronous orbit over a period of 11 years. The figure shows that the proton fluence decreases as proton energy increases; the low fluence of high-energy protons is even further attenuated by the coverglass, and hence their damaging effect is expected to be relatively small during a 10-year mission. Analysis of the data of Figure 2 can also provide information to determine the optimum coverglass protection desirable for GaAs cells in a specific space mission. Furthermore, it is very encouraging that our early results on annealing studies indicate that low-energy proton damage in GaAs cells may be substantially reduced by annealing at temperatures as low as 150 to 200°C .

In the thermal annealing study, we limit our experiments to the single proton energy of 200 keV and a fluence of $1 \times 10^{11} \text{ p cm}^{-2}$. We chose the 200 keV protons because they generate defects and produce severe damage within the active region of the GaAs solar cells. Our choice of 200 keV for the proton energy thus leads to the worst case. As far as the fluence is concerned, we select a value of $10^{11} \text{ p cm}^{-2}$ because it corresponds to the highest value for all protons capable of traversing a 12 mil coverglass during 11 years in geosynchronous orbit and corresponds again to the worst possible case. We performed four cycles of periodic thermal annealing experiments in this study. The GaAs solar cells were first subjected to 200 keV of proton irradiation and subsequently to isothermal annealing.

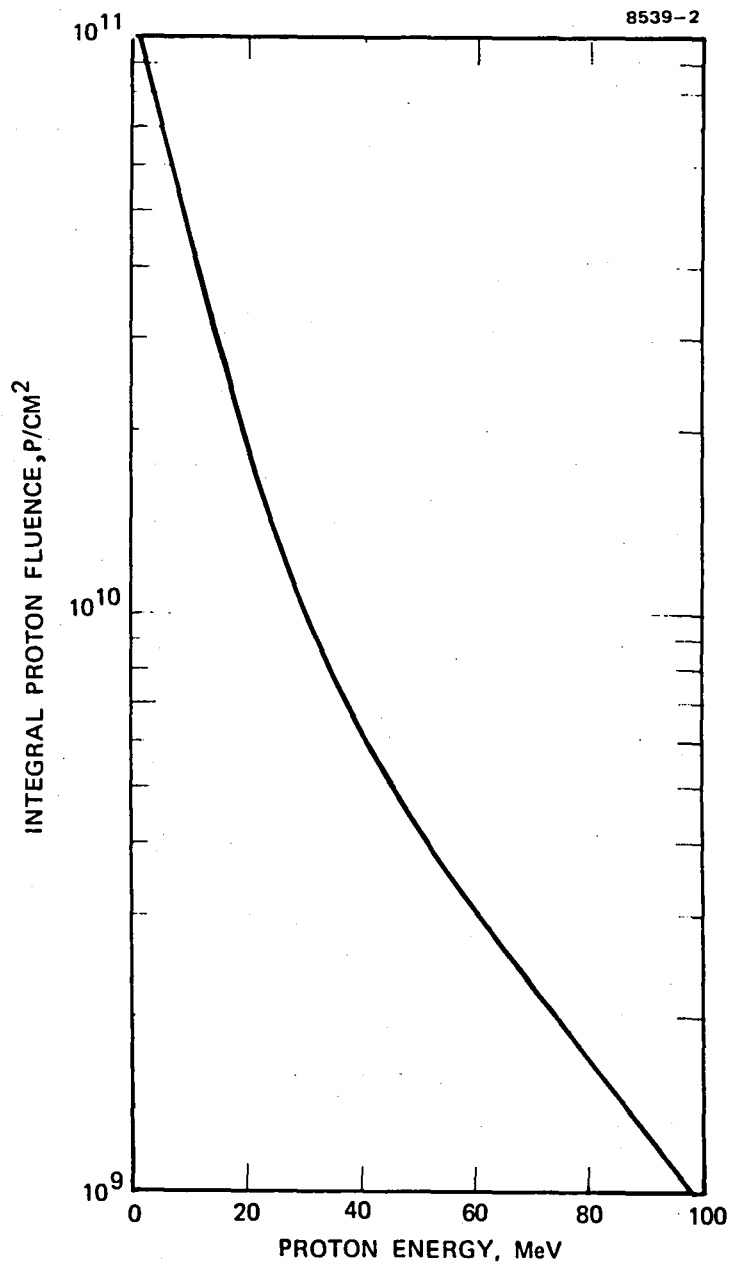


Figure 3. Integral proton fluence as a function of proton energy. Cumulative solar protons for 20th solar cycle, 11 years.

Figure 4, we compare two sets of GaAs cells which were irradiated to the same level by 200 keV protons; one set was subjected to periodic annealing and the other was not. The data show that after the second periodic anneal cycle (at 200°C) of the power ratio P_A/P_0 (P_A = power output after annealing, P_0 = initial cell power before irradiation) is maintained at 65% without appreciable further degradation.

In the continuous annealing experiment, we studied the effect of proton flux, 1×10^{10} versus 1×10^{11} p cm⁻² hr⁻¹, in our GaAs solar cells at temperatures of 25°C and 200°C, respectively. Figure 5 shows the power ratio after irradiation as a function of fluence in this continuous annealing experiment. The result shows that after continuous annealing at 200°C to a fluence of 1×10^{11} p cm⁻² the cells which were irradiated with low proton flux of 1×10^{10} p cm⁻² hr⁻¹ had 6% more power over the cells which were irradiated at a flux of 1×10^{11} p cm⁻² hr⁻¹. Thus the extra hours of annealing during irradiation at 200°C at low flux did improve the cells' radiation resistance

Although our data on annealing show a substantial reduction of the radiation damage to our GaAs solar cells when annealed at temperatures as low as 200°C, there is still damage that cannot be annealed at 200°C under the conditions of our experiment. Our results, in conjunction with the analysis of the nature of the defects obtained from deep level transient spectroscopy (DLTS) measurements, lead us to believe that these harder defects are caused by complexes that are formed by the high flux rates used in terrestrial laboratory experiments. In the space environment we expect fluxes on the order of 10^3 p cm⁻² sec⁻¹, which is about six orders of magnitude lower; the slower flux rate is expected to result mainly in simple annealable defects. Our GaAs cells now is used on NTS II support this expectation. The data on these cells show that the damage is considerably less than would be expected in view of their excessive junction depth of 1 μm. We believe that the reduced damage results from a degree of annealing at the 100°C temperature that the panel reaches during the NTS II orbit. Ultimately, our studies on annealing lead us to expect that with proper annealing and optimum cell design, the need for coverglass protection could be minimized, if not eliminated, resulting in a substantial increase in the power-to-weight ratio for the solar panel.

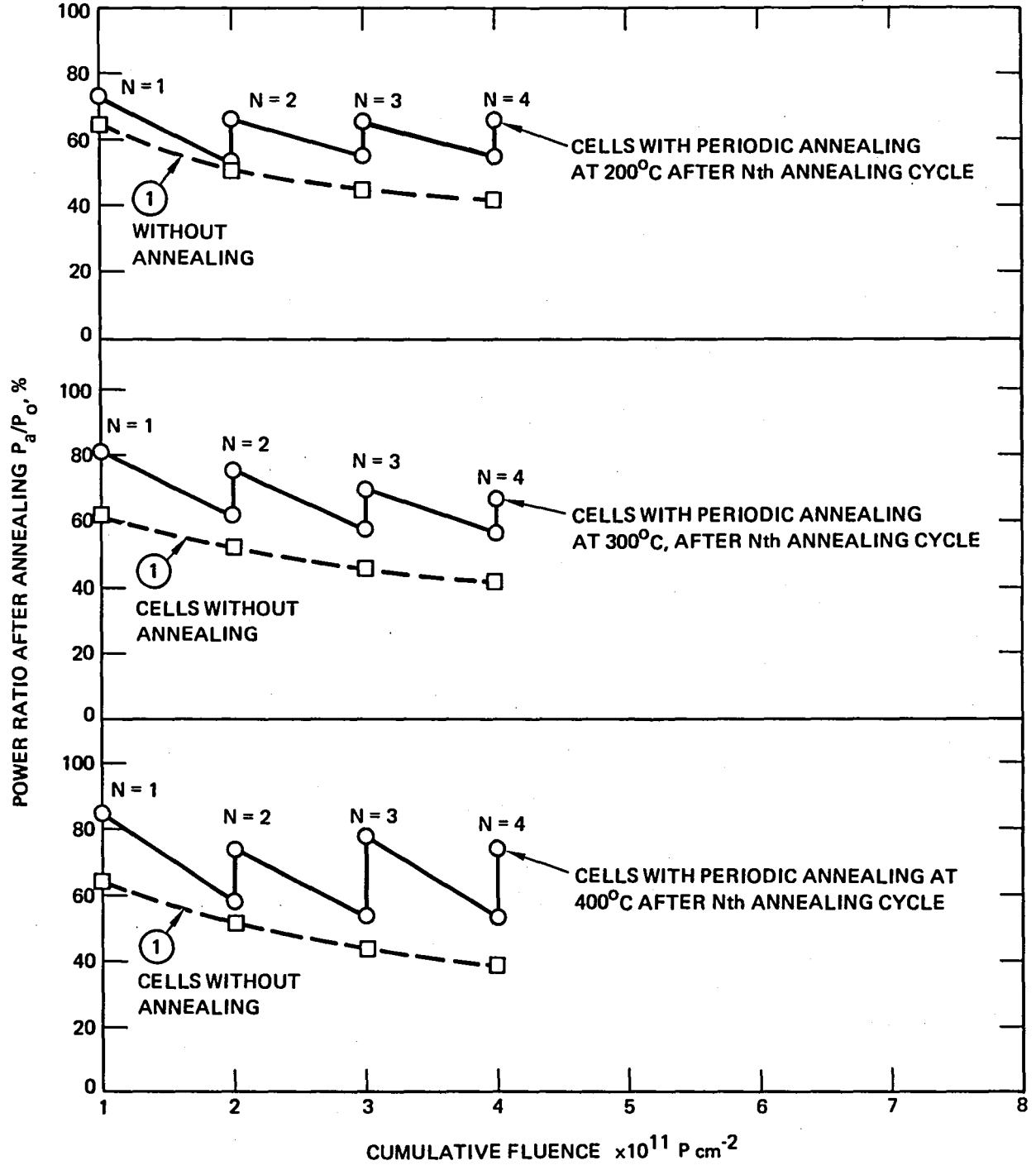


Figure 4. Periodic thermal annealing at (a) 200° C, (b) 300°C, and (c) 400°C, after proton irradiation at 200 keV.

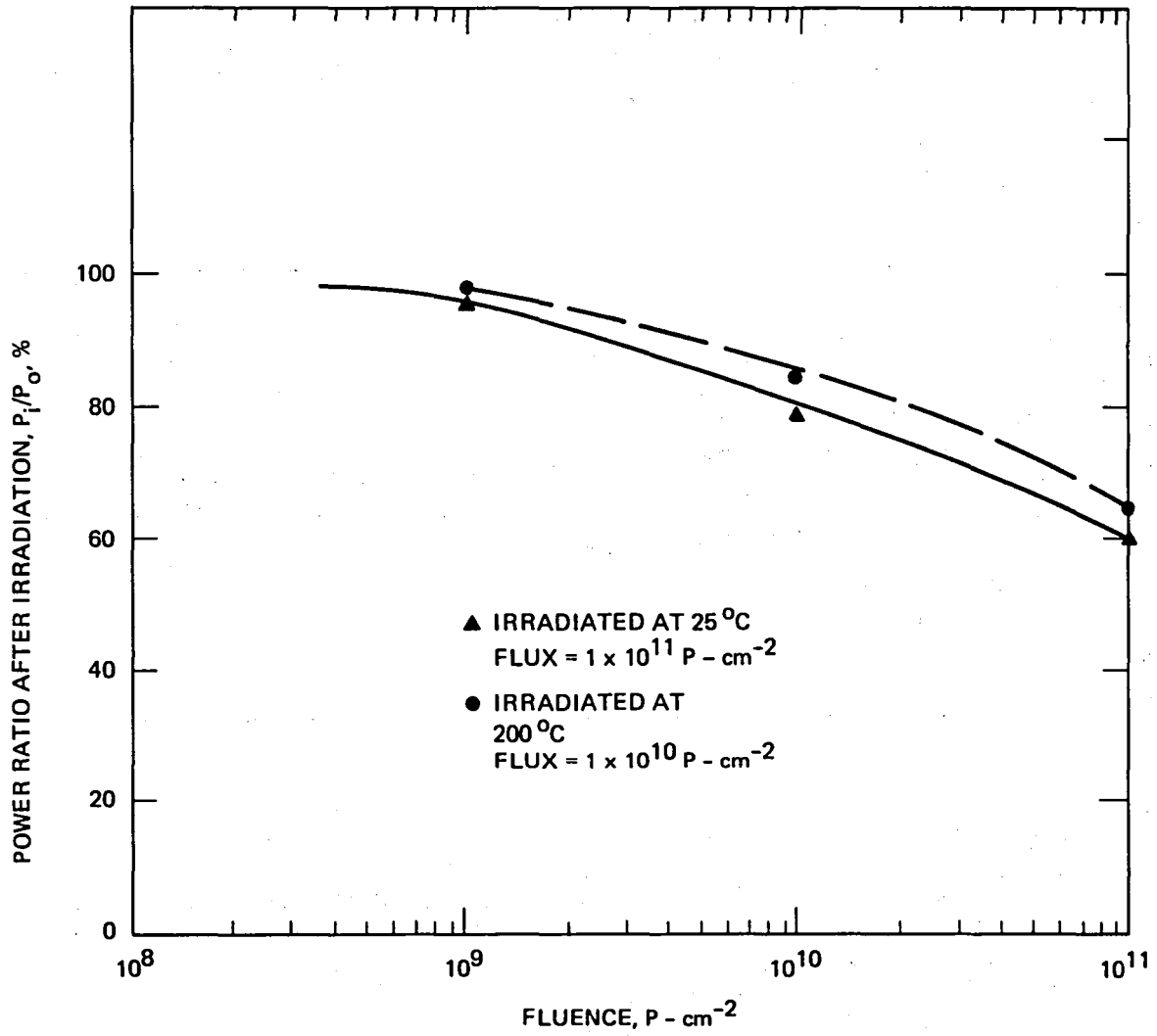


Figure 5. GaAs solar cell 200 keV proton damage study.

SECTION 2

MEDIUM-ENERGY PROTON RADIATION DAMAGE

Table 1 gives the full test matrix of GaAs and silicon cells used in our investigation. As seen in the table, a number of GaAs solar cells protected with 12-mil-thick coverglass were included to verify the shielding effect of glass against the protons.

Table 1. Test Matrix

Fluence, P cm ⁻²	GaAs Solar Cell		Si Solar Cell I.D. No.
	Without Coverglass	12-mil-Thick Coverglass	
<u>2 MeV Proton Energy</u>			
1x10 ¹⁰	4166, 4167, 4171	3890	14, 15, 42
1x10 ¹¹	4172, 4175, 4177	3896	16, 17, 43
1x10 ¹²	4180, 4190, 4195	3892	18, 19, 44
1x10 ¹³	4199, 4207, 4209	3893	20, 21, 45
<u>5 MeV Proton Energy</u>			
1x10 ¹⁰	4101, 4095, 4093		26, 34
1x10 ¹¹	4035, 4033, 4030		27, 35
1x10 ¹²	4029, 4028, 4010	3901	28, 36
1x10 ¹³	4006, 4000, 4026	3990	
<u>10 MeV Proton Energy</u>			
1x10 ¹⁰	4068, 4064, 4063		22, 30
1x10 ¹¹	4062, 4113, 4109		23, 31
1x10 ¹²	4107, 4106, 4105	3988	24, 32
1x10 ¹³	4104, 4103, 4102	3992	25, 33

T7433

Figures B-1 through B-42 in Appendix B show the air mass zero (AMO) photo I-V characteristics of GaAs solar cells before and after proton irradiation with energies of 2, 5, and 10 MeV. Table 2 has been completed from these I-V characteristics and gives the following characteristics of the individual cells: I_{sc} ; V_{oc} ; fill factor (FF); maximum power output, P_{max} ; and power conversion efficiency, η .

Table 2 gives the results using both the HRL (xenon) and Spectrolab's (X-25) simulators. The agreement is good between the two simulators at proton fluence less than 1×10^{12} p cm⁻². However, above 1×10^{12} p cm⁻², the short-circuit currents measured at HRL were consistently a little lower than those measured at Spectrolab. This discrepancy is a result of the difference between the light spectra of the two simulators. The HRL solar simulator is indeed richer than the AMO in the long wavelength region. Thus we expect, as observed, that the GaAs solar cell yields less current after irradiation when measured using the HRL solar simulator than when measured using the Spectrolab X-25 simulator because a substantial part of the radiation damage occurs in the long wavelength part of the spectrum.

Figure 2 shows the power ratio P_I/P_O as a function of proton energy (P_O and P_I are the maximum solar cell output power before and after proton radiation, respectively). Figure 2 also includes data obtained with 0.8 MeV protons. These data were not obtained under this contract, but are shown here for information purposes. As expected, the low-energy proton does more damage to the GaAs solar cell than the high-energy proton. This is because the low-energy protons are stopped and produce damages inside the active region of the cell. In space missions, the solar cell is usually shielded against low-energy protons by a coverglass, while there is no protection against the high-energy protons. The dotted curve in Figure 2 illustrates the effect of 12-mil-thick coverglass used to shield against the low-energy protons. It is effective for proton energies up to at least 5 MeV. In actual practice, the high-energy protons lose some of their energy while penetrating through the coverglass and these, again, are capable of damaging the cell.

Table 2. (AlGa)As-GaAs Solar Cell Characteristics Before and After Proton Irradiation

Cell No.	Proton		I_{sc} , mA	V_{oc} , V	FF	P_{max} , mW	η , %
	Energy, MeV	Fluence $p\text{ cm}^{-2}$					
4166	0	0 (HRL)	114	0.98	0.76	84.4	15.6
	2	1×10^{10} (HRL)	114	0.96	0.75	81.4	15.0
	"	" (SL)	113	0.97	0.75	81.8	15.1
4167	0	0 (HRL)	112	0.99	0.75	83	15.3
	2	1×10^{10} (HRL)	110	0.97	0.74	79	14.6
	"	" (SL)	108	0.97	0.75	79	14.6
4171	0	0 (HRL)	115	0.99	0.76	86.1	15.9
	2	1×10^{10} (HRL)	112	0.97	0.76	82	15.2
	"	" (SL)	112	0.97	0.76	82	15.2
*3890	0	0 (HRL)	114	1.0	0.76	87	16.0
	2	1×10^{10} (HRL)	114	1.0	0.76	87	16.0
	"	" (SL)	112	0.99	0.77	86	15.8
4172	0	0 (HRL)	114	0.99	0.76	86.1	15.9
	2	1×10^{11} (HRL)	105	0.94	0.76	74.8	13.8
	"	" (SL)	106	0.94	0.77	76.6	14.1
4177	0	0 (HRL)	116	0.99	0.74	85.3	15.8
	2	1×10^{11} (HRL)	107	0.93	0.75	74.7	13.8
	"	" (SL)	108	0.93	0.75	75.0	13.8
4175	0	0 (HRL)	114	0.98	0.74	82.6	15.3
	2	1×10^{11} (HRL)	107	0.93	0.75	74.5	13.8
	"	" (SL)	108	0.94	0.75	76.0	14.0
*3896	0	0 (HRL)	113.5	0.99	0.77	86.6	16.0
	2	1×10^{11} (HRL)	113.5	0.99	0.77	86.6	16.0
	"	" (SL)	110	0.98	0.77	83.4	15.4
4180	0	0 (HRL)	114	1.0	0.75	85.9	15.9
	2	1×10^{12} (HRL)	93	0.87	0.76	60.6	11.2
	"	" (SL)	96	0.87	0.76	63.6	11.8
4190	0	0 (HRL)	115	1.0	0.74	85.5	15.8
	2	1×10^{12} (HRL)	93	0.86	0.74	59.3	10.9
	"	" (SL)	96	0.87	0.75	62.3	11.5

Table 2 cont.

Cell No.	Proton		I_{sc} , mA	V_{oc} , V	FF	P_{max} , mW	η , %
	Energy, MeV	Fluence, $p\text{ cm}^{-2}$					
4195	0	0 (HRL)	116	1.0	0.75	88.4	16.3
	2	1×10^{12} (HRL)	92	0.86	0.74	58.9	10.9
	"	" (SL)	95	0.87	0.73	60.4	11.2
*3892	0	0 (HRL)	113	0.99	0.75	85.8	15.8
	2	1×10^{12} (HRL)	110	0.975	0.77	82.7	15.2
	"	" (SL)	110	0.98	0.75	80.4	14.9
4199	0	0 (HRL)	117	1.0	0.74	86.7	16.0
	2	1×10^{13} (HRL)	73	0.74	0.71	38.4	7.1
	"	" (SL)	76	0.76	0.72	41.4	7.6
4207	0	0 (HRL)	113	0.99	0.75	84.2	15.6
	2	1×10^{13} (HRL)	72	0.74	0.71	37.8	7.0
	"	" (SL)	76	0.75	0.73	41.5	8.0
4209	0	0 (HRL)	113	1.0	0.76	85.5	15.8
	2	1×10^{13} (HRL)	70	0.74	0.72	37.2	6.9
	"	" (SL)	75	0.75	0.73	40.9	8.0
*3893	0	0 (HRL)	114	1.0	0.76	86.6	16.0
	2	1×10^{13} (HRL)	116	0.925	0.76	81.9	15.1
	"	" (SL)	112	0.93	0.77	80.1	14.8
4093	0	0 (HRL)	111	0.99	0.76	83	15.3
	5	1×10^{10} (SL)	111	0.98	0.76	83	15.3
	"	" (SL)	112	0.98	0.76	83.6	15.4
4101	0	0 (HRL)	112	1.0	0.77	85.6	15.8
	5	1×10^{10} (HRL)	112	1.0	0.77	85.6	15.8
	"	" (SL)	112	0.98	0.77	85.3	15.8
4095	0	0 (HRL)	110	1.0	0.76	83.2	15.4
	5	1×10^{10} (HRL)	110	1.0	0.76	83.2	15.4
	"	" (SL)	112	0.98	0.77	84.7	15.7

7433

Table 2 cont.

Cell No.	Proton			I_{sc} , mA	V_{oc} , V	FF	P_{max} , mW	η , %
	Energy, MeV	Fluence, $p\text{ cm}^{-2}$						
4033	0	0	(HRL)	113	1.0	85.3	0.76	15.8
	5	1×10^{11}	(HRL)	105	0.96	77	0.76	14.2
	"	"	(SL)	106	0.96	77	0.87	14.2
4030	0	0	(HRL)	112	0.99	0.77	85.5	15.8
	5	1×10^{11}	(HRL)	104	0.96	0.78	77	14.2
	"	"	(SL)	104	0.96	0.78	77	14.2
4035	0	0	(HRL)	114	1.01	0.76	87.2	16.1
	5	1×10^{11}	(HRL)	105	0.96	0.76	77	14.2
	"	"	(SL)	106	0.96	0.76	77.0	14.2
4028	0	0	(HRL)	110	1.0	0.78	85.9	15.9
	5	1×10^{12}	(HRL)	92	0.90	0.77	63.8	11.8
	"	"	(SL)	96	0.90	0.76	65.5	12.1
4029	0	0	(HRL)	109	1.0	0.77	84	15.5
	5	1×10^{12}	(HRL)	92	0.90	0.77	63.8	11.8
	"	"	(SL)	97	0.89	0.75	64.7	12.0
*3901	0	0	(HRL)	117	0.99	0.77	89.2	16.5
	5	1×10^{12}	(SL)	113	0.98	0.77	85.7	15.8
4006	0	0	(HRL)	114	1.0	0.76	86.5	16.5
	5	1×10^{13}	(HRL)	78	0.79	0.72	44.0	8.1
	"	"	(SL)	84	0.80	0.73	48.8	9.0
4026	0	0	(HRL)	110	1.0	0.77	84.2	15.6
	5	1×10^{13}	(HRL)	78	0.80	0.72	44	8.1
	"	"	(SL)	82	0.80	0.72	47.5	9.0
*3990	0	0	(HRL)	116	1.01	0.77	89.9	16.6
	5	1×10^{13}	(SL)	114	0.97	0.76	84.2	15.6
4064	0	0	(HRL)	111	0.99	0.77	84.2	15.5
	10	1×10^{10}	(HRL)	111	0.98	0.77	83.4	15.4
	"	"	(SL)	110	0.98	0.76	82.4	15.2

7433

Table 2 cont.

Cell No.	Proton		I_{sc} , mA	V_{oc} , V	FF	P_{max} mW	η , %
	Energy, MeV	Fluence, $p\text{ cm}^{-2}$					
4068	0	0 (HRL)	112	1.0	0.76	83.6	15.5
	10	1×10^{10} (HRL)	112	1.0	0.76	83.6	15.5
	"	" (SL)	112	0.98	0.75	82.4	15.2
4063	0	0 (HRL)	110	1.0	0.76	83.6	15.5
	10	1×10^{10} (HRL)	110	1.0	0.76	83.6	15.5
	"	" (SL)	108	0.98	0.77	81.8	15.1
4062	0	0 (HRL)	112	1.0	0.75	83.64	15.5
	10	1×10^{11} (HRL)	108	0.97	0.76	79.4	14.7
	"	" (SL)	110	0.96	0.76	80.4	14.9
4109	0	0 (HRL)	113	0.99	0.75	84	15.5
	10	1×10^{11} (HRL)	109	0.96	0.77	80.4	14.9
	"	" (SL)	113	0.96	0.75	81.6	15.1
4113	0	0 (HRL)	111	1.0	0.77	84.9	15.7
	10	1×10^{11} (HRL)	109	0.97	0.77	81.8	15.1
	"	" (SL)	110	0.96	0.78	82.6	15.3
4105	0	0 (HRL)	112	1.0	0.77	86.3	15.9
	10	1×10^{12} (HRL)	100	0.92	0.78	71.8	13.3
	"	" (SL)	104	0.92	0.77	73.3	13.5
4106	0	0 (HRL)	113	0.99	0.75	84	15.5
	10	1×10^{12} (HRL)	101	0.92	0.76	70.8	13.0
	"	" (SL)	105	0.92	0.76	73.5	13.6
4107	0	0 (HRL)	110	1.0	0.76	84.1	15.5
	10	1×10^{12} (HRL)	98	0.92	0.78	69.9	12.9
	"	" (SL)	102	0.91	0.78	72.4	13.4
*3988	0	0 (HRL)	116	1.0	0.76	88.2	16.3
	10	1×10^{12} (HRL)	97	0.91	0.77	67.9	12.5
	"	" (SL)	102	0.90	0.77	70.8	13.1
4104	0	0 (HRL)	110	0.99	0.77	83.8	15.5
	10	1×10^{13} (HRL)	83	0.82	0.74	50.2	9.3
	"	" (SL)	88	0.82	0.74	53.6	10.0

7433

Table 2 cont.

Cell No.	Proton		I_{sc} , mA	V_{oc} , V	FF	P_{max} mW	η , %
	Energy, MeV	Fluence, $p\text{ cm}^{-2}$					
4102	0	0 (HRL)	111	1.0	0.76	83.4	15.4
	10	1×10^{13} (HRL)	85	0.82	0.74	51.0	9.3
	"	" (SL)	89	0.82	0.73	53.1	10.0
4103	0	1×10^{13} (HRL)	111	0.99	0.76	83.4	15.4
	10	1×10^{13} (HRL)	84	0.82	0.74	51.2	9.5
	"	" (SL)	89	0.82	0.74	54.4	10.1
(3992)	0	0 (SL)	117	1.0	0.77	90.5	16.7
	10	1×10^{13} (HRL)	83	0.81	0.73	49.0	9.0
	"	" (SL)	90	0.80	0.74	53.1	10.0

*Cells protected by 12-mil-thick coverglass.

HRL: Photo I-V measurement performed at HRL using xenon light source.

SL: Photo I-V measurement performed at Spectrolab using X-25 simulator.

Table 3 gives the electrical characteristics of Si solar cells. The Si cells used for the intermediate proton energy study do not have back surface fields (BSF); they have lower beginnings of life power than the other groups of cells with BSF that were used in the low- and high-energy proton studies. Furthermore, it is known that the BSF cells degrade at a faster rate at low fluences than do the cells without BSF. Once the effect of the BSF is gone, all the Si cells have similar degradation characteristics*. Table 4 gives the various groups of Si cells used in our proton damage studies.

Figures 6(a) through 6(c) show the GaAs short-circuit current of the solar cells, the open-circuit voltage and fill factor as a function of proton energy. Again these experimental data show that the low-energy protons degrade the cell both in the bulk and the junction. This is consistent with our prediction that the cell damage is correlated to the penetration depth of the proton.

Figures 7(a) through 7(c) show the average spectral response of the GaAs solar cell before and after proton irradiation with proton energies of 2, 5, and 10 MeV, respectively. The 2 MeV protons degrade the cell more than the 5 and 10 MeV protons because the 5 and 10 MeV protons produce damages farther away from the active region of the cell. The change in the spectral response of the GaAs solar cells is in good agreement with the change in I_{sc} after irradiation.

Figures 8(a) through 8(c) show the spectral response of the GaAs cells protected with 12-mil-thick coverglass. Clearly, the 12-mil-thick coverglass shields the proton from damaging the cell at energy below 5 MeV. The 10 MeV protons demonstrate that they lose some of their energy while traveling through the coverglass and cause damage in the active region of the cell.

In summary, the GaAs solar cells show more radiation resistance than the Si cells at energy above 5 MeV. However, at proton energy below 5 MeV, where GaAs cells are more susceptible to damage, they can be effectively shielded

* B.E. Anspaugh, J.A. Scott-Monck, R.G. Downing, D.W. Moffett, and T.F. Miyahira "Influence of Processing on the Electrical Performance of Proton Irradiated Silicon Solar Cells," Proc. IEEE Photovoltaic Specialist Conf., pp. 847-852, Jan. 1980.

by coverglass. Some of the high-energy protons also can cause damage to the cell by losing part of their energy while penetrating through the coverglass. But in this case, the amount of damage depends on their number and on their energy distribution. In general, the number of these protons is relatively small, as shown previously in Figure 3.

Table 3. Silicon Solar Cell Characteristics
Before and After Proton Irradiation

Cell No.	Proton Energy, MeV	Fluence, $p\text{ cm}^{-2}$	I_{sc} , mA	V_{oc} , v	FF	P_{max} , mW	η , %
14	0	0	147	0.56	0.80	65.6	12
14	2	1×10^{10}	148	0.56	0.78	64	11.8
15	0	0	147	0.56	0.79	65.3	12
15	2	1×10^{10}	148	0.56	0.78	64	11.8
16	0	0	148	0.56	0.79	65.1	12
16	2	1×10^{11}	135	0.53	0.76	54	10
17	0	0	145	0.56	0.79	64.1	11.8
17	2	1×10^{11}	132	0.53	0.77	54	9.8
18	0	0	146	0.56	0.79	64.9	12
18	2	1×10^{12}	110	0.49	0.75	40	7.4
19	0	0	146	0.56	0.80	65.1	12
19	2	1×10^{12}	110	0.49	0.75	40	7.4
26	0	0	147	0.56	0.80	65.3	12
26	5	1×10^{10}	146	0.55	0.78	63	11.6
34	0	0	146	0.56	0.66	54.7	10
34	5	1×10^{10}	144	0.56	0.65	52.3	9.7
27	0	0	149	0.56	0.79	65.8	12.2
27	5	1×10^{11}	138	0.53	0.77	56.3	10
35	0	0	145	0.57	0.73	60	11
35	5	1×10^{11}	131	0.54	0.67	47	8.7
28	0	0	147	0.56	0.80	65.8	12
28	5	1×10^{12}	118	0.50	0.76	44.6	8.2
36	0	0	148	0.56	0.72	59.4	10.9
36	5	1×10^{12}	118	0.50	0.69	40.1	7.4

7433

Table 3 (Continued)

Cell No.	Proton Energy, MeV	Fluence, $p\text{ cm}^{-2}$	I_{sc} , mA	V_{oc} , v	FF	P_{max} , mW	η , %
22	0	0	148	0.56	0.79	65.2	12
22	10	1×10^{10}	148	0.56	0.78	64.4	11.9
30	0	0	144	0.56	0.79	63.2	11.6
30	10	1×10^{10}	146	0.56	0.77	62.3	11.5
31	0	0	146	0.57	0.71	60	11
31	10	1×10^{11}	140	0.54	0.69	52.3	9.7
23	0	0	146	0.56	0.78	63	11.6
23	10	1×10^{11}	140	0.54	0.76	57.6	10.6
24	0	0	146	0.56	0.80	66	12.2
24	10	1×10^{12}	122	0.51	0.76	47.2	8.7
32	0	0	150	0.56	0.68	56.3	10.4
32	10	1×10^{12}	122	0.51	0.65	40	7.4

7433

Table 4. Cell Description

Type of Cell	Shallow Junction, $\sim 0.2 \mu\text{m}$	Back Surface Field	Back Surface Reflector	Textured Surface	Cell Size, cm x cm	Typical Parameters			Proton Used in
						I_{sc} , mA	V_{oc} , V	P_{max} , mW	
A	X	X			2 x 2.2	170	0.59	76	Low-energy proton (50 to 300 keV)
B	X		X		2 x 2	148	0.56	65	Intermediate proton (800 keV to 10 MeV)
C	X	X	X	X	2 x 2.1	180	0.59	80	High-energy proton (15 to 40 MeV)

7433

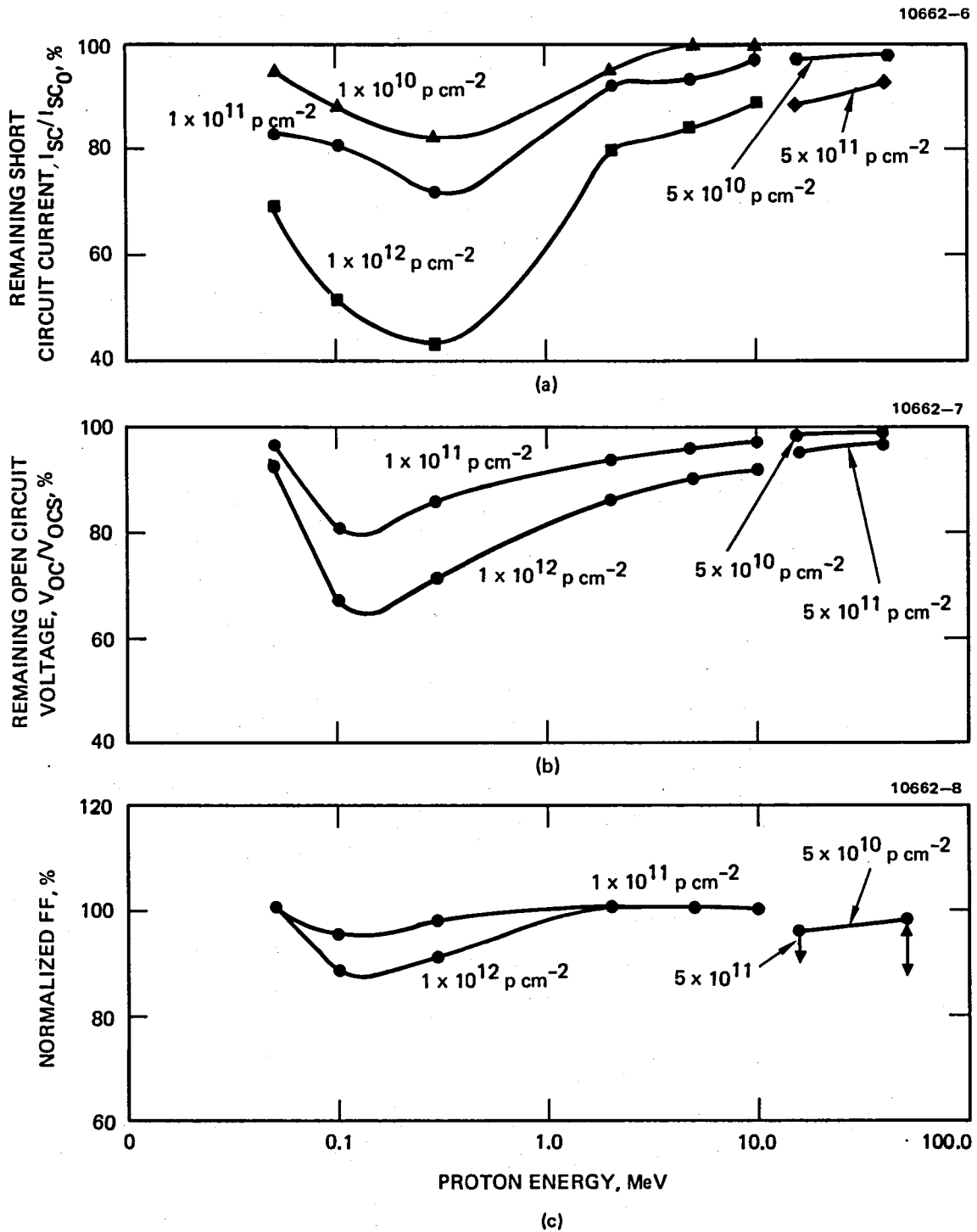


Figure 6. (AlGa)As-GaAs solar cell. (a) short-circuit current as a function of proton energy, (b) open circuit voltage as a function of proton energy, (c) (AlGa)As-GaAs solar cell's fill factor as a function of proton energy.

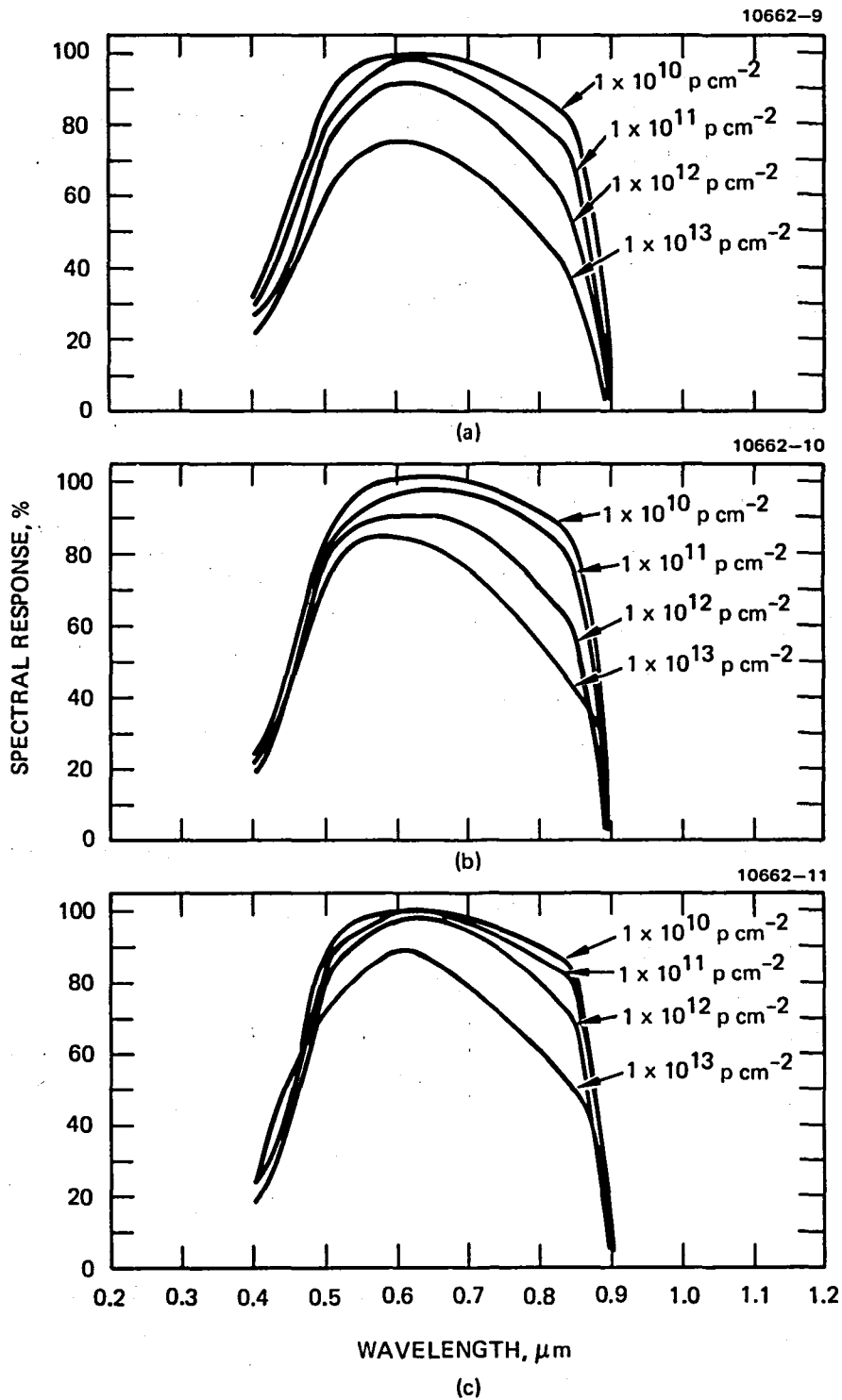


Figure 7. Spectral response of (AlGa)As-GaAs solar cells. (a) After 2 MeV proton irradiation (without coverglass), (b) after 5 MeV proton irradiation (without coverglass), (c) after 10 MeV proton irradiation (without coverglass).

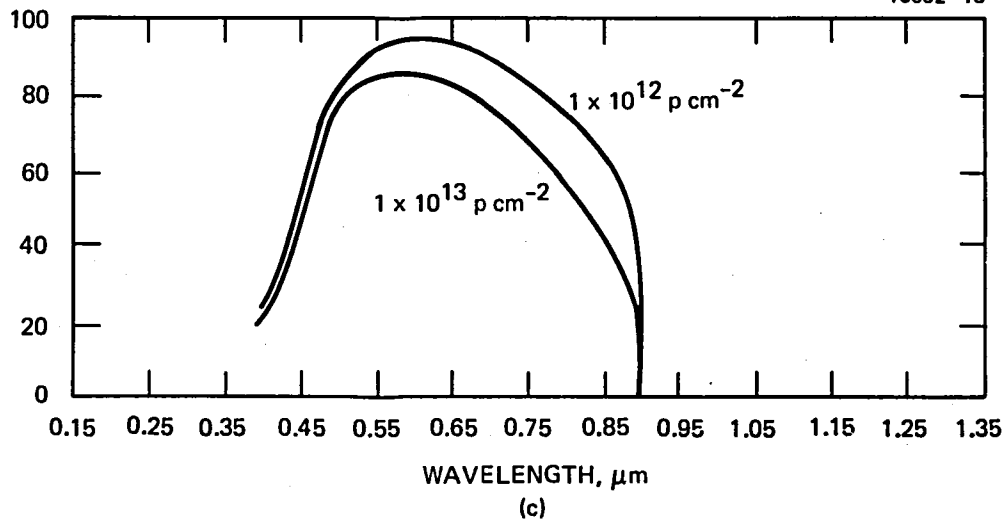
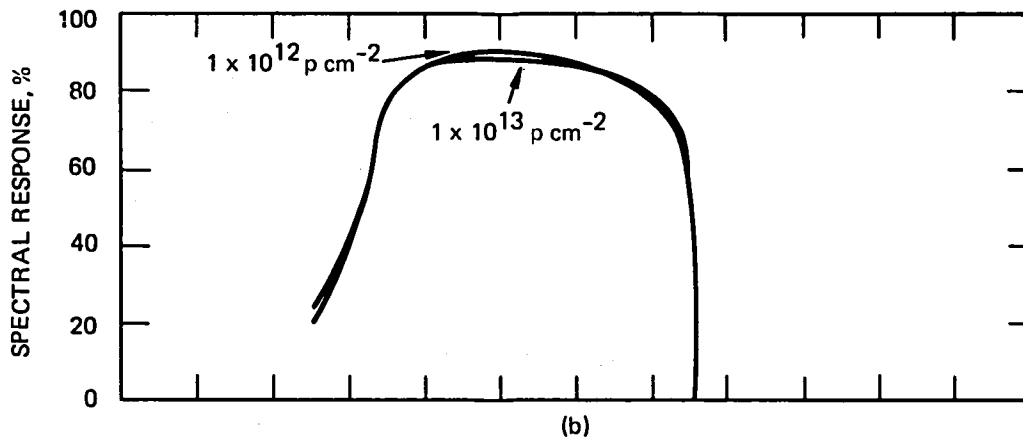
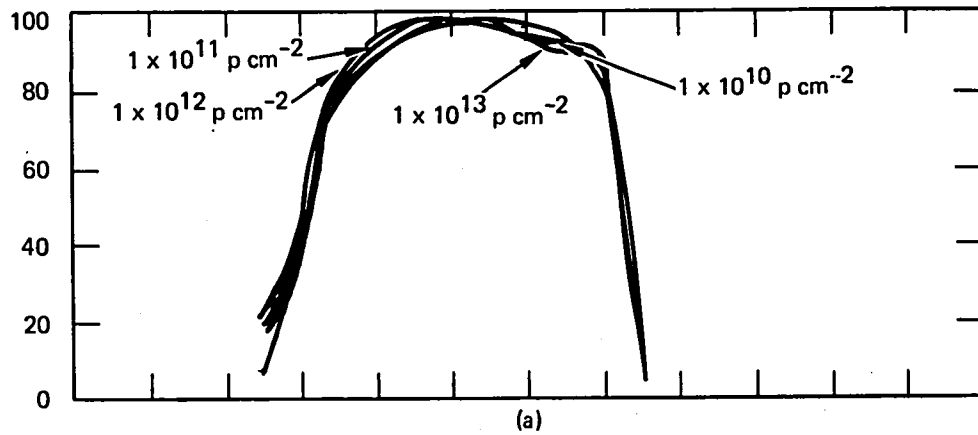


Figure 8. Spectral response of (AlGa)As-GaAs solar cells. (a) After 2 MeV proton irradiation (with 12 mil cover glass), (b) after 5 MeV proton irradiation (with 12 mil cover glass), and (c) After 10 MeV proton irradiation (with 12 mil cover glass).

This Page Intentionally Left Blank

SECTION 3

PERIODIC THERMAL ANNEALING

In the periodic thermal annealing experiment, we chose to study the single-proton energy of 200 keV with incremental fluences of 1×10^{11} p cm⁻² for the reasons given in Section 1. Figure 9 shows the flow chart of the periodic thermal annealing experiments. The GaAs solar cells were first subjected to 200 keV proton irradiation and subsequently to isothermal annealing at various temperatures. The proton irradiation and thermal annealing were repeated again. Finally, the periodically annealed cells were compared to the cells that have been subjected to the same proton irradiation without annealing.

Figure 10 shows the cross-sectional diagram of the annealing system. It consists of a mechanical pump, a cryogenic vacuum pump, a vacuum chamber, a power supply, and a temperature controller. The vacuum chamber is located directly on top of the cryogenic pump. They are separated by a 3-in.-high vacuum valve. The system is capable of reaching 3×10^{-7} Torr in less than 10 min. At least 20 GaAs solar cells can be loaded into a Ta basket, which is then placed in a small oven inside the vacuum chamber. A resistance heater is embedded in the oven wall, as shown in Figure 10. One of the thermocouples is inserted inside the cell basket on top of the cells and the other thermocouple is placed next to the oven wall to permit the controller to maintain the cell temperature within $\pm 5^{\circ}\text{C}$ up to 700°C .

Figures 11(a) through 11(c) show the power ratio (P_A/P_O) as a function of annealing time at temperatures of 200, 300, and 400°C . At 200°C , the annealing process occurs in less than 10 hours, and at 300 and 400°C , the recovery process is almost instantaneous. Consequently, the annealable damage can be quickly recovered at temperatures above 200°C . The photo I-V characteristics before and after each cycle of irradiation and annealing are also displayed in Figures 12 through 22. Figures 23 through 25 show the average spectral response after each cycle of irradiation and annealing. These data are also consistent with our photo I-V measurements.

The periodic annealing characteristics of our GaAs solar cells are summarized in Tables 5, 7, and 9. Figure 4 compares the power output of the periodic annealed cells with the cells that have been subjected to the same

irradiation but not annealed, Tables 6, 8, and 10. By inspection of these tables and figures, we observe that periodic thermal annealing at temperatures as low as 200°C considerably reduces the radiation damage to the GaAs solar cells. The remaining power of the solar cells is maintained at 65% when annealed at 200°C, even when the proton influence exceeds $4 \times 10^{11} \text{ p cm}^{-2}$. The first 35% power loss can only be partially annealed at temperatures higher than 200°C. The power loss is only 28 and 22% after being annealed at 300 and 400°C, respectively. Finally, the cells that were irradiated to a total fluence of $4 \times 10^{11} \text{ p cm}^{-2}$ and subsequently annealed, also recovered to the same final power output as those that were periodically annealed after each dose of $1 \times 10^{11} \text{ p cm}^{-2}$. The net advantages of periodic annealing, compared with one single post-annealing step under the conditions of an experiment, is that the maximum power loss through the whole sequence is smaller with periodic annealing than with single-step annealing, as expected a priori. ($P/P_0 = 0.39$ after irradiation to a fluence of $4 \times 10^{11} \text{ p cm}^{-2}$ and prior to single-step annealing, compared to $P/P_0 = 0.55$ after irradiation to the same influence with periodic annealing prior to the last annealing step.) (See Tables 5 through 10.) The fluence at which periodic annealing was initiated in these experiments ($1 \times 10^{11} \text{ p cm}^{-2}$), however, still seems too high to avoid the formation of those complex defect centers that are more difficult to anneal (higher activation energy) and which could be prevented by avoiding accumulation of the simpler defect centers (annealing before the density of the latter has reached an excessive value). As will be shown in the next section, even keeping the incremented proton fluence down to 10^9 p/cm^2 is not low enough.

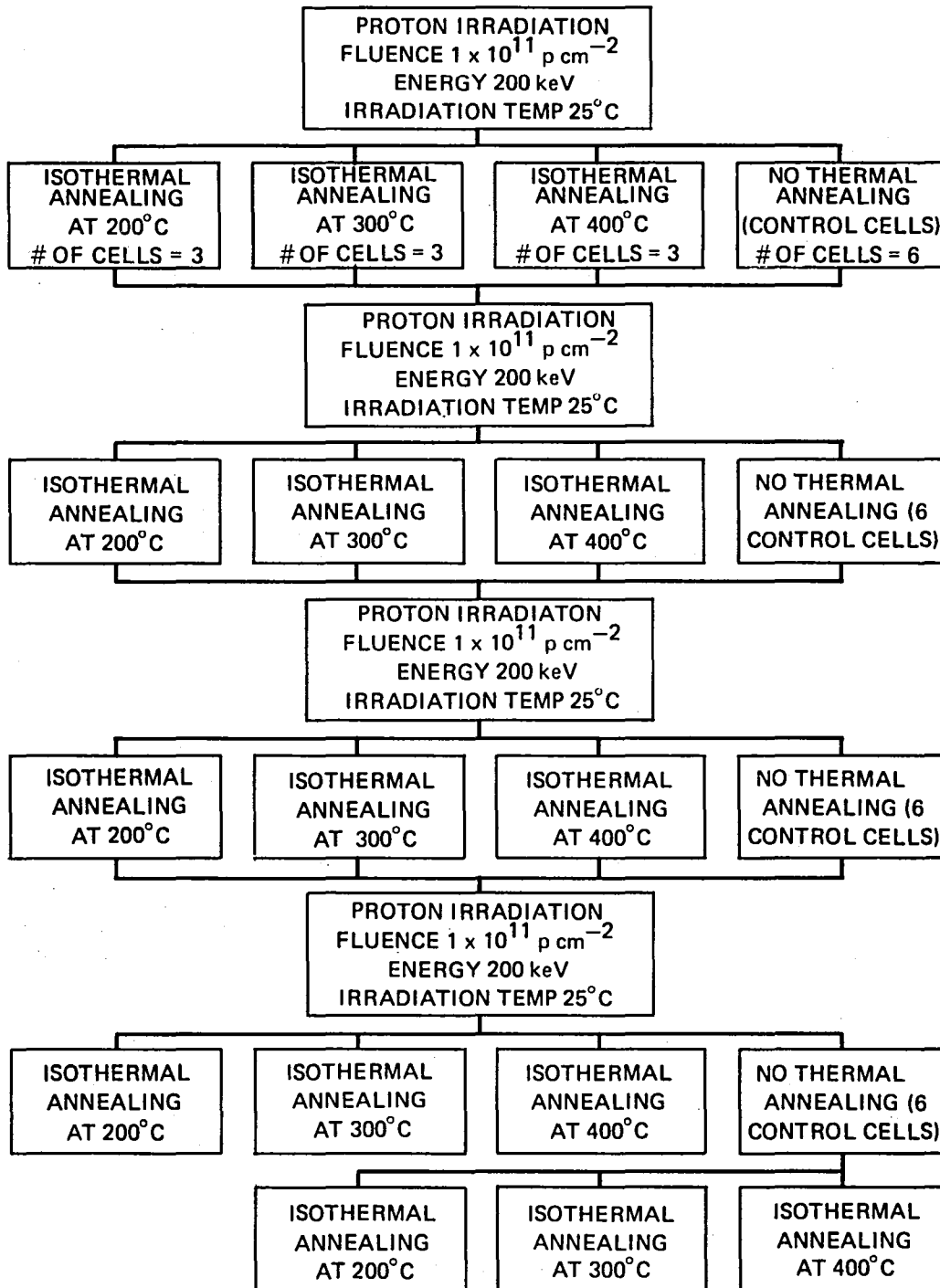


Figure 9. Periodic thermal annealing flow chart.

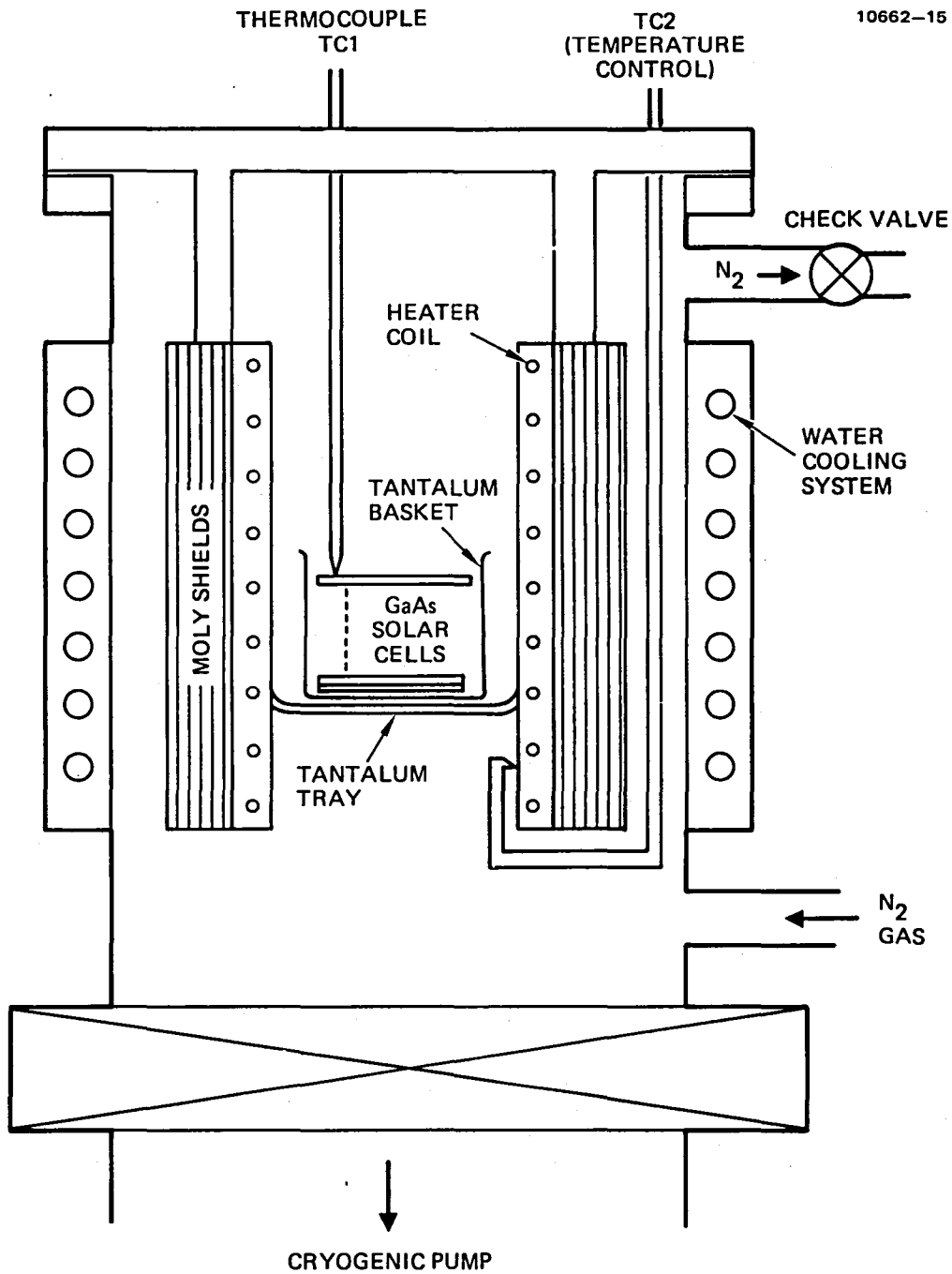


Figure 10. The annealing system.

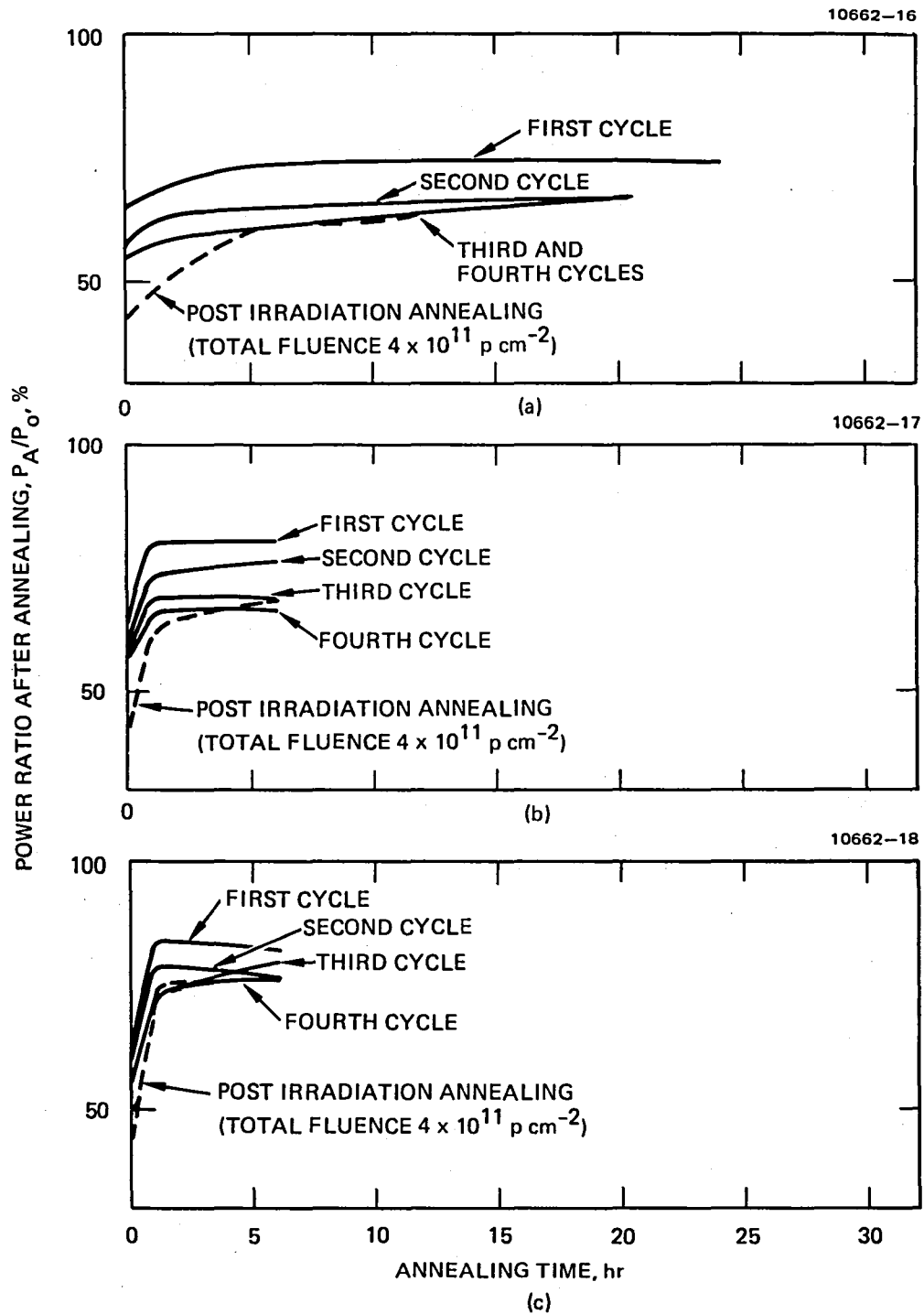


Figure 11. Isothermal annealing. (a) 200°C, (b) 300°C, and (c) 400°C.

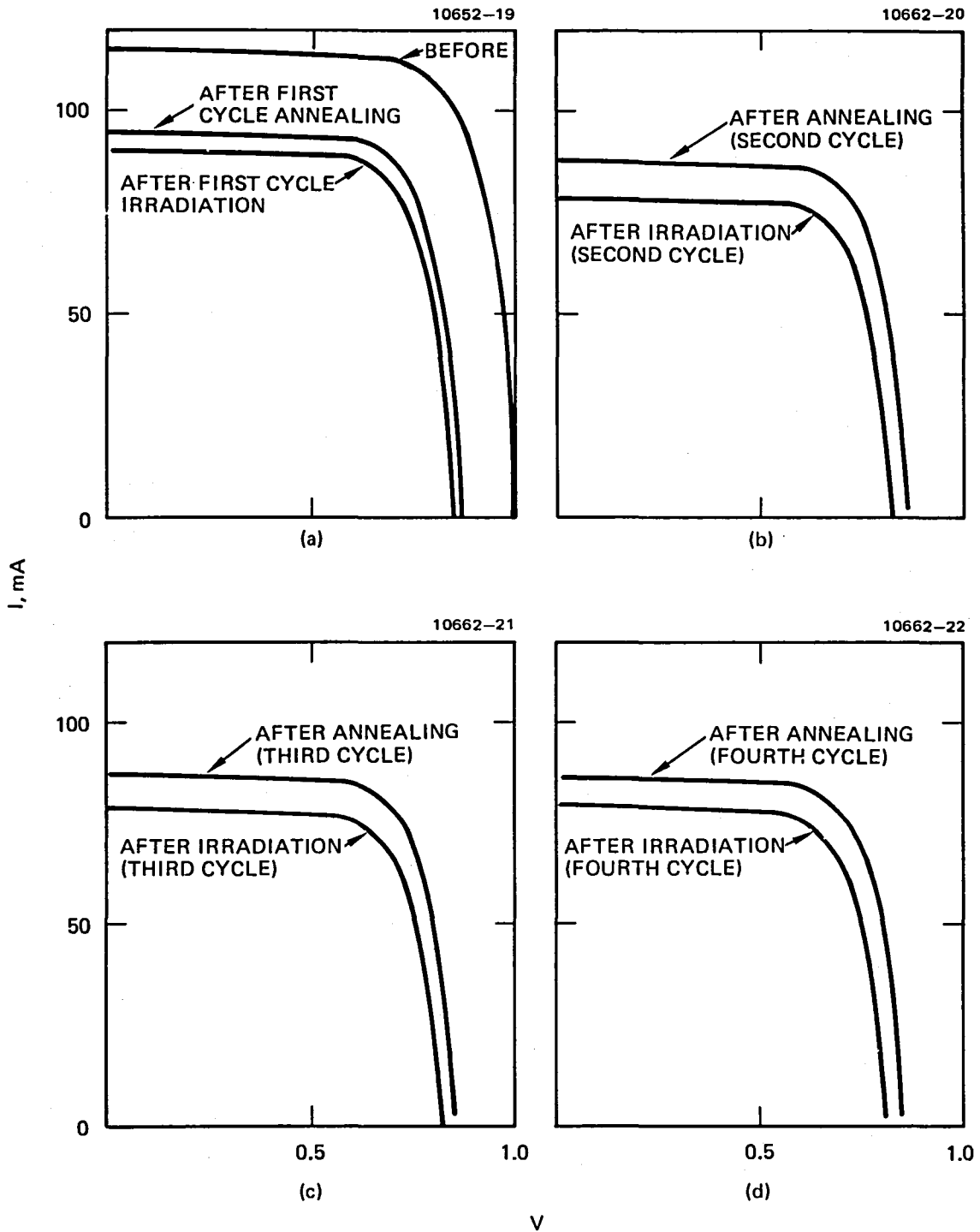


Figure 12. Photo I-V characteristics of (AlGa)As-GaAs solar cell before and after 200 keV; 1×10^{11} pcm^{-2} proton irradiation and after isothermal annealing at temperature of 200°C. (a) first cycle), (b) second cycle, (c) third cycle, and (d) fourth cycle (Cell 5549).

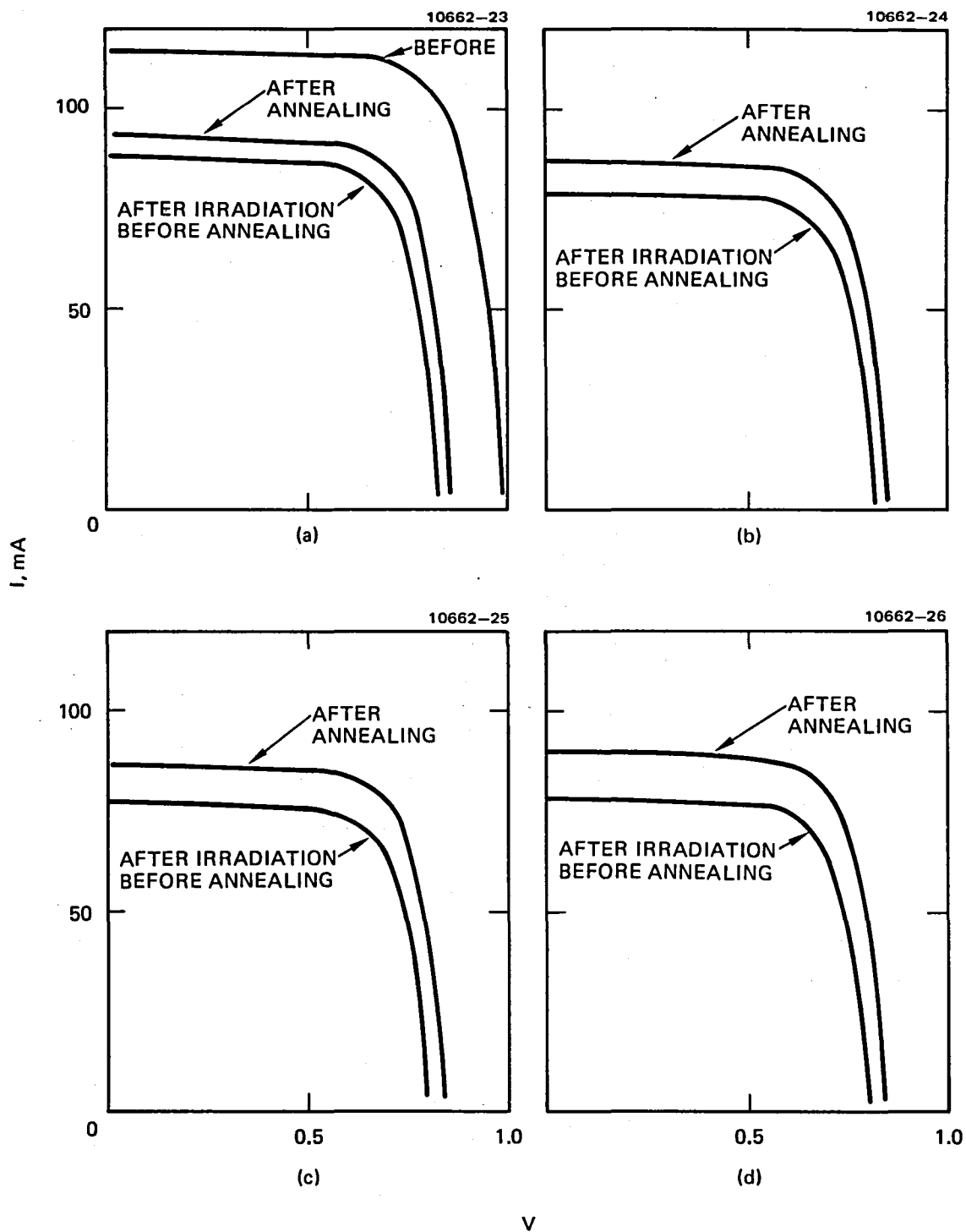


Figure 13. Photo I-V characteristics of (AlGa)As-GaAs solar cell before and after 200 keV; 1×10^{11} pcm^{-2} proton irradiation and after isothermal annealing at temperature of 200°C. (a) first cycle, (b) second cycle, (c) third cycle, and (d) fourth cycle. (Cell 5551).

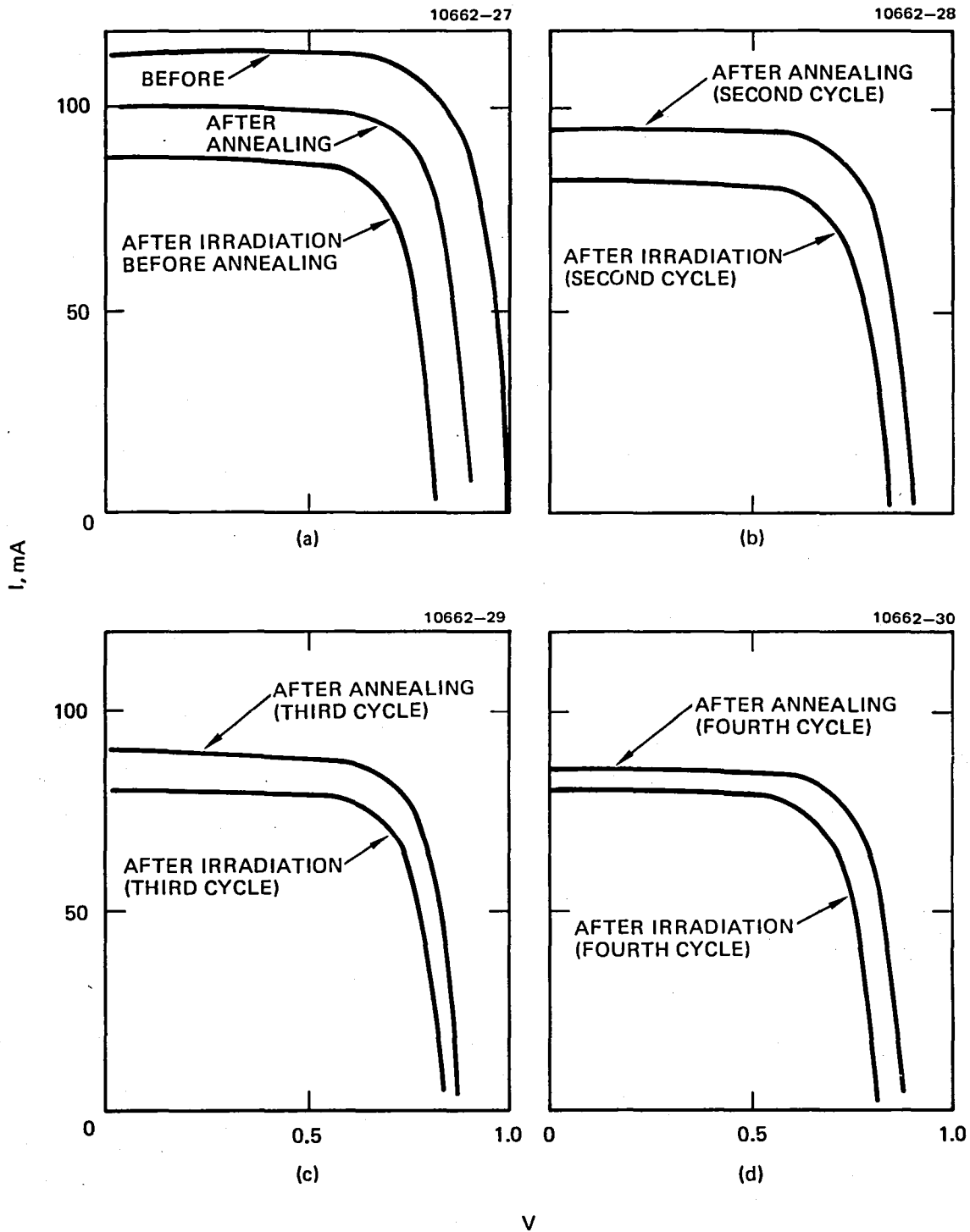


Figure 14. Photo I-V characteristics of (AlGa)As-GaAs solar cell before and after 200 keV, $1 \times 10^{11} \text{ pcm}^{-2}$ proton irradiation and after isothermal annealing at temperature of 300°C. (Cell 5552).

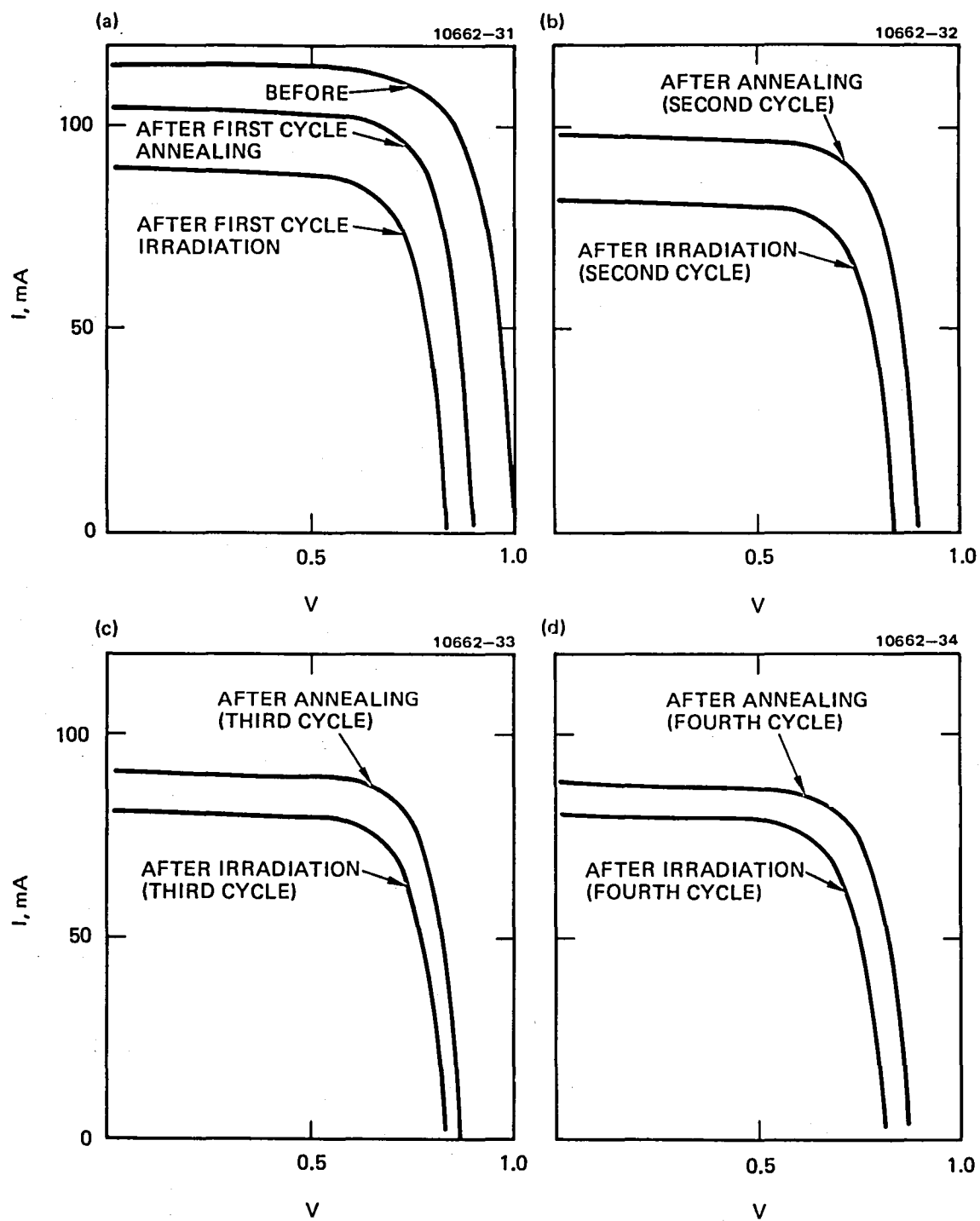


Figure 15. Photo I-V characteristics of (AlGa)As-GaAs solar cell before and after 200 keV, $1 \times 10^{11} \text{ pcm}^{-2}$ proton irradiation and after isothermal annealing at temperature of 300°C. (a) first cycle, (b) second cycle, (c) third cycle, and (d) fourth cycle (Cell 5554).

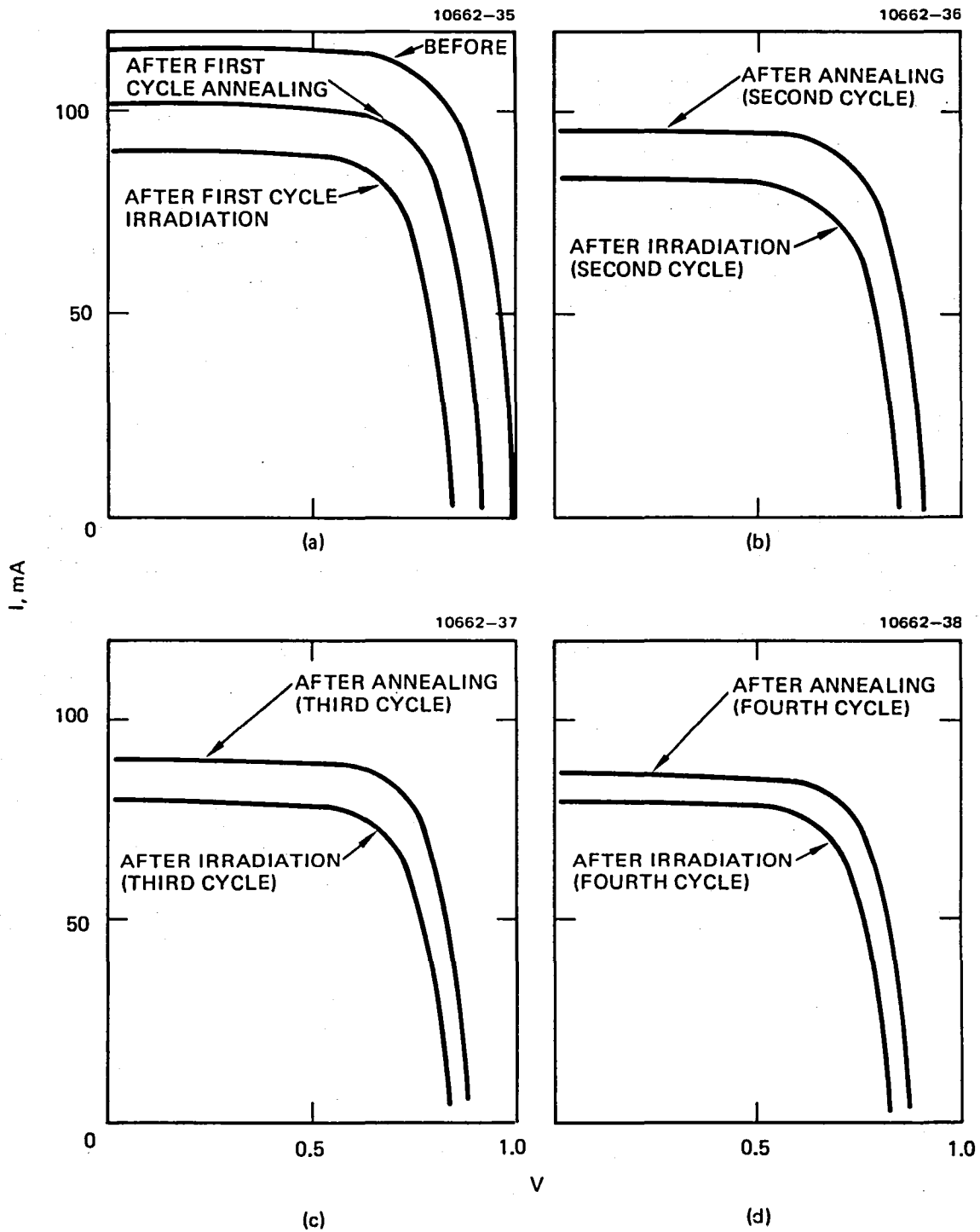


Figure 16. Photo I-V characteristics of (AlGa)As-GaAs solar cell before and after 200 keV, $1 \times 10^{11} \text{ pcm}^{-2}$ proton irradiation and after isothermal annealing at temperature of 300°C. (a) first cycle, (b) second cycle, (c) third cycle, and (d) fourth cycle (cell 5555).

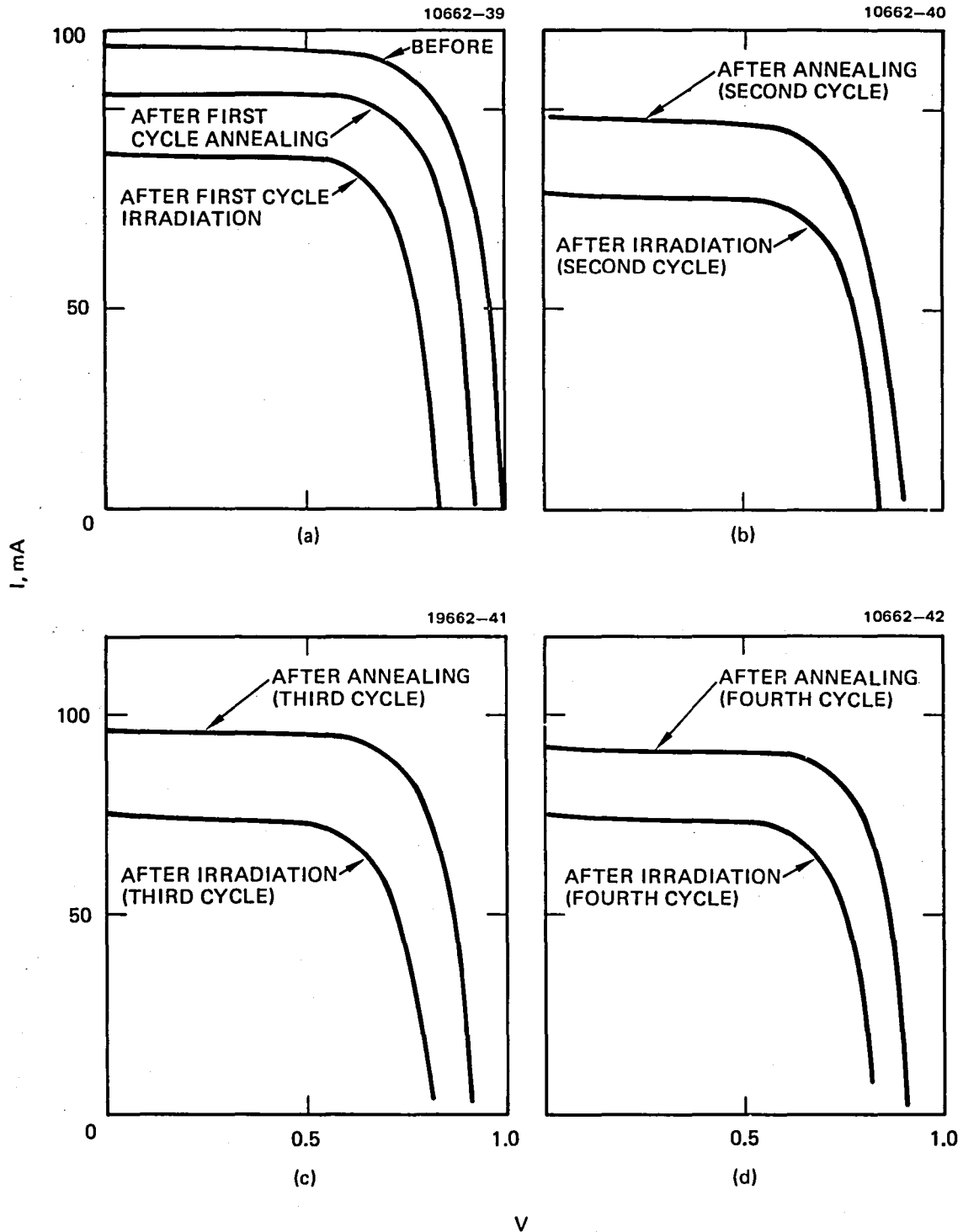


Figure 17. Photo I-V characteristics of (AlGa)As-GaAs solar cell before and after 200 keV, $1 \times 10^{11} \text{ pcm}^{-2}$ proton irradiation at temperature of 400°C. (a) first cycle, (b) second cycle, (c) third cycle, and (d) fourth cycle (cell 5556).

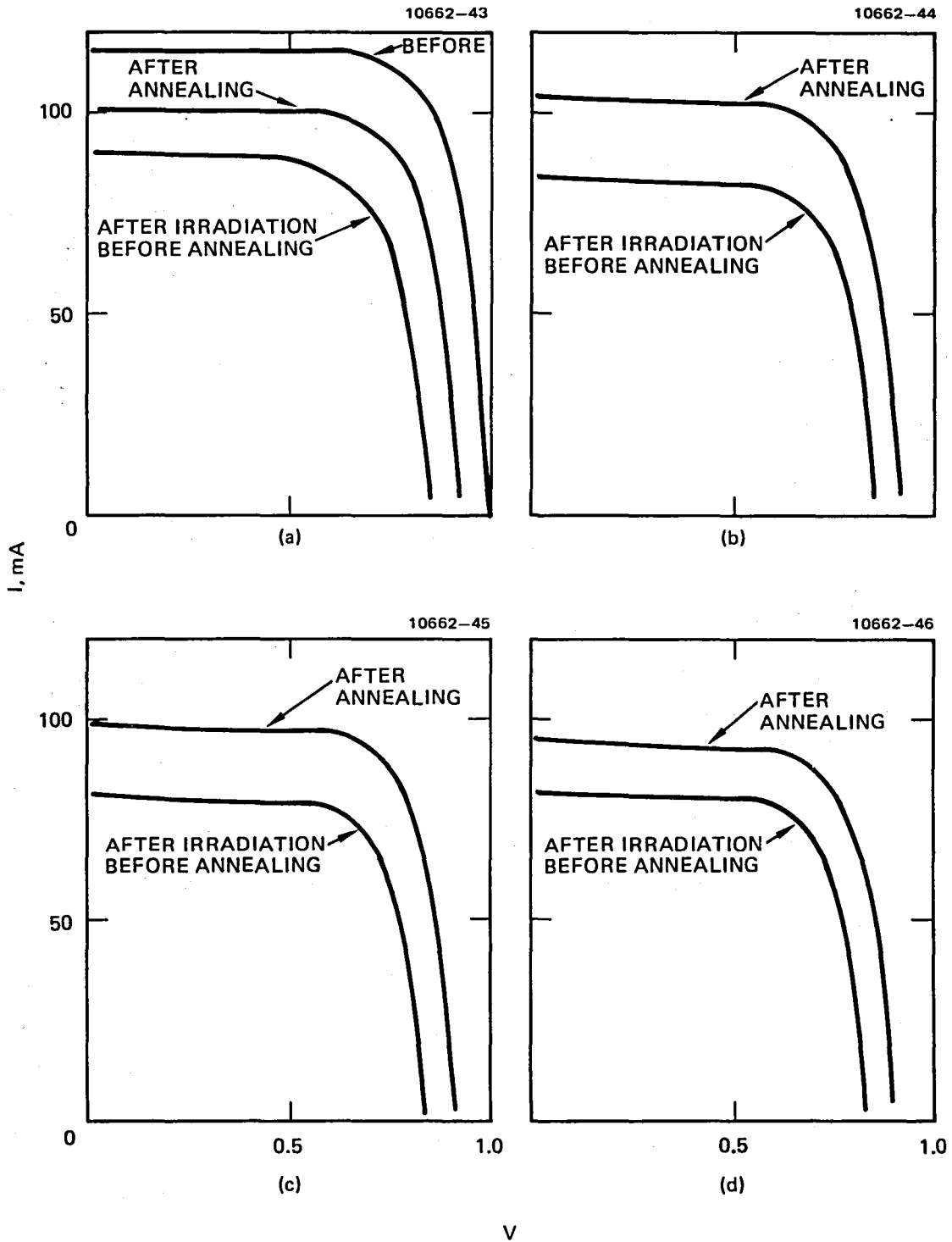


Figure 18. Photo I-V characteristics before and after 200 keV; $1 \times 10^{11} \text{ pcm}^{-2}$ proton irradiation and after isothermal annealing at temperature of 400°C. (a) first cycle, (b) second cycle, (c) third cycle, and (d) fourth cycle (cell 5557).

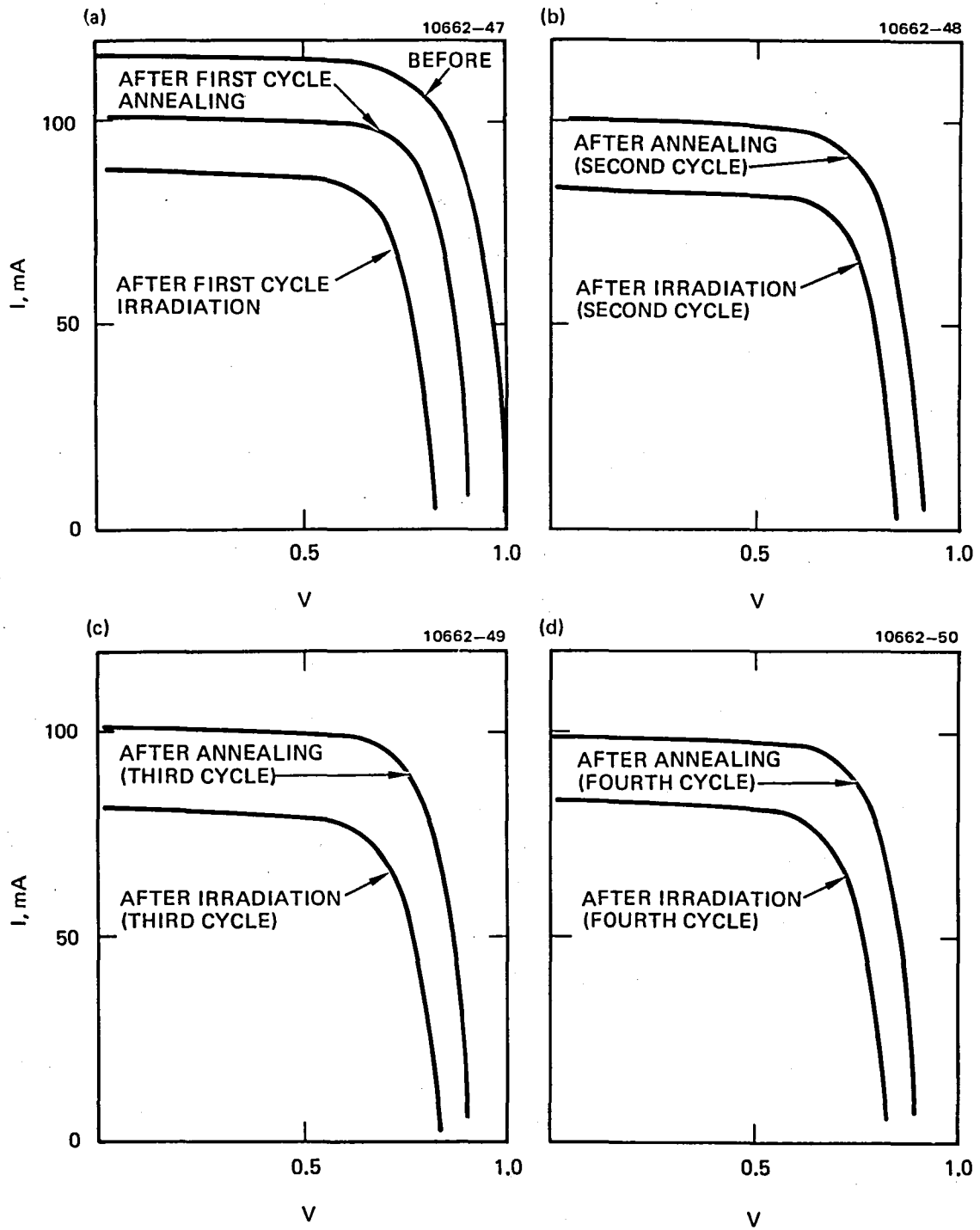


Figure 19. Photo I-V characteristics before and after 200 keV; 1×10^{11} pcm^{-2} proton irradiation and after isothermal annealing at temperature of 400°C. (a) first cycle, (b) second cycle, (c) third cycle, and (d) fourth cycle (cell 5558).

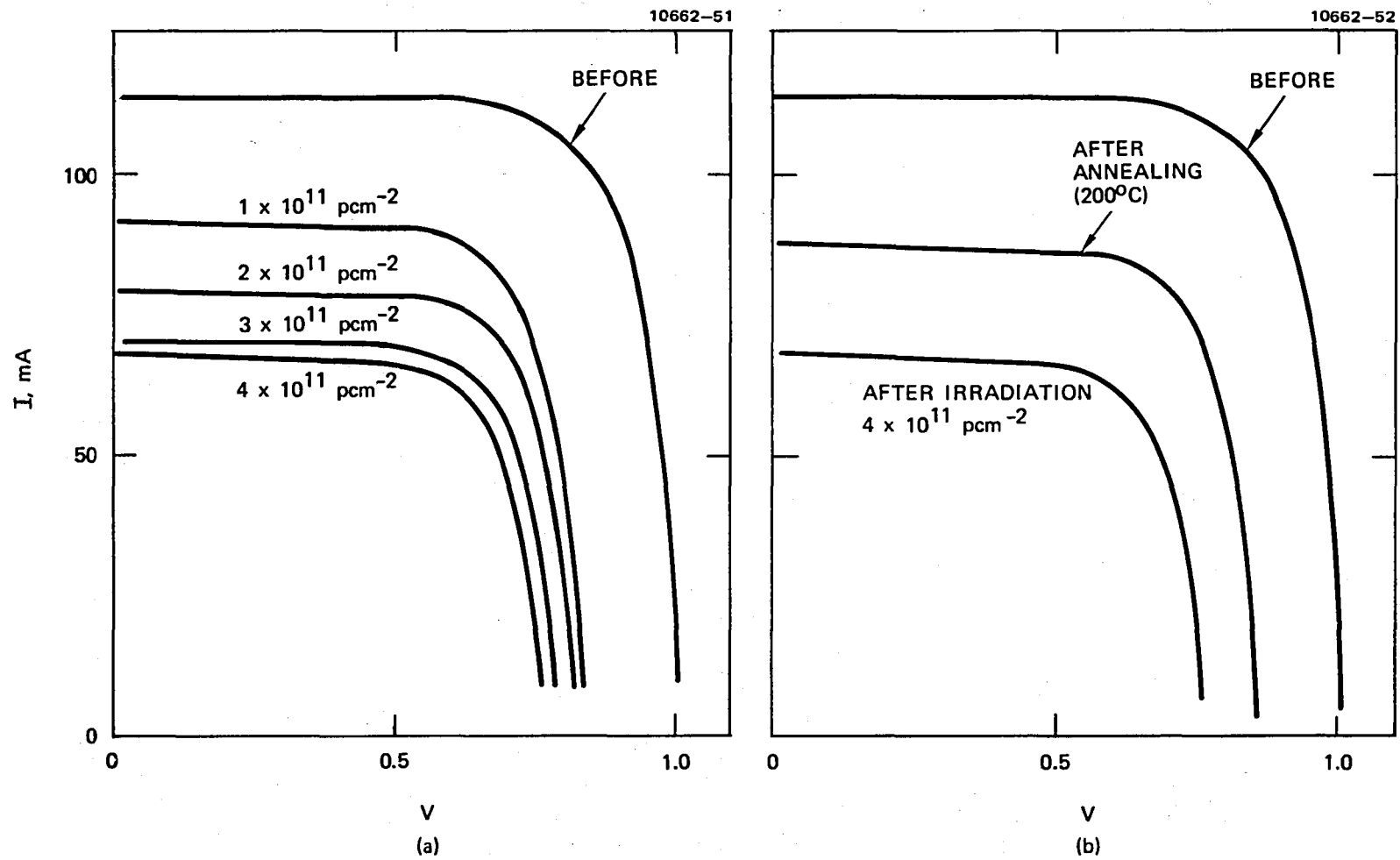


Figure 20. Photo I-V characteristics of (AlGa)As-GaAs solar cell before and after 200 keV; $4 \times 10^{11} \text{ p cm}^{-2}$ irradiation and after 200°C isothermal annealing. (Cell 5591.)

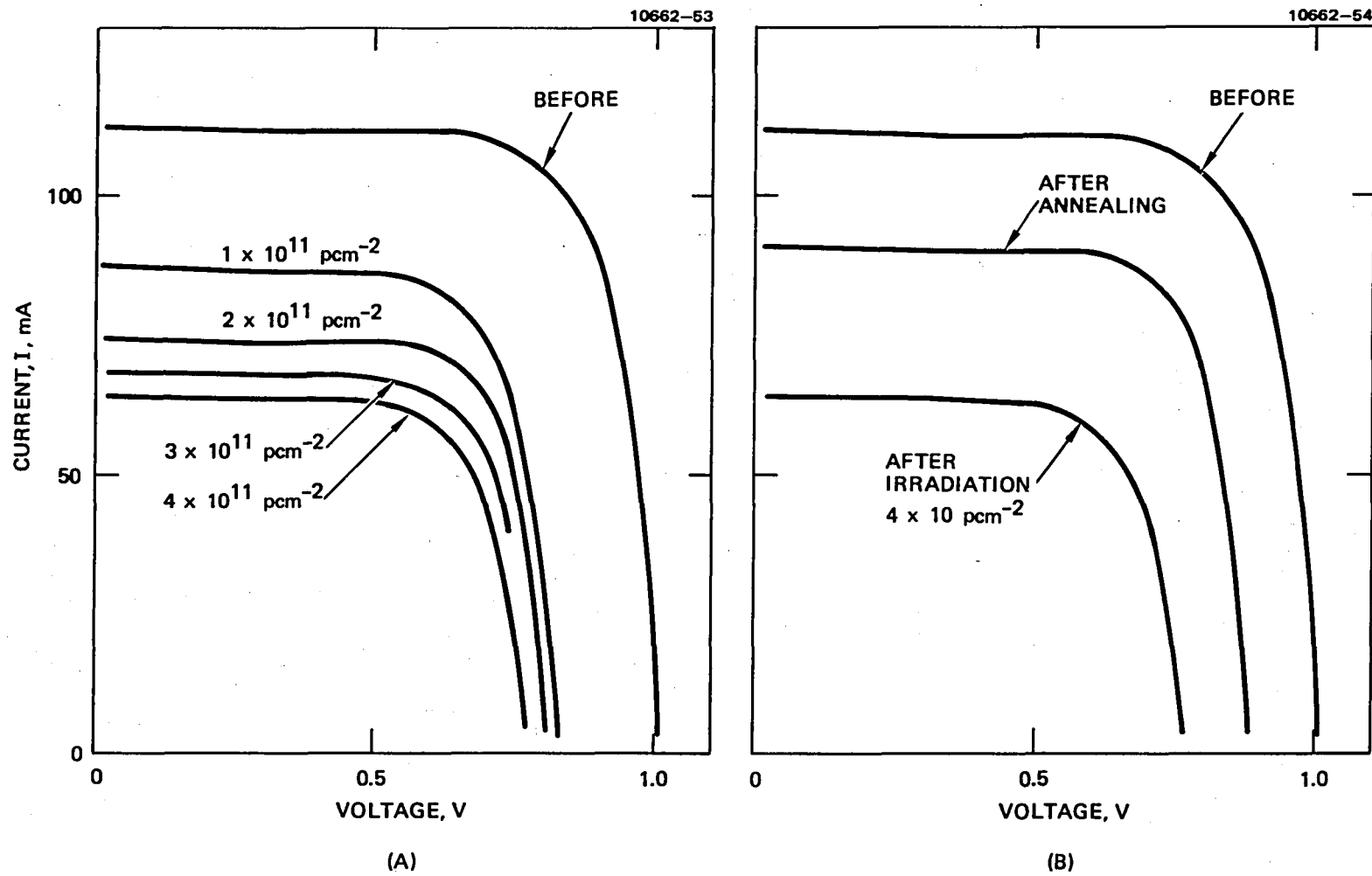
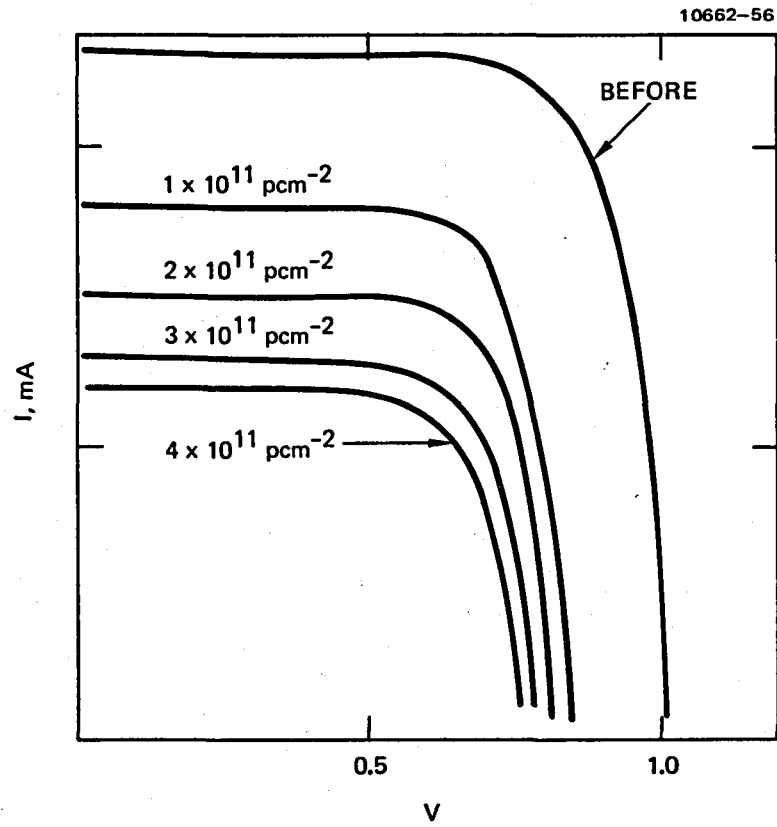
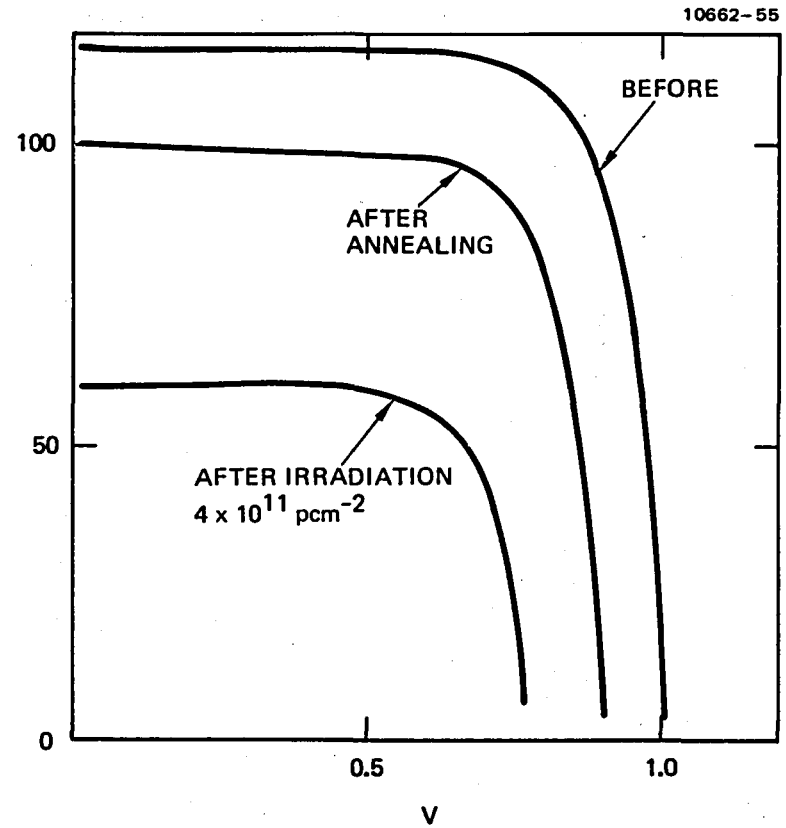


Figure 21. Photo I-V characteristics of (AlGa)As-GaAs solar cell before and after 200 keV proton irradiations and after 300°C isothermal annealing (cell 5563).



(a)



(b)

Figure 22. Photo I-V characteristics of (AlGa)As-GaAs solar cell before and after 200 keV proton irradiation and after 400°C isothermal annealing (cell 5560).

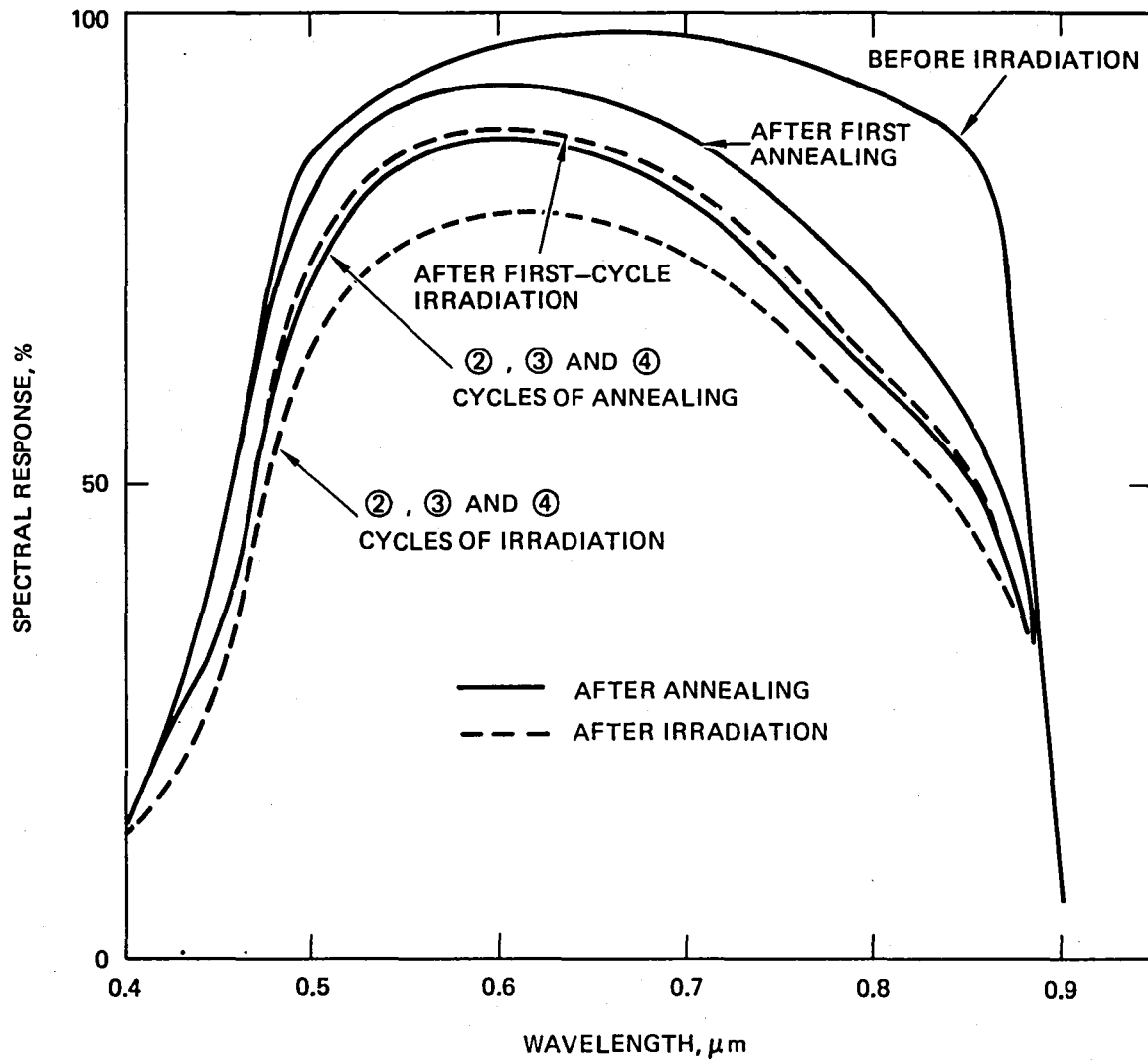


Figure 23. Spectral response of (AlGa)As-GaAs solar cell before and after 200 keV proton irradiation and after 200°C isothermal annealing (cell 5549).

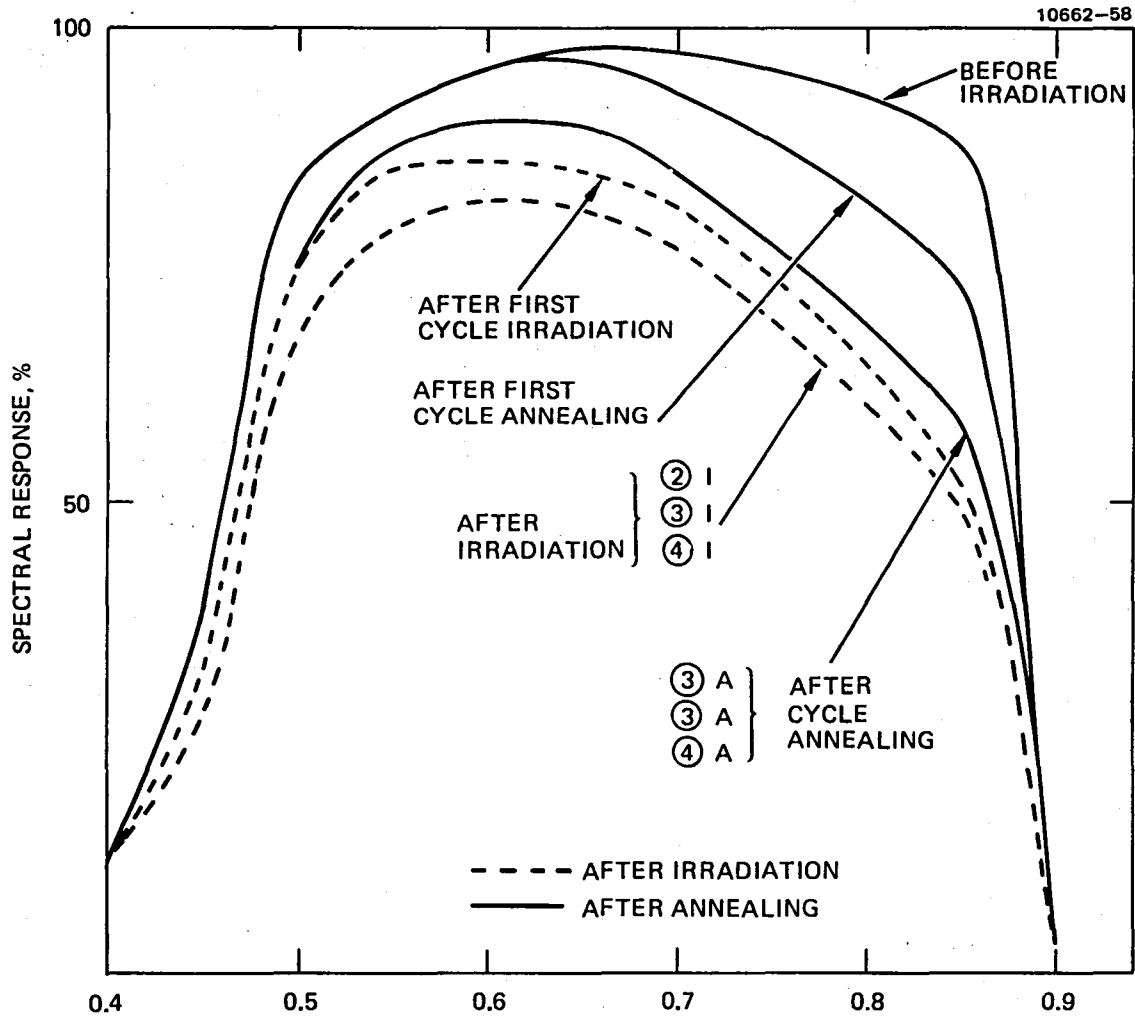


Figure 24. Spectral response of (AlGa)As-GaAs solar cell before and after 200 keV proton irradiation and after 400°C isothermal annealing (cell 5558).

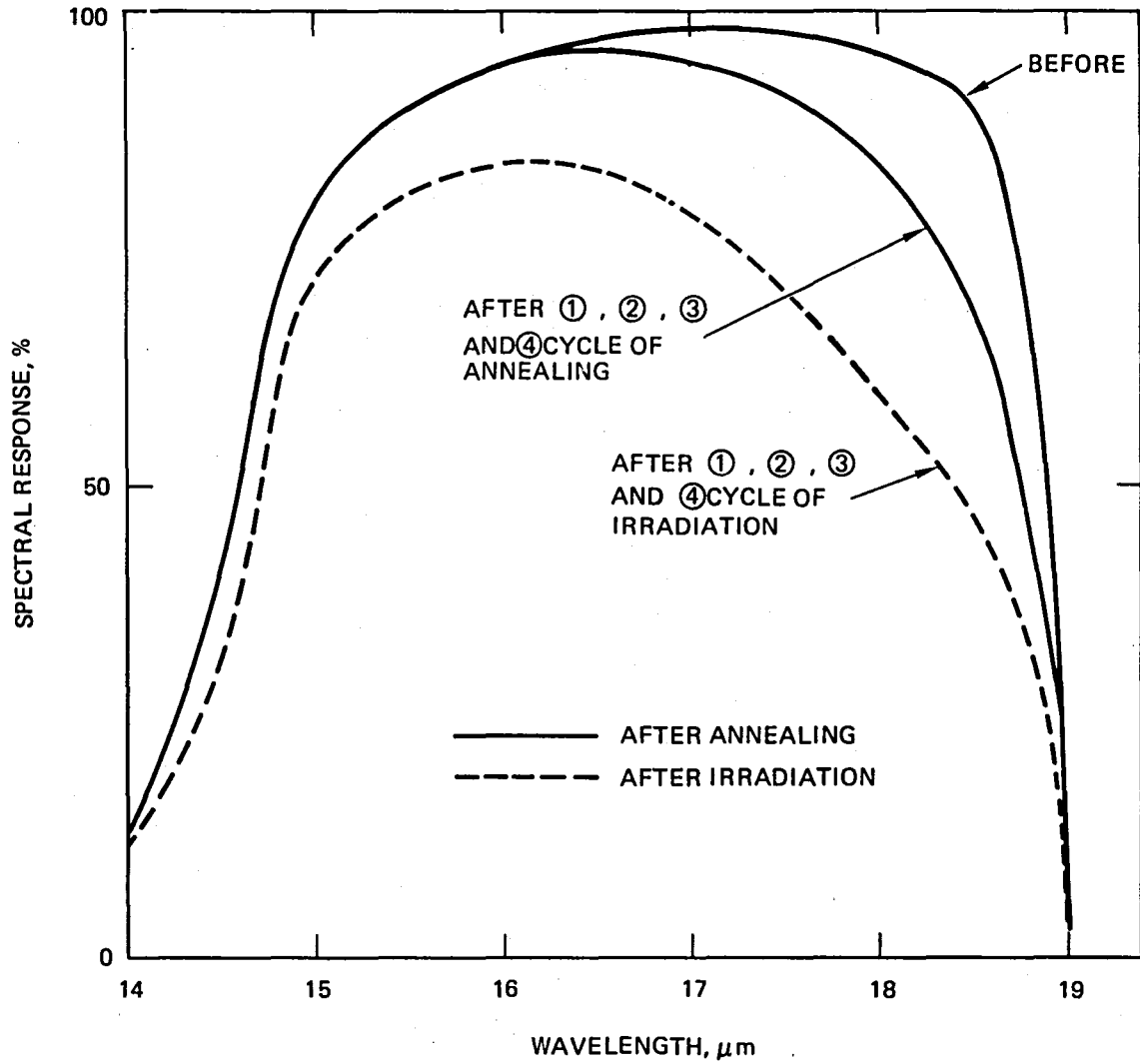


Figure 25. Spectral response of (AlGa)As-GaAs solar cell before and after 200 keV proton irradiation and after 400°C isothermal annealing.

Table 5. Periodic Thermal Annealing Results on (AlGa)As-GaAs Solar Cells Damaged by 200 KeV Protons

Cell No.	Periodic Annealing Cycle	Cumulative Proton Fluence, p cm ⁻²	Thermal Annealing		I _{sc} ' mA	V _{oc} ' V	FF	P _{max} ' mW	η, %	P _A /P ₀ ' %
			Temp., °C	Time, Hour						
5549	1st	1x10 ¹⁸	200	1	114	1.0	0.75	85.3	15.8	
				6	90	0.84	0.74	55.8	10.5	65
				24	92	0.86	0.75	58.8	10.9	69
					96	0.87	0.74	62.1	11.5	73
	2nd	2x10 ¹⁸	200	1	79	0.83	0.74	48.3	8.9	56.3
				20	85	0.85	0.75	54.3	10.0	63.3
					89	0.86	0.75	57.2	10.6	67
	3rd	3x10 ¹⁸	200	2	79	0.82	0.74	47.6	8.8	55.7
				18	81	0.83	0.74	49.7	9.2	58.2
					88	0.85	0.74	55.3	10.2	64.6
	4th	4x10 ¹⁸	200	5	80	0.81	0.73	47.5	8.8	55.7
				21	85	0.84	0.73	52.4	9.7	61.5
					87	0.85	0.75	55.3	10.2	65.0
5551	1st	1x10 ¹⁸	200	1	114	1.0	0.75	85.7	15.8	
				6	88	0.83	0.75	54.4	10.1	64
				20	90	0.85	0.76	57.9	10.7	68
					94	0.86	0.75	61.1	11.3	72
	2nd	2x10 ¹⁸	200	1	79	0.82	0.74	47.9	8.9	56.3
				20	85	0.85	0.76	54.6	10.1	63.9
					87	0.85	0.76	56	10.3	65.2
	3rd	3x10 ¹⁸	200	2	77	0.81	0.74	46.2	8.5	53.8
				20	83	0.83	0.75	51	9.4	59.5
					87	0.84	0.75	54.5	10.1	63.9
	4th	4x10 ¹⁸	200	5	78.5	0.80	0.74	46.2	8.5	54
				21	83.5	0.84	0.74	51.8	9.6	61
					90	0.85	0.75	57.1	10.5	67
5561	1st	1x10 ¹⁸	200	5	113	1.0	0.75	84.7	15.6	
		2x10 ¹⁸		83	0.81	0.73	48.8	9.0	58.0	
		3x10 ¹⁸		70	0.80	0.73	41.0	7.6	48.7	
		4x10 ¹⁸		61	0.77	0.73	34.0	6.3	40.7	
				56	0.74	0.72	29.7	5.5	35.3	
				78	0.83	0.74	47.6	8.8	56.4	
				82	0.84	0.74	50.72	9.4	60.0	
5591	1st	1x10 ¹⁸	200	5	113	1.02	0.76	87.7	16.2	
		2x10 ¹⁸		91	0.84	0.74	56.2	10.4	64.2	
		3x10 ¹⁸		79	0.83	0.75	49	9.0	55.6	
		4x10 ¹⁸		71	0.79	0.74	41.3	7.6	46.9	
				68	0.77	0.72	38.1	7.0	43.2	
				84	0.85	0.74	52.9	9.8	60.5	
				88	0.87	0.75	56.8	10.5	65	
5554	1st	1x10 ¹⁸	300	1	115	1.01	0.75	87.2	16.1	
				6	90	0.84	0.74	55.9	10.3	64
					102.5	0.90	0.76	70.5	13.0	81
	2nd	2x10 ¹⁸	300	1	104	0.91	0.76	71.6	13.2	82
				6	82	0.84	0.74	51.2	9.5	59
					95	0.89	0.76	64	11.8	73.2
				98	0.90	0.76	66.8	12.3	76.3	

7433

Table 5. (Continued)

Cell No.	Periodic Annealing Cycle	Cumulative Proton Fluence $p\text{ cm}^{-2}$	Thermal Annealing		I_{sc} , mA	V_{oc} , V	FF	P_{max} , mW	η , %	P_A/P_0 , %
			Temp., °C	Time, Hour						
5555	3rd	3×10^{19}	300	1	81	0.83	0.74	49.7	9.2	57.1
				6	92	0.88	0.74	59.8	11.0	68.3
				6	91	0.87	0.75	59.4	11.0	68.3
	4th	4×10^{19}	300	1	81	0.82	0.74	48.5	9.0	56
				6	89	0.87	0.73	56.8	10.5	65.2
				6	89	0.87	0.74	57.2	10.6	66
	1st	1×10^{20}	300	1	115	1.0	0.74	85.3	15.8	
				6	90	0.84	0.74	55.8	10.3	65
				6	100	0.92	0.75	69.2	12.8	81
	2nd	2×10^{20}	300	1	83	0.84	0.74	51.8	9.6	60.8
				6	92	0.89	0.75	61.3	11.3	71.5
				6	95	0.91	0.75	64.5	11.9	75.3
3rd	3×10^{20}	300	1	80	0.84	0.73	49	9.0	57	
			6	89	0.88	0.75	58.4	10.8	68.4	
			6	90	0.88	0.75	59	10.9	69	
4th	4×10^{20}	300	1	80	0.82	0.74	48.4	8.9	56.3	
			6	88	0.87	0.74	56.2	10.4	66	
			6	87	0.87	0.75	56.5	10.4	66	
5552	1st	1×10^{20}	300	1	114.5	1.01	0.74	85.5	15.8	
				6	88	0.82	0.74	53.6	9.9	63
				6	101	0.90	0.75	68.1	12.6	80
	2nd	2×10^{20}	300	1	83	0.84	0.74	51.8	9.6	61
				6	93	0.89	0.75	62.5	11.6	73.4
				6	96	0.90	0.75	65	12.0	76
	3rd	3×10^{20}	300	1	81	0.84	0.74	50	9.2	58.2
				6	90	0.87	0.75	59	10.9	69
				6	90	0.88	0.75	59	10.9	69
	4th	4×10^{20}	300	1	81	0.82	0.73	48.6	9.0	57
				6	85.5	0.87	0.76	56.2	10.4	66
				6	86.5	0.86	0.75	56.1	10.4	66
5563	1st	1×10^{20}	300	1	112	1.01	0.76	85.5	15.8	
				6	88	0.83	0.73	52.9	9.8	62
				6	75	0.82	0.74	45.2	8.4	53.2
	2nd	2×10^{20}	300	1	69	0.79	0.74	40.3	7.5	47.5
				6	65	0.77	0.72	36.2	6.7	42.4
				6	88	0.88	0.75	57.7	10.7	68
	3rd	3×10^{20}	300	1	92	0.88	0.76	61.3	11.3	72
				6	92	0.88	0.76	61.3	11.3	72
				6	92	0.88	0.76	61.3	11.3	72
	4th	4×10^{20}	300	1	114	1.02	0.75	86.3	15.8	
				6	85	0.82	0.73	50.8	9.4	60
				6	73	0.81	0.74	43.6	8.0	50.6
1st	1×10^{21}	300	1	68	0.79	0.72	38.7	7.2	45.3	
			6	68	0.79	0.72	38.7	7.2	45.3	
			6	63.5	0.76	0.72	34.7	6.4	40.5	
2nd	2×10^{21}	300	1	88	0.87	0.74	56.9	10.5	66.5	
			6	95	0.88	0.66	55.4	10.2	65	
			6	95	0.88	0.66	55.4	10.2	65	
5556	1st	1×10^{21}	400	1	115.5	1.0	0.73	84.2	15.6	
				6	89	0.83	0.74	54.4	10.1	65
				6	106	0.92	0.75	73	13.5	87
				6	104	0.92	0.75	72	13.3	85

7433

Table 5. (Continued)

Cell No.	Periodic Annealing Cycle	Cumulative Proton Fluence, $p\text{ cm}^{-2}$	Thermal Annealing		I_{sc} mA	V_{oc} V	FF	P_{max} mW	η , %	P_A/P_{O_2} %
			Temp., °C	Time, Hour						
5557	2nd	2×10^{19}	400	1 6	79	0.84	0.74	49	9.3	58
					98	0.92	0.74	66.4	12.0	79
					98	0.90	0.72	63.2	11.7	75
	3rd	3×10^{19}	400	1 6	75	0.82	0.70	42.9	7.9	50.6
					90	0.89	0.73	58.2	10.8	69.2
					96	0.92	0.74	65.3	12.1	78
	4th	4×10^{19}	400	1 6	75	0.82	0.73	45	8.3	53
					93	0.92	0.73	61.4	11.3	72.4
					93	0.91	0.75	63	11.6	74
	1st	1×10^{20}	400	1 6	116	1.0	0.75	86.9	16.1	
					89	0.84	0.73	54.5	10.1	63
					104	0.92	0.75	71.3	13.2	82
2nd	2×10^{20}	400	1 6	101	0.92	0.75	69.8	12.9	80	
				83	0.85	0.74	52.4	9.7	60	
				96	0.91	0.76	66	12.2	76	
3rd	3×10^{20}	400	1 6	104	0.92	0.73	70	12.9	80	
				81	0.84	0.73	49.6	9.2	57	
				95	0.90	0.74	63.5	11.7	73	
4th	4×10^{20}	400	1 6	99	0.91	0.73	66.1	12.2	76	
				82.5	0.83	0.73	49.6	9.2	57	
				97	0.90	0.73	63.7	11.8	73	
5558	1st	1×10^{20}	400	1 6	95	0.90	0.73	62.1	11.5	72
					115	1.01	0.75	87.2	16.1	
					87	0.83	0.74	53.7	9.9	
	2nd	2×10^{20}	400	1 6	104	0.93	0.76	73.2	13.5	84
					101	0.93	0.76	71.2	13.2	82
					83	0.85	0.75	53.2	9.8	61
	3rd	3×10^{20}	400	1 6	97	0.92	0.77	68.5	12.7	79
					100	0.91	0.74	67.3	12.4	77
					81	0.83	0.73	98.9	9.0	56
	4th	4×10^{20}	400	1 6	95	0.90	0.74	63.6	11.8	73.3
					101	0.91	0.75	69	12.8	80
					83	0.83	0.73	50.3	9.28	58
5559	1st	1×10^{21}	400	1 6	99	0.89	0.75	65.7	12.1	75
					99	0.90	0.75	68.5	12.6	78.3
					115	1.01	0.75	87.2	16.1	
	2nd	2×10^{21}	400	1 6	90	0.84	0.74	55.8	10.3	64
					79	0.82	0.75	48.3	8.9	55.3
					67	0.78	0.74	38.4	7.1	44
	3rd	3×10^{21}	400	1 6	63	0.76	0.73	35	6.5	40.4
					83	0.83	0.73	50.3	9.28	58
					99	0.90	0.73	65.0	12.0	75
	4th	4×10^{21}	400	1 6	99	0.90	0.75	66.4	12.3	76.4
					99	0.90	0.75	66.4	12.3	76.4
					115	1.01	0.75	87.2	16.1	
5560	1st	1×10^{22}	400	1 6	90	0.84	0.74	55.8	10.3	64
					79	0.82	0.75	48.3	8.9	55.3
					67	0.78	0.74	38.4	7.1	44
	2nd	2×10^{22}	400	1 6	63	0.76	0.73	35	6.5	40.4
					83	0.83	0.73	50.3	9.28	58
					99	0.90	0.73	65.0	12.0	75
	3rd	3×10^{22}	400	1 6	99	0.90	0.75	66.4	12.3	76.4
					99	0.90	0.75	66.4	12.3	76.4
					115	1.01	0.75	87.2	16.1	
	4th	4×10^{22}	400	1 6	90	0.84	0.74	55.8	10.3	64
					79	0.82	0.75	48.3	8.9	55.3
					67	0.78	0.74	38.4	7.1	44
1st	1×10^{23}	400	1 6	63	0.76	0.73	35	6.5	40.4	
				83	0.83	0.73	50.3	9.28	58	
				99	0.90	0.73	65.0	12.0	75	
2nd	2×10^{23}	400	1 6	99	0.90	0.75	66.4	12.3	76.4	
				99	0.90	0.75	66.4	12.3	76.4	
				115	1.01	0.75	87.2	16.1		
3rd	3×10^{23}	400	1 6	90	0.84	0.74	55.8	10.3	64	
				79	0.82	0.75	48.3	8.9	55.3	
				67	0.78	0.74	38.4	7.1	44	
4th	4×10^{23}	400	1 6	63	0.76	0.73	35	6.5	40.4	
				83	0.83	0.73	50.3	9.28	58	
				99	0.90	0.73	65.0	12.0	75	
1st	1×10^{24}	400	1 6	99	0.89	0.75	65.7	12.1	75	
				101	0.90	0.75	68.5	12.6	78.3	
				118	1.01	0.76	90.5	16.7		
2nd	2×10^{24}	400	1 6	91	0.85	0.75	57.3	10.6	63.5	
				77	0.82	0.75	47.3	8.7	52.1	
				66	0.79	0.74	38.4	7.1	42.5	
3rd	3×10^{24}	400	1 6	61.5	0.77	0.73	34.1	6.3	38	
				83	0.83	0.73	50.3	9.28	58	
				99	0.90	0.73	65.0	12.0	75	
4th	4×10^{24}	400	1 6	99	0.90	0.75	66.4	12.3	76.4	
				99	0.90	0.75	66.4	12.3	76.4	
				118	1.01	0.76	90.5	16.7		
1st	1×10^{25}	400	1 6	91	0.85	0.75	57.3	10.6	63.5	
				77	0.82	0.75	47.3	8.7	52.1	
				66	0.79	0.74	38.4	7.1	42.5	
2nd	2×10^{25}	400	1 6	61.5	0.77	0.73	34.1	6.3	38	
				83	0.83	0.73	50.3	9.28	58	
				99	0.90	0.73	65.0	12.0	75	
3rd	3×10^{25}	400	1 6	99	0.90	0.75	66.4	12.3	76.4	
				99	0.90	0.75	66.4	12.3	76.4	
				118	1.01	0.76	90.5	16.7		
4th	4×10^{25}	400	1 6	91	0.85	0.75	57.3	10.6	63.5	
				77	0.82	0.75	47.3	8.7	52.1	
				66	0.79	0.74	38.4	7.1	42.5	
1st	1×10^{26}	400	1 6	61.5	0.77	0.73	34.1	6.3	38	
				83	0.83	0.73	50.3	9.28	58	
				99	0.90	0.73	65.0	12.0	75	

SECTION 4

CONTINUOUS ANNEALING

In the continuous annealing experiment we again chose to study the single proton energy of 200 keV. The purpose of this experiment was to study the effect of proton flux (1×10^{10} versus 1×10^{11} p cm⁻² hr⁻¹) in our GaAs cells at the temperatures of 200°C and 25°C, respectively. Table 6 gives the test matrix of the continuous annealing experiment. Table 7 gives the electrical characteristics before and after 200 keV proton irradiation. Appendix C shows the photo I-V characteristics of each individual cell. Figure 26 shows the power ratio after irradiation as a function of proton fluence. The GaAs solar cells which were irradiated at a flux of 1×10^{10} p cm⁻² hr⁻¹ for 10 hours at 200°C have 6% more power (or $P/P_0 = 66\%$) than both the cells which were irradiated at room temperature under the same irradiation condition and the cells that were irradiated at 200°C for one hour at a flux of 1×10^{11} p cm⁻² hr⁻¹. The cells which were subjected to room temperature irradiation, and those that were subjected to a higher flux of 1×10^{11} p cm⁻² hr⁻¹ at 200°C, have the same power degradation, $P/P_0 = 60\%$. The result clearly shows that during proton irradiation, the annealing time (one hour at 200°C) was not long enough to have any significant effect on the cell performance.

In another set of continuous annealing experiments, we irradiated our GaAs solar cells with 200 keV protons at a flux of 1×10^{10} p cm⁻² hr⁻¹ to a fluence of 1×10^9 p-cm⁻² at 200°C. We repeated this experiment 10 times. Each time we added 1 hour of annealing at 200°C before the next irradiation, until the final fluence accumulated to 1×10^{10} p cm⁻². Table 8 gives the electrical characteristics before and after the irradiation. These results show that the one hour annealing time between each step of irradiation is not effective in improving the cells radiation resistance, even though the incremental flux between each step was kept as low as 10^9 p cm⁻².

We have also completed the post annealing experiments on the GaAs cells which had first been continuously annealed at 200°C (irradiation at 200°C at the two fluxes of 1×10^{10} p cm⁻² hr⁻¹ and 1×10^{11} p cm⁻² hr⁻¹, respectively). The results of these measurements are given in Tables 7 and 8. The GaAs cells which were irradiated at a lower flux of 1×10^{10} p cm⁻² hr⁻¹ for

ten hours at 200°C (continuous annealing) did not improve their efficiency with additional annealing at 200°C. This indicates that the annealing time provided under continuous annealing under this low flux was adequate. Only those cells which were irradiated at room temperature and at high flux ($1 \times 10^{11} \text{ p cm}^{-2} \text{ hr}^{-1}$ at 200°C) showed an increase in efficiency with 200°C post annealing. This correlates with the observation that the time available (<1 hr) at the annealing temperature of 200° under high flux continuous annealing was insufficient for substantial annealing. In conclusion, these results show that the continuous annealing experiment at 200°C at lower flux provided sufficient time for annealing, even though the cells which were irradiated at room temperature exhibited more power output ($P_1/P_0 = 74\%$) than the continuously annealed cells ($P_1/P_0 = 66\%$). Thus, within the limits of our experiments, the data indicate that continuous annealing does not seem more favorable than periodic annealing on GaAs solar cells, at least for 200 keV proton radiation damage at fluxes $>10^{10} \text{ p cm}^{-2} \text{ hr}^{-1}$ and fluences $>10^{10} \text{ p cm}^{-2}$.

Table 6. 200 keV Proton - Continuous Annealing Experiment

Task	Temp., °C	Flux, $\text{p cm}^{-2} \text{ hr}^{-1}$	Time, hr	Fluence, p cm^{-2}	GaAs Cell I.D. No.
1	200	1×10^{11}	1	1×10^{11}	7742, 7755, 7756
2	25	1×10^{10}	10	1×10^{11}	7743, 7744, 7746
3	200	1×10^{10}	10	1×10^{11}	7757, 7758, 7814
4 ^a	200	1×10^{10}	0.1	1×10^9	7810, 8259, 8256
5	200	1×10^{11}	0.1	1×10^{10}	7831, 7869, 8258

^aAnneal once an hour and repeat for ten times. The final fluence should be $1 \times 10^{10} \text{ p cm}^{-2}$.

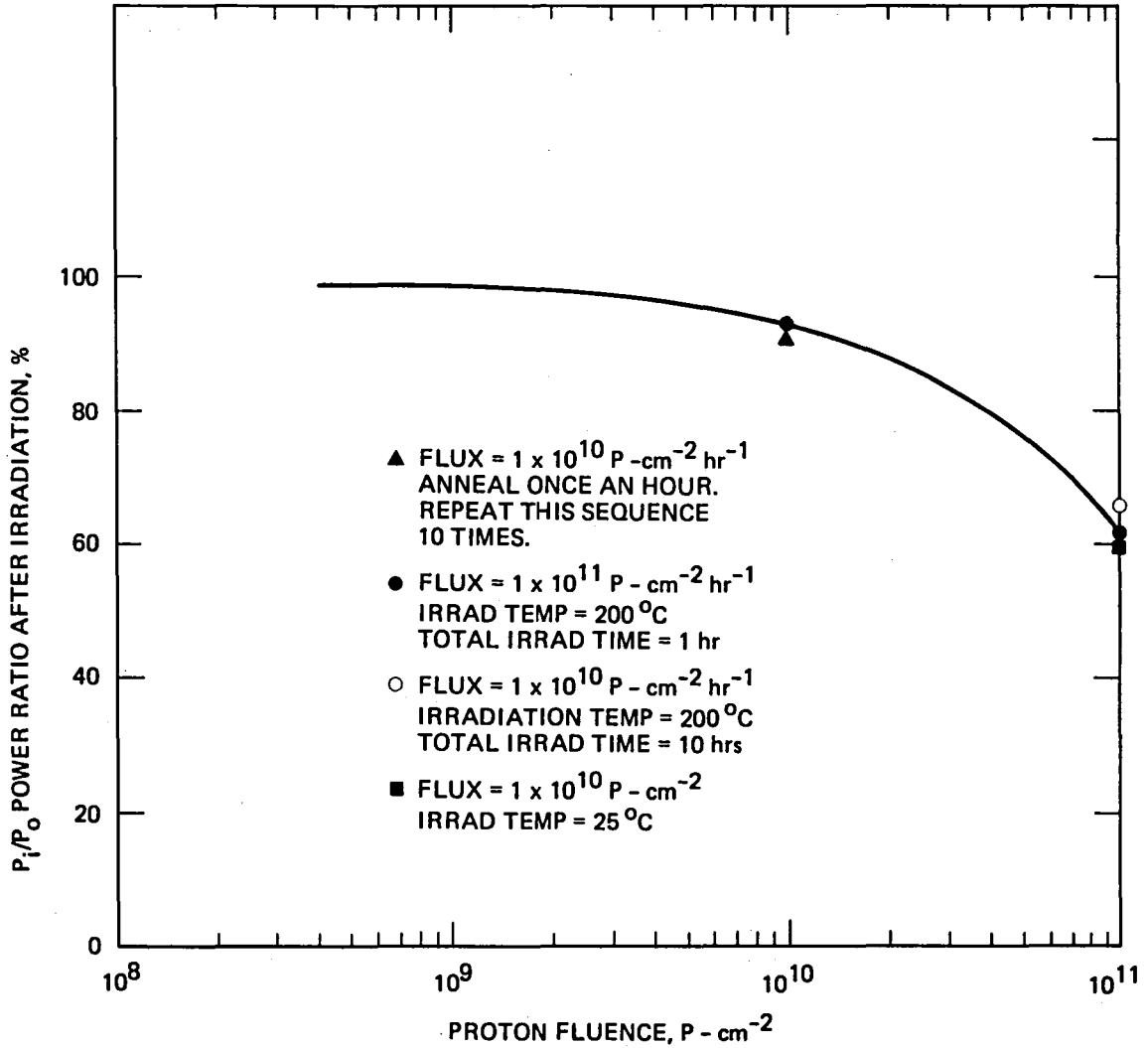


Figure 26. Continuous annealing experiment.

Table 7. Annealing of Proton Radiation Damage,
Fluence 1×10^{11} p cm⁻²

Cell No.	Irradiation			Post Anneal		Performance					
	Flux, p cm ⁻² Hr ⁻¹	Temp., °C	Time, Hr	Temp., °C	Time, Hr	I _{SC} , mA	V _{OC} , V	FF	P _m , mW	η, %	P/P ₀ , %
7743	0	0				113	1.0	0.78	87.6	16.2	
	1×10^{10}	25	10			75	0.92	0.79	54.5	10.0	61.7
				200	6	88	0.945	0.79	65.6	12.1	74.7
				200	10	88	0.94	0.78	64.8	12.0	74.7
7744	0	0				113	1.0	0.77	86.9	16.1	
	1×10^{10}	25	10			76.5	0.90	0.78	53.5	9.89	61.4
				200	6	90	0.925	0.78	65.2	12.0	74.5
				200	10	90	0.92	0.78	64.7	12.0	74.5
7746	0	0				113	1.01	0.769	87.7	16.2	
	1×10^{10}	25	10			75	0.90	0.787	53.1	9.8	60.5
				200	6	87	0.93	0.78	62.8	11.6	71
				200	10	89	0.92	0.78	63.5	11.7	71
7757	0	0				117.5	1.02	0.78	93.3	17.2	
	1×10^{10}	200	10			80	0.97	0.78	60.6	11.2	65.1
				200	6	77	0.98	0.79	59.6	11.0	64
				200	10	78	0.97	0.78	59	10.9	64
7758	0	0				117	1.01	0.78	91.8	17.0	
	1×10^{10}	200	10			80	0.96	0.79	60.7	11.2	66
				200	6	79	0.98	0.79	61	11.3	66
				200	10	77	0.96	0.79	58.6	10.8	65
7814	0	0				115	1.01	0.79	91.2	16.8	
	1×10^{10}	200	10			86	0.89	0.77	59.3	11	65.5
				200	6	84	0.90	0.78	59.3	11	65.5
				200	10	83	0.89	0.78	57.8	10.7	65
7742	0	0				114	1.0	0.78	88.8	16.4	
	1×10^{11}	200	1			86	0.89	0.77	59.3	11.0	67
				200	6	88	0.905	0.79	62.7	11.6	71
				200	10	89	0.89	0.79	62.3	11.5	71
7755	0	0				115	1.01	0.775	90.1	16.7	
	1×10^{11}	200	1			73	0.96	0.784	54.9	10.2	61
				200	6	79	0.98	0.79	60.9	11.3	67.7
				200	10	81	0.97	0.78	61.4	11.3	67.7
7756	0	0				117	1.01	0.78	91.8	17	
	1×10^{11}	200	1			73	0.96	0.79	55.4	10.2	60
				200	6	80	0.98	0.78	61.0	11.3	66
				200	10	82	0.97	0.78	62.3	11.5	66

Figure 8. Annealing of Proton Radiation Damage,
200 keV; 1×10^{10} p cm⁻²

Cell No.	Irradiation			Post Anneal		Performance					
	Flux, p cm ⁻² Hr ⁻¹	Temp., °C	Time, Hr	Temp., °C	Time, Hr	I _{SC} , mA	V _{OC} V	FF	P _m , mW	η, %	P/P ₀ %
8256	1×10^{11}	200	0.1	200	9	113	1.0	0.74	83.6	15.5	
						103	0.98	0.77	78	14.4	93
						103	0.98	0.77	78	14.4	93
8259	1×10^{11}	200	0.1	200	9	114	0.99	0.75	84	15.6	
						105.5	0.94	0.79	77.4	14.3	92
						105.5	0.94	0.79	77.4	14.3	92
7810	1×10^{11}	200	0.1	200	9	114	1.01	0.786	90.5	16.7	
						104	0.95	0.785	77.6	14.3	85.6
						104	0.95	0.79	77.6	14.3	85.6
7831*	1×10^{10}	200	10			117	1.02	0.768	90.9	16.8	
						108	0.99	0.76	81.3	15.0	89.3
7869*		200	10			117	1.0	0.80	93.7	17.3	
						110	0.97	0.79	84.6	15.6	90
8258*		200	10			115	1.01	0.74	85.5	15.8	
						105	0.98	0.77	80	14.7	93

* Irradiated to a fluence of 1×10^9 p cm⁻² and then annealed once an hour. This has been repeated for ten times until the final fluence is 1×10^{10} p cm⁻².

This Page Intentionally Left Blank

SECTION 5

CONCLUSION

We have studied the radiation damage characteristics of GaAs solar cells under medium-energy proton irradiation at 2, 5, and 10 MeV. This study is a continuation of our previous work on low-energy (50 to 300 keV) and high-energy (15 to 50 MeV) proton irradiation in GaAs solar cells. The key observation is that the GaAs solar cells are superior in radiation hardness to Si solar cells at all proton energies higher than 5 MeV. In the region below 5 MeV, the only proton energy region where GaAs cells are more susceptible to damage, conventional coverglass offers sufficient protection to virtually eliminate all damages. Some high-energy protons lose some of their energy while penetrating through the coverglass and cause damage as low-energy protons. In the geosynchronous orbit, (Figure 3), there are relatively fewer high-energy than low-energy protons. For example, there are only $\sim 2 \times 10^{10}$ p cm⁻² in the energy range between 20 MeV to 40 MeV, whereas in the proton energy between 0 to 200 keV, there are $\sim 1 \times 10^{10}$ p cm⁻². Therefore, our GaAs solar cells protected by the coverglass should suffer relatively small deterioration by proton irradiation in the orbit.

Under this contract we also performed periodic thermal annealing and continuous annealing experiments on our GaAs solar cells. Our data show that the cells subjected to periodic thermal annealing have improved end-of-life efficiency compared to the cells without annealing. In the periodic thermal annealing, results at 200°C appear to be almost as good as the annealing results at temperatures of 300 and 400°C. In general, a 10-hour annealing time at 200°C is sufficient. Higher temperatures reduce annealing time, becoming almost instantaneous at temperatures above 300°C. In our experiments, the remaining power (P/P_0) stays constant at 65% after the second cycle of periodic annealing at 200°C.

The results from the continuous annealing at 200°C show that one hour annealing at 200°C during proton irradiation was not long enough to have a substantial effect on the cell performance. The effect of proton flux is important only to provide more time for cell annealing at 200°C. Within the limits of four experiments in the laboratories, the question that still

remains unanswered is whether or not the effective annealing temperature can be lowered below 200°C if the cells are subjected to the very low flux in the geosynchronous orbit of the order of $\sim 10^3$ p cm⁻² see⁻¹. The alternative approach to continuous annealing is to incorporate annealing into a space concentrator system with modest solar concentration of ~ 100 suns. Such a system can be used to protect the cell from radiation damage. Also, the generated heat by the concentrated sunlight can be utilized for annealing cell damage. Consequently, it is highly desirable to continue these annealing studies in detail since there are strong indications that with proper panel design and the use of only modest solar concentrations, it should be possible to achieve desired annealing and tolerate a very severe radiation environment while maintaining the end-of-life efficiency close to the beginning-of-life value. Alternatively, it may be possible to decrease the thickness of the required protective coverglass or to eliminate it in some cases. Such approaches could be very desirable to ensure reliable operation of GaAs space cells in space missions with power levels remaining close to their beginning-of-life values under severe radiation exposure and in economically attractive systems. We plan to make this an important thrust of future programs.

REFERENCES

1. J. B. Marion and F. C. Young, Nuclear Reaction Analysis (American Elsevier Publishing Company, New York, 1968), pp. 30-31.
2. C. F. Williamson, Jean-Paul Boujot and Jean Picard, Tables of Range and Stopping Power of Chemical Elements for Charged Particles of Energy 0.05 to 500 MeV (Département de Physique Nucléaire SACLAY, 1966), p.69.

This Page Intentionally Left Blank

APPENDIX A

MEDIUM ENERGY PROTON IRRADIATION (CALTECH)

Proton beams from the ONR-CIT EN tandem accelerator were energy analyzed using a previously calibrated 90° bending magnet. The beams were spread over the area of four 2 cm x 2 cm cells by multiple scattering in 0.2-mil to 1.5-mil-thick gold foils. The geometry of the target system is shown in Figure A-1. The target was electrically isolated so that the proton flux could be measured by integrating the current deposited on the target. The target was biased at +45 V to prevent secondary electrons from escaping, while the upstream aperture was biased at -300 V to suppress secondary electrons from the gold foils. Measurements of beam current are thus accurate to ±2%. There are two major sources of systematic error in beam fluence and energy. The multiply scattered beam will have a Gaussian angular profile. The half angle of the scattered beam was calculated¹ and is shown in Table A-1, along with the percentage difference in flux indicated between the center and outside corners of the cells. The second source of error is caused by the mechanism of energy loss of the beam passing through the gold foil. Energy is lost because of a large number of collisions between the protons and electrons in the foil. Statistical deviations in the number of collisions cause a spread in the energy of the scattered beam. The total energy loss,² and the calculated energy spread of the scattered beam are also shown in Table A-1.

Table A-1. Calculated Energy Spread of the Scattered Proton Beam

Energy MeV	Gold Foil Thickness, Mil	Energy Loss, MeV	Scattering Half Angle	Flux Ratio*	Energy Spread
10.0	1.57	1.37	3.8	0.81	±0.09 MeV
4.8	1.20	1.30	6.6	0.93	±0.07 MeV
2.0	0.40	0.91	9.1	0.96	±0.04 MeV
0.8	0.15	0.45	12.4	0.98	±0.02 MeV

*Ratio between the flux at the corner of the target farthest from the center (lowest point) and the flux at the corner in the center (highest flux point)

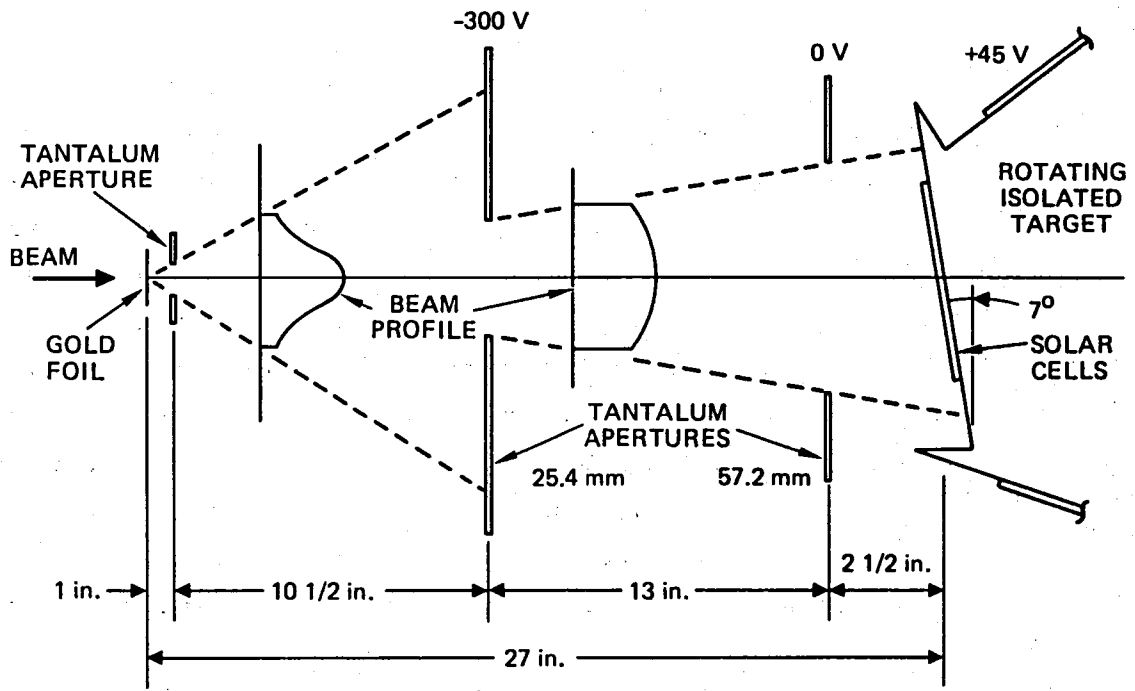


Figure A-1. Medium energy proton target system.

APPENDIX B

PHOTO I-V CHARACTERISTICS OF (AlGa)As-GaAs SOLAR CELLS
BEFORE AND AFTER MEDIUM-ENERGY PROTON IRRADIATION

This Page Intentionally Left Blank

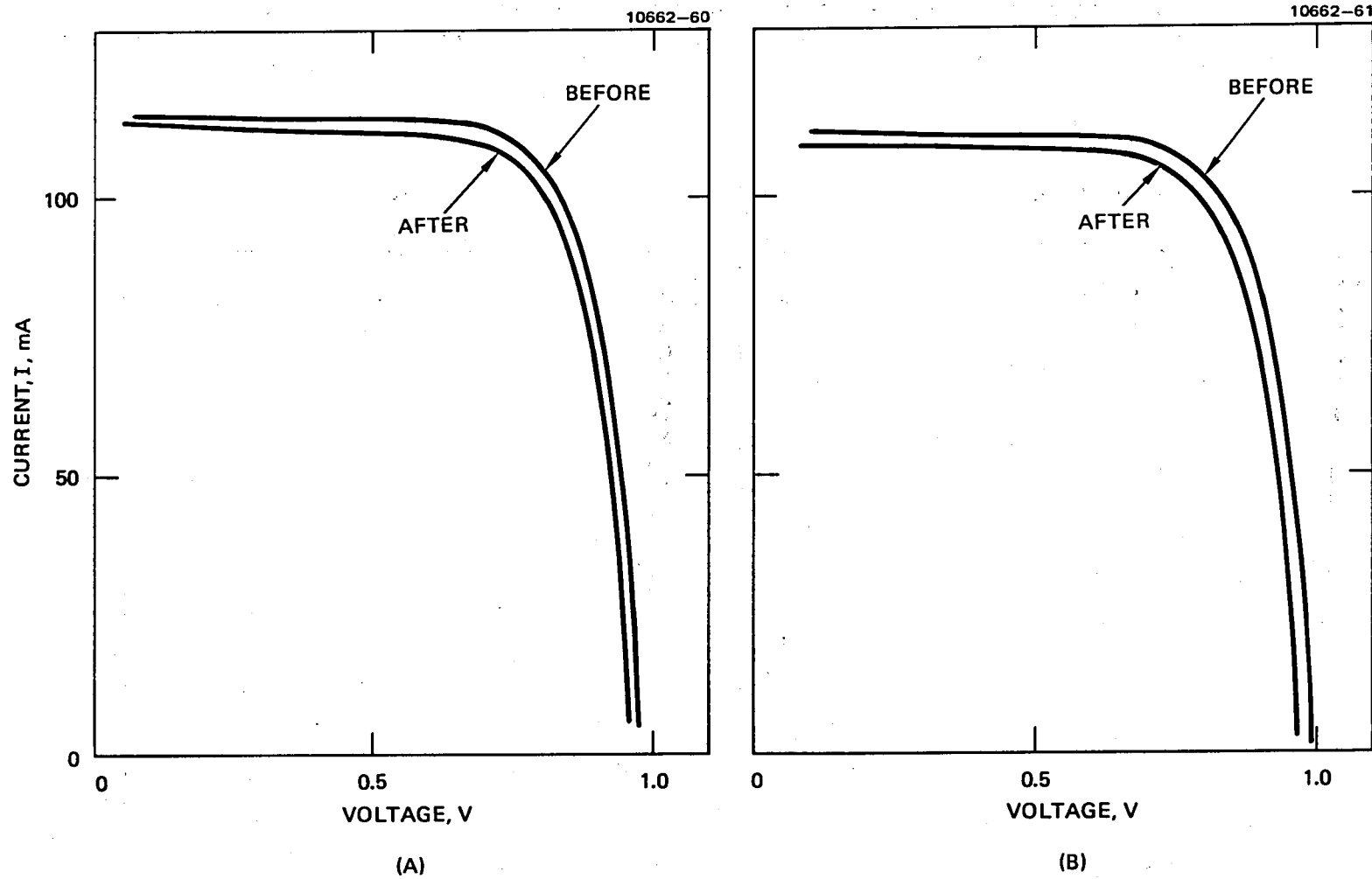


Figure B-1. Photo I-V characteristics before and after $2 \text{ MeV}; 1 \times 10^{10} \text{ p cm}^{-2}$ proton irradiation.
(a) Cell 4166 without coverglass.
(b) Cell 4167 without coverglass.

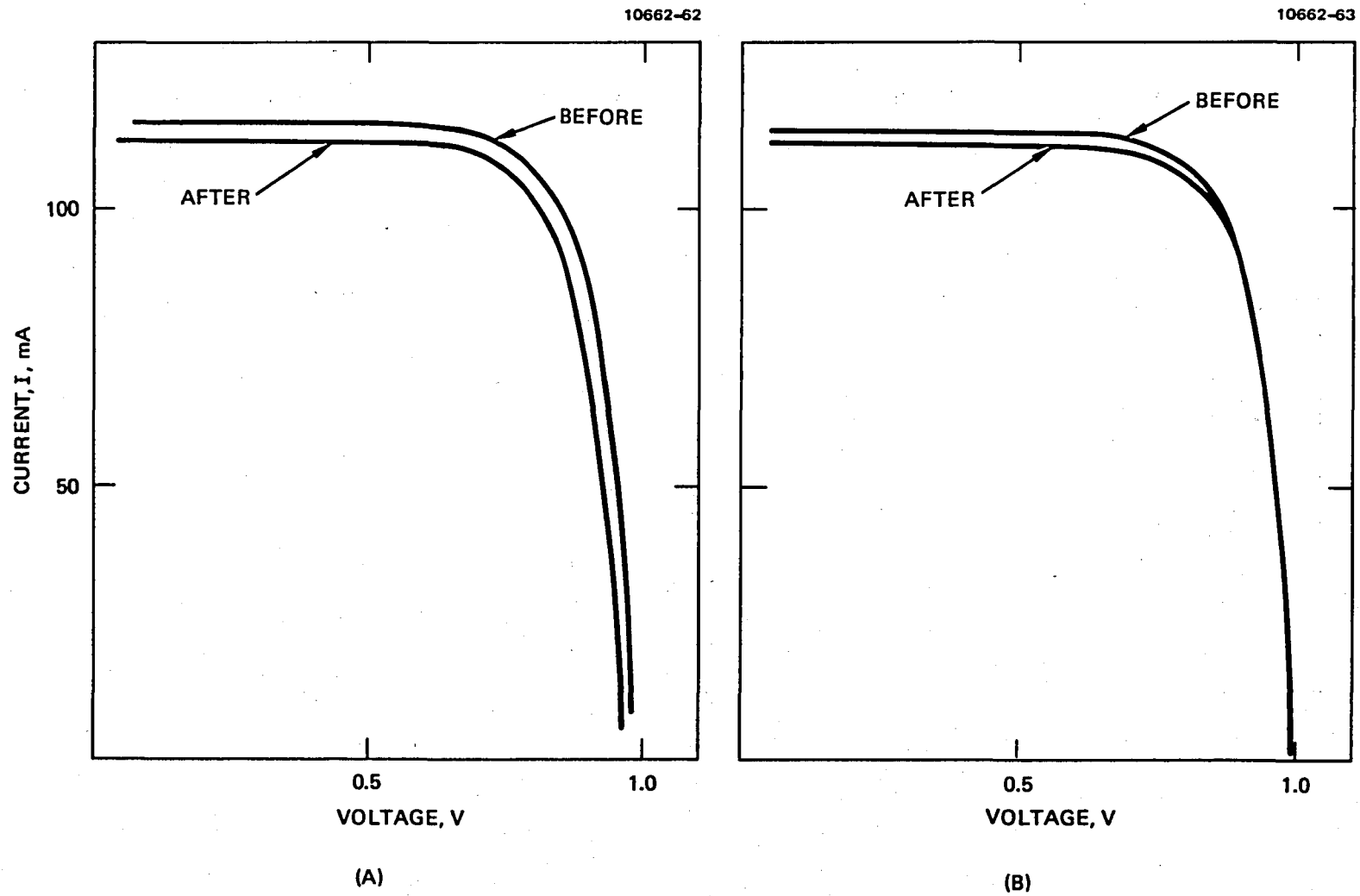
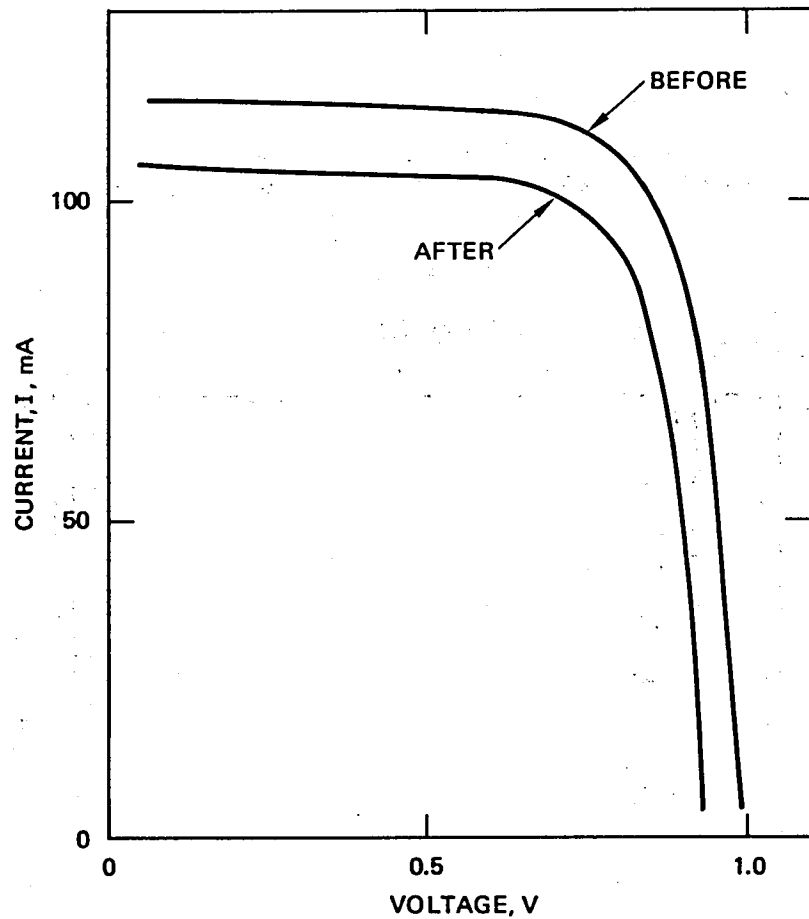


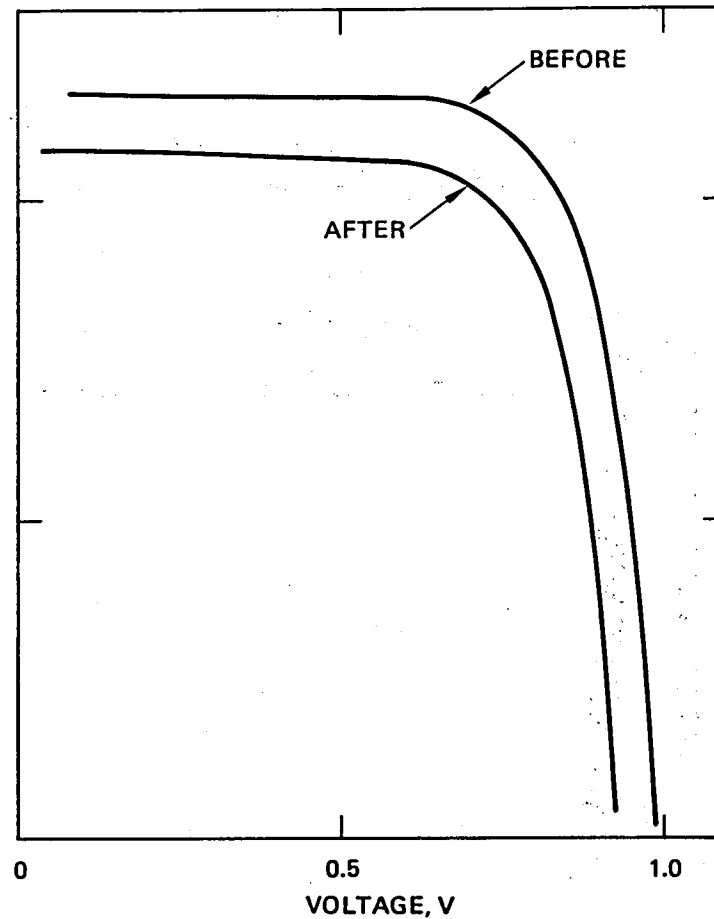
Figure B-2. Photo I-V characteristics before and after $2 \text{ MeV}; 1 \times 10^{10} \text{ p cm}^{-2}$ proton irradiation. (a) Cell 4171, without coverglass; (b) Cell 3890, with coverglass.

10662-64



(A)

10662-65



(B)

Figure B-3. Photo I-V characteristics before and after $2 \text{ MeV}; 1 \times 10^{11} \text{ p cm}^{-2}$ proton irradiation. (a) Cell 4172, without coverglass; (b) Cell 4177, without coverglass.

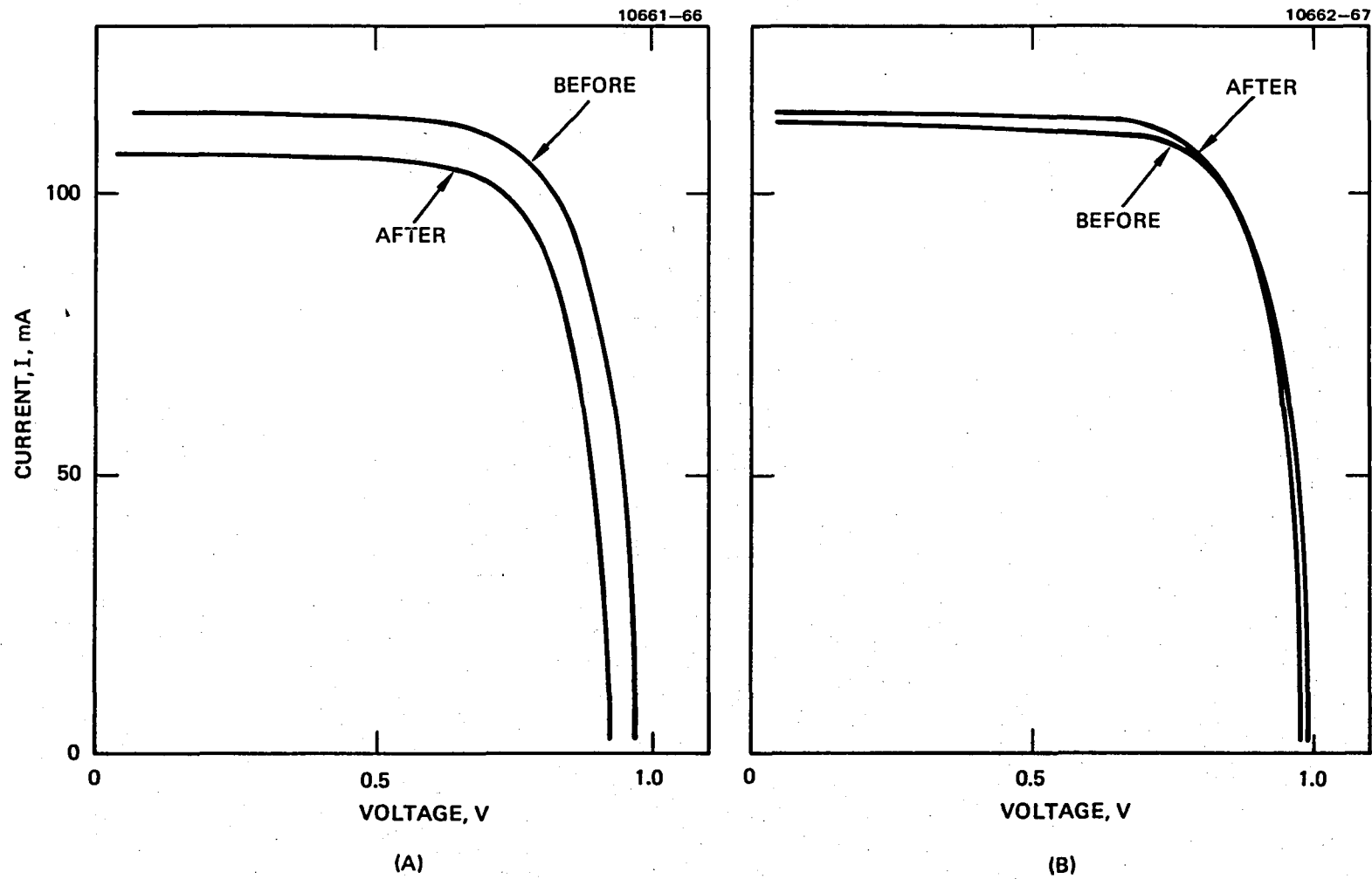


Figure B-4. Photo I-V characteristics before and after 2 MeV; 1×10^{11} p cm⁻² proton irradiation. (a) Cell 4175, without coverglass; (b) Cell 3896, with coverglass.

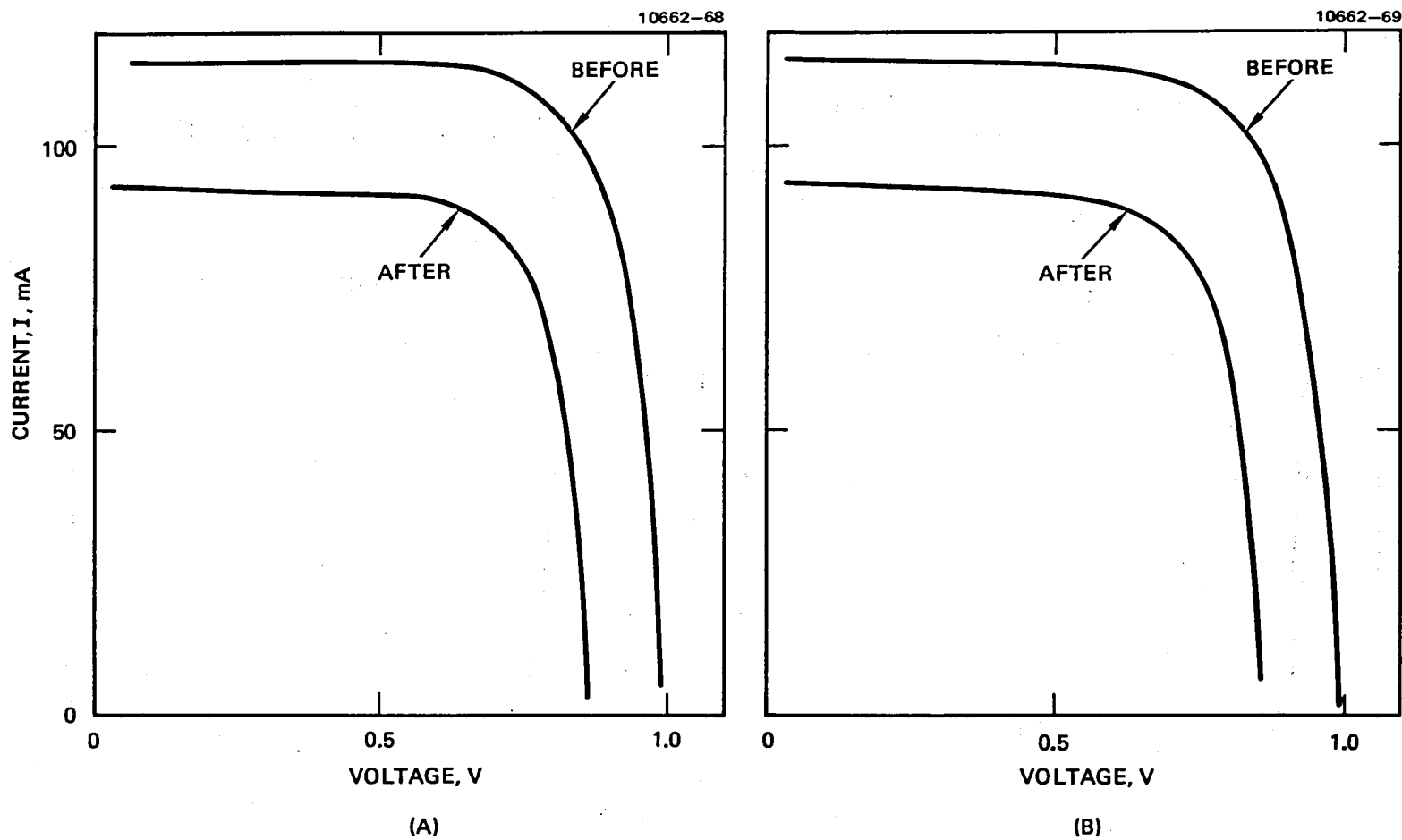


Figure B-5. Photo I-V characteristics before and after $2 \text{ MeV}; 1 \times 10^{12} \text{ p cm}^{-2}$ proton irradiation. (a) Cell 4180, without coverglass; (b) 4190, without coverglass.

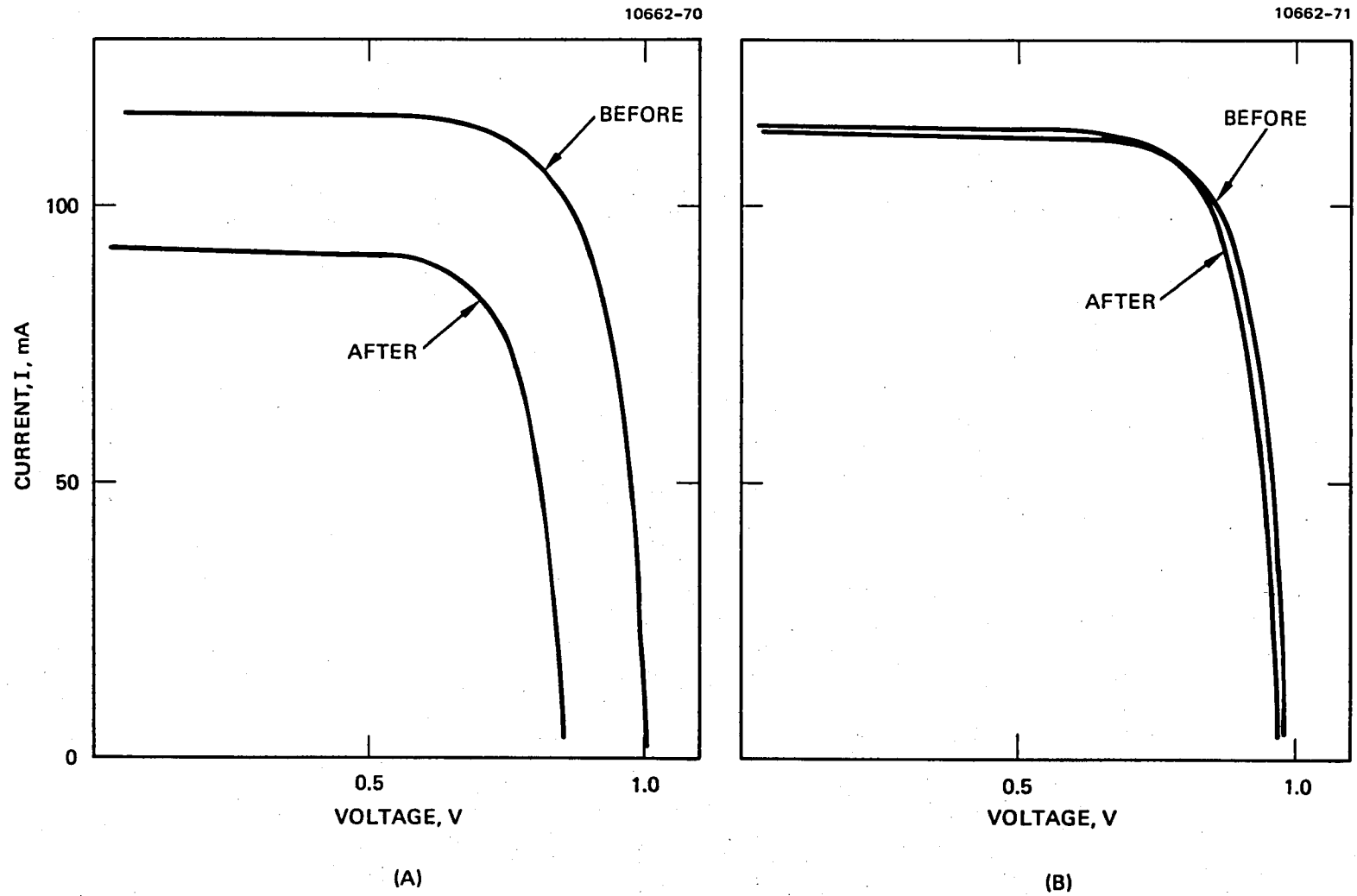


Figure B-6. Photo I-V characteristics before and after $2 \text{ MeV}; 1 \times 10^{12} \text{ p cm}^{-2}$ proton irradiation. (a) Cell 4195, without coverglass, (b) Cell 3892, with coverglass.

10662-72

10662-73

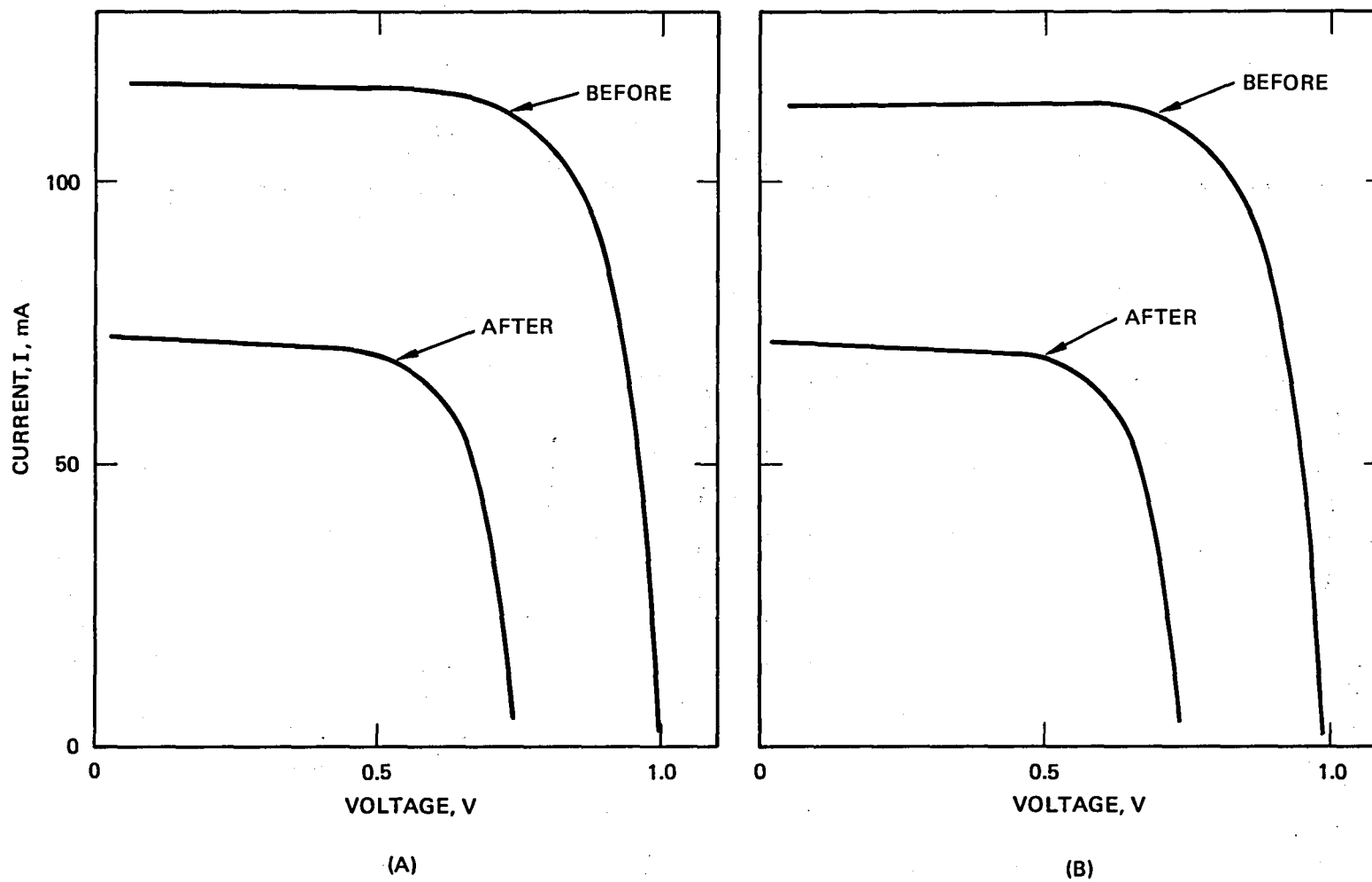


Figure B-7. Photo I-V characteristics before and after $2 \text{ MeV}; 1 \times 10^{13} \text{ p cm}^{-2}$ proton irradiation. (a) Cell 4166, without coverglass, (b) Cell 4207, without coverglass.

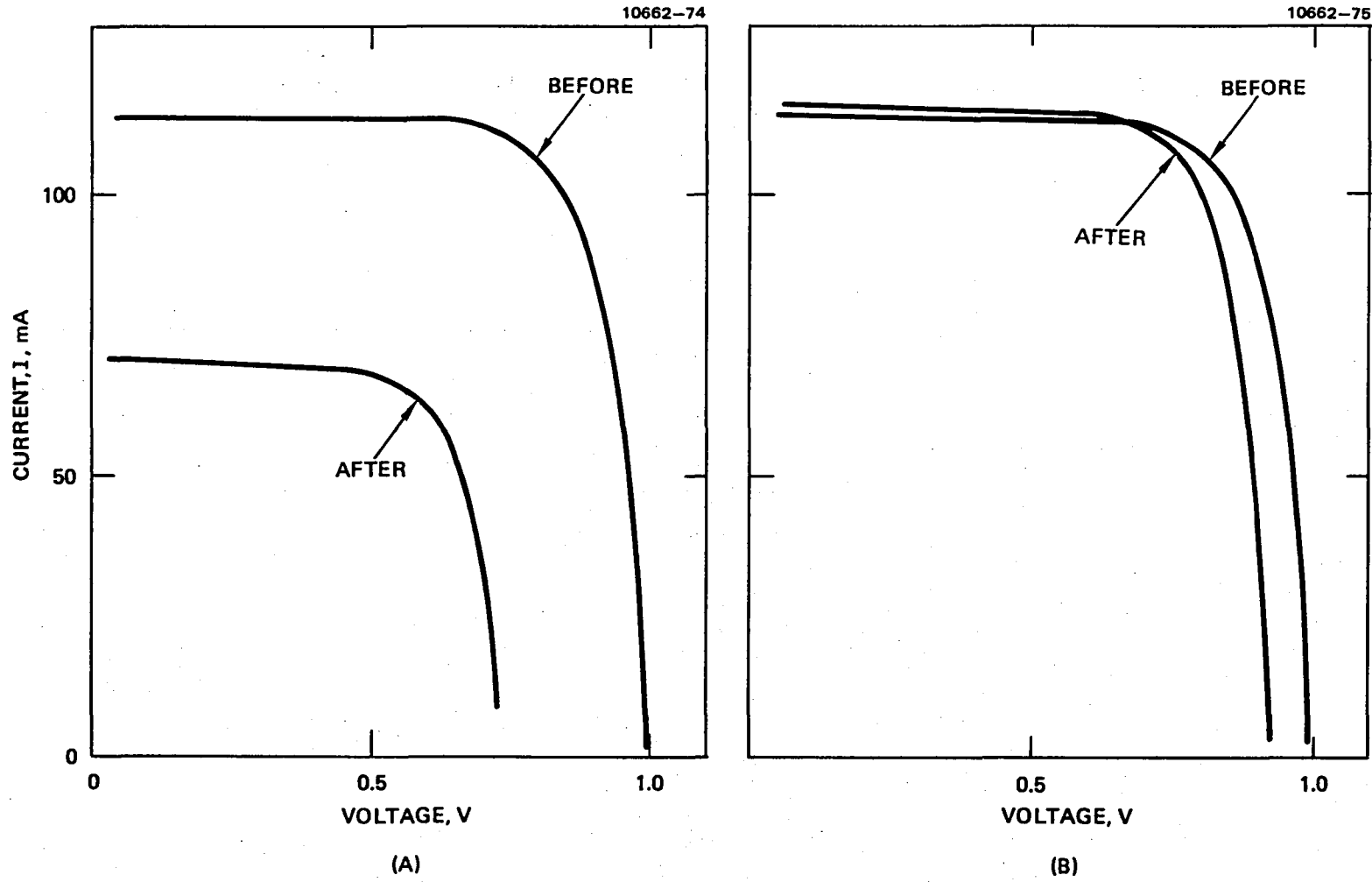


Figure B-8. Photo I-V characteristics before and after $2 \text{ MeV}; 1 \times 10^{13} \text{ p cm}^{-2}$ proton irradiation. (a) Cell 4209, without coverglass, (b) Cell 3893, with coverglass.

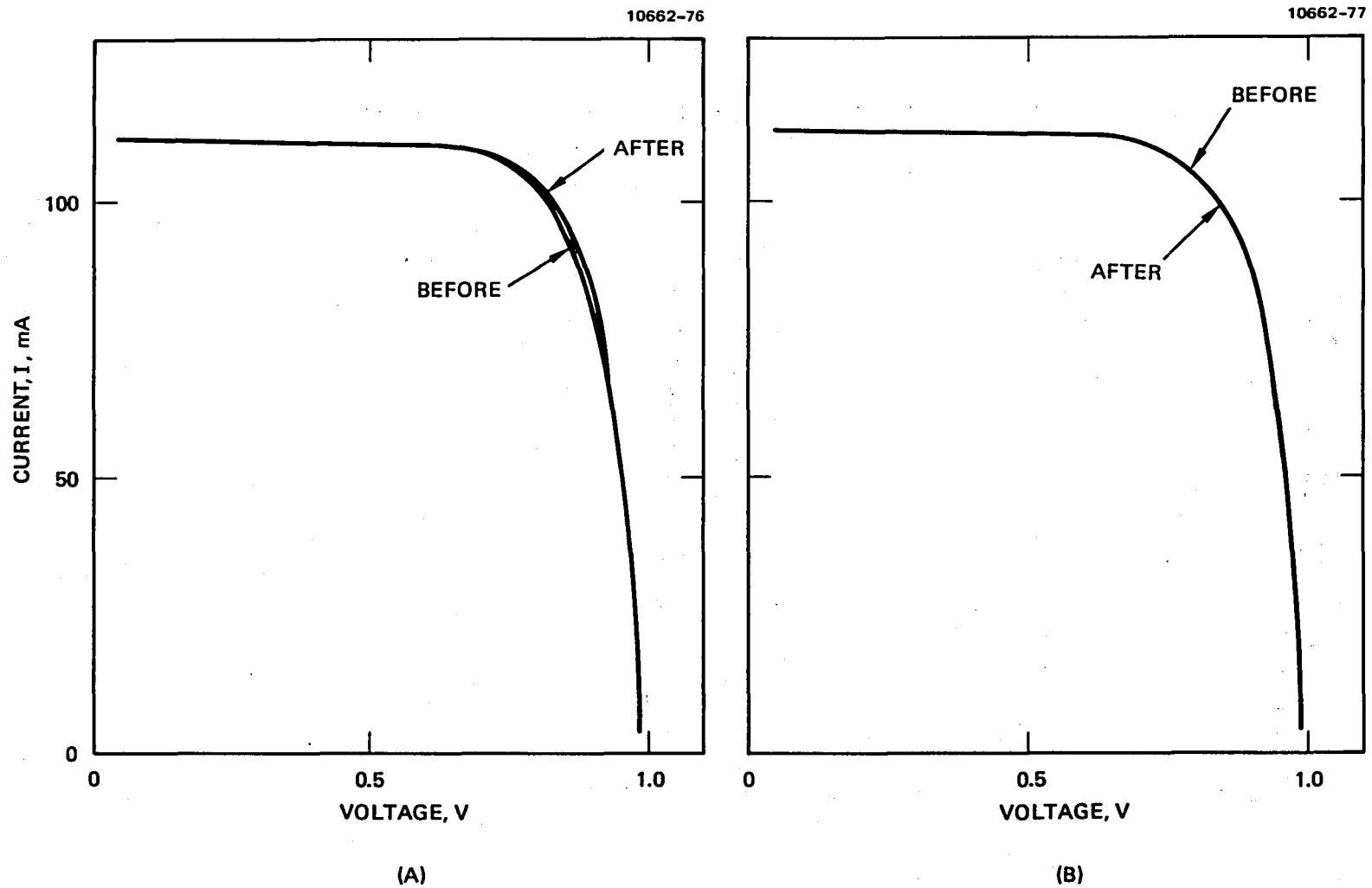


Figure B-9. Photo I-V characteristics before and after 5 MeV; $1 \times 10^{10} \text{ p cm}^{-2}$ proton irradiation. (a) Cell 4093, without coverglass, (b) Cell 4101, without coverglass.

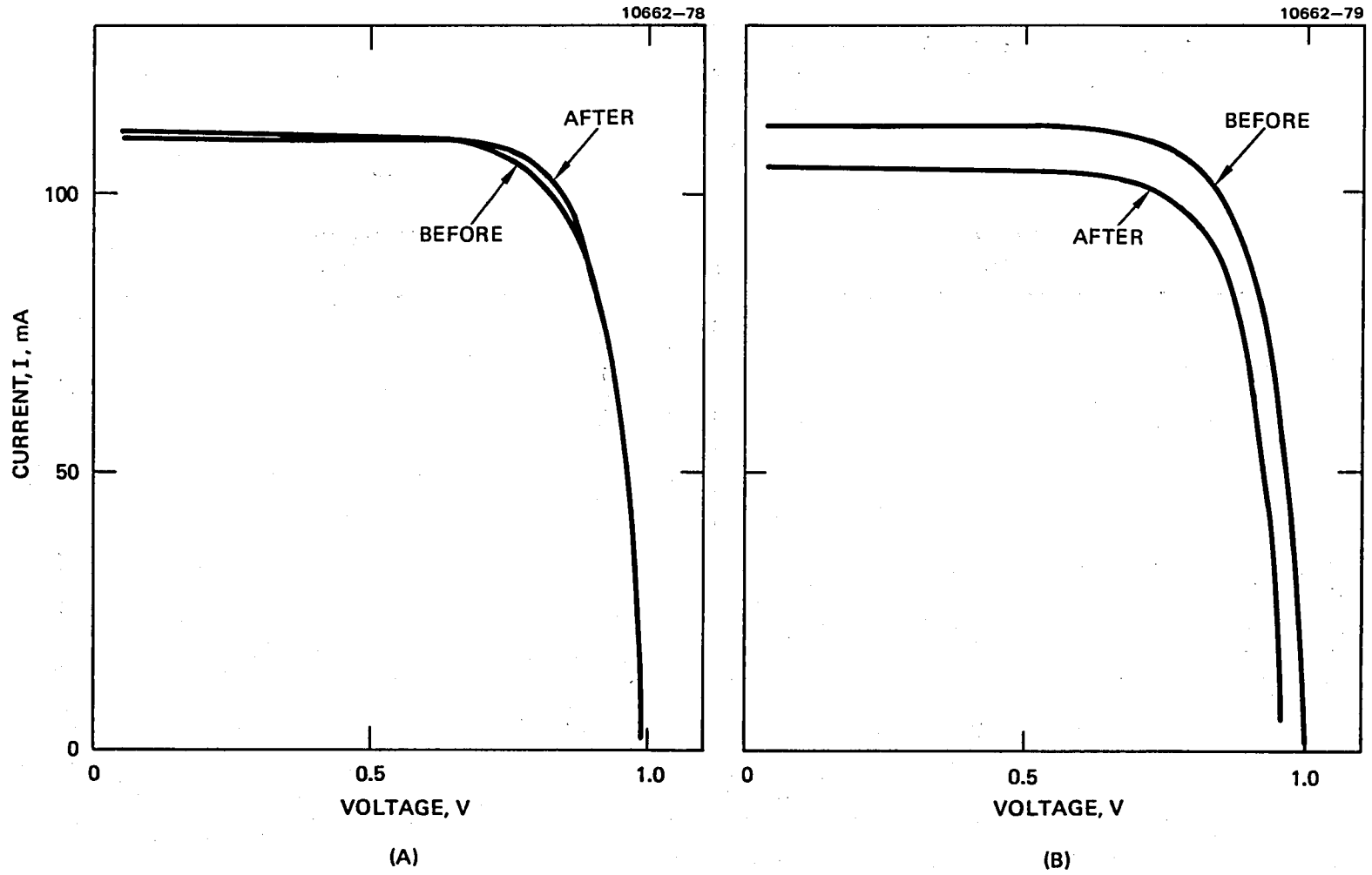


Figure B-10, Photo I-V characteristics before and after $5 \text{ MeV}; 1 \times 10^{10} \text{ p cm}^{-2}$ proton irradiation. (a) Cell 4095, without coverglass, (b) Cell 4033, without coverglass.

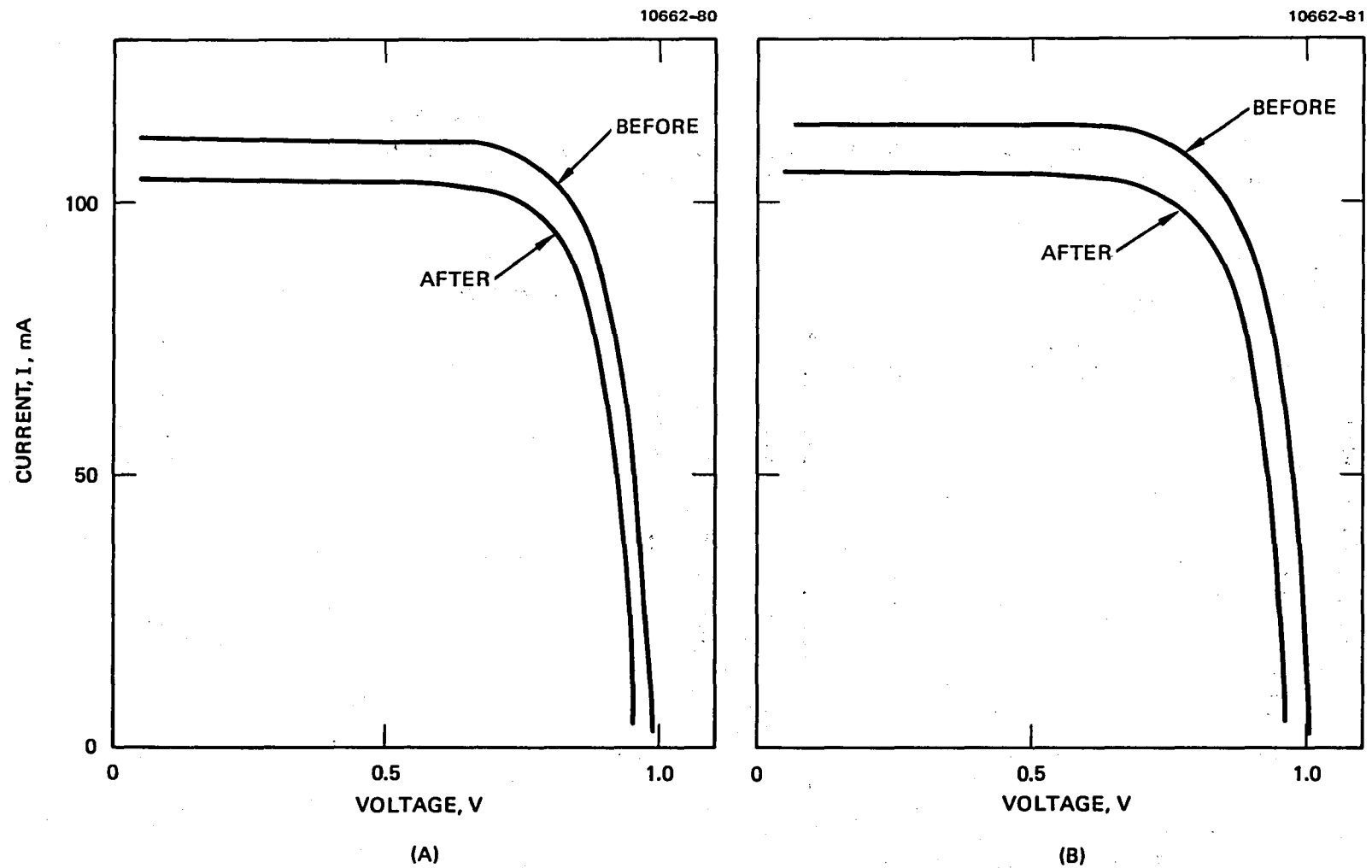


Figure B-11. Photo I-V characteristics before and after $5 \text{ MeV}; 1 \times 10^{11} \text{ p cm}^{-2}$ proton irradiation. (a) Cell 4030, without coverglass, (b) Cell 4035, without coverglass.

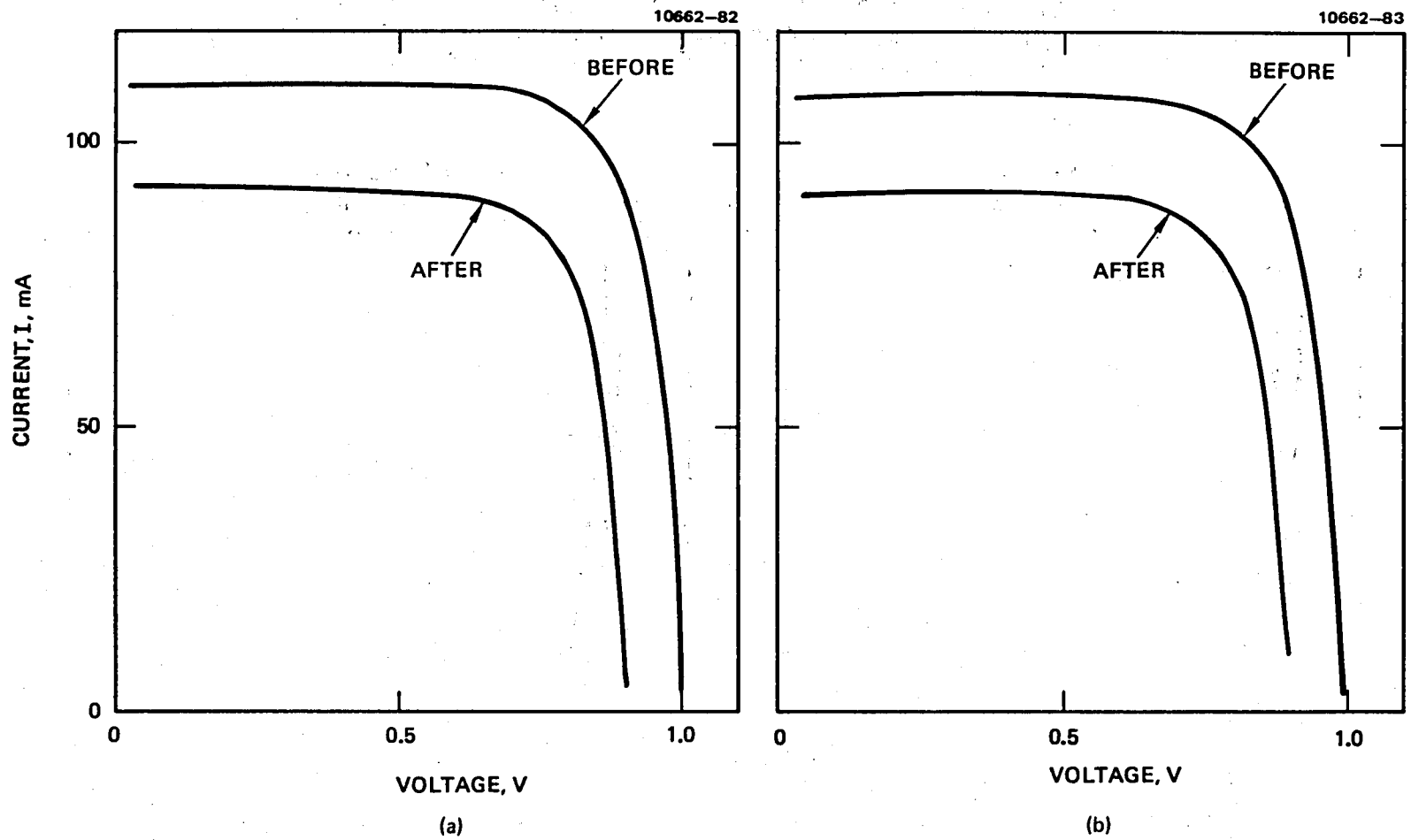


Figure B-12. Photo I-V characteristics before and after $5 \text{ MeV}; 1 \times 10^{12} \text{ p cm}^{-2}$ proton irradiation. (a) Cell 4028, without coverglass, (b) Cell 4029, without coverglass.

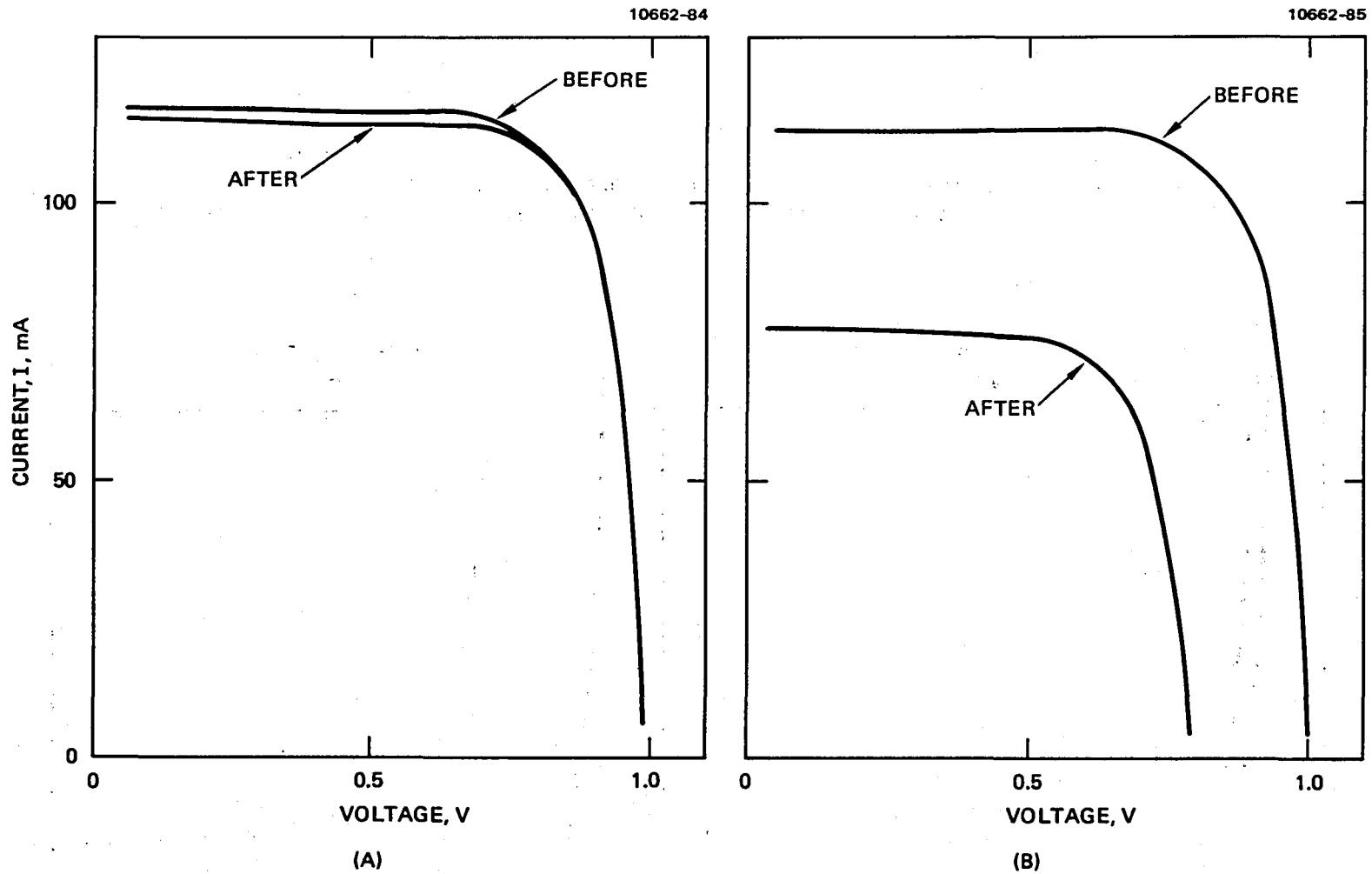


Figure B-13. Photo I-V characteristics before and after $5 \text{ MeV}; 1 \times 10^{12} \text{ p cm}^{-2}$ proton irradiation. (a) Cell 3901, with coverglass, (b) Cell 4006, without coverglass.

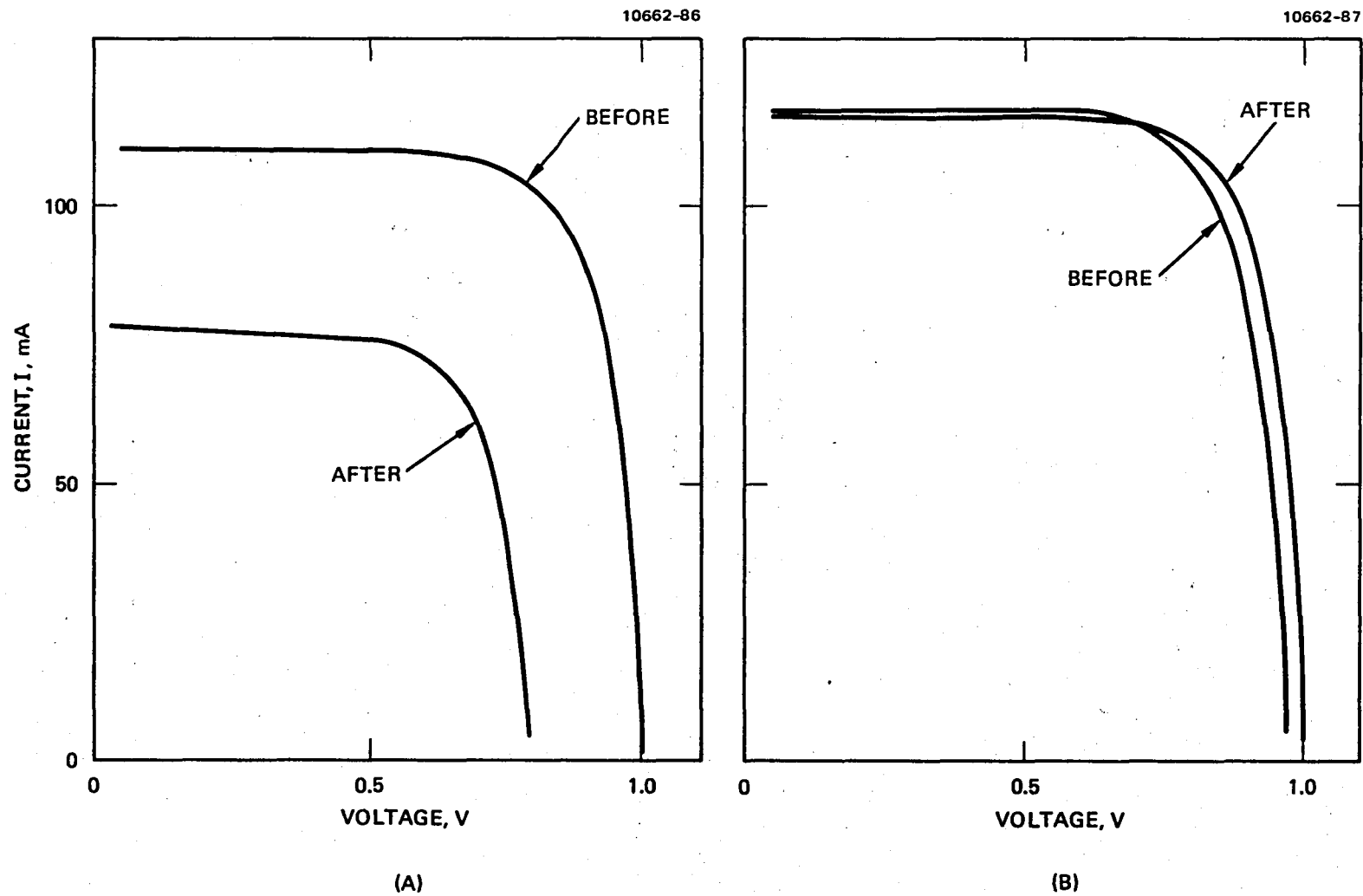


Figure B-14. Photo I-V characteristics before and after $5 \text{ MeV}; 1 \times 10^{13} \text{ p cm}^{-2}$ proton irradiation. (a) Cell 4026, without coverglass, (b) Cell 3990, with coverglass.

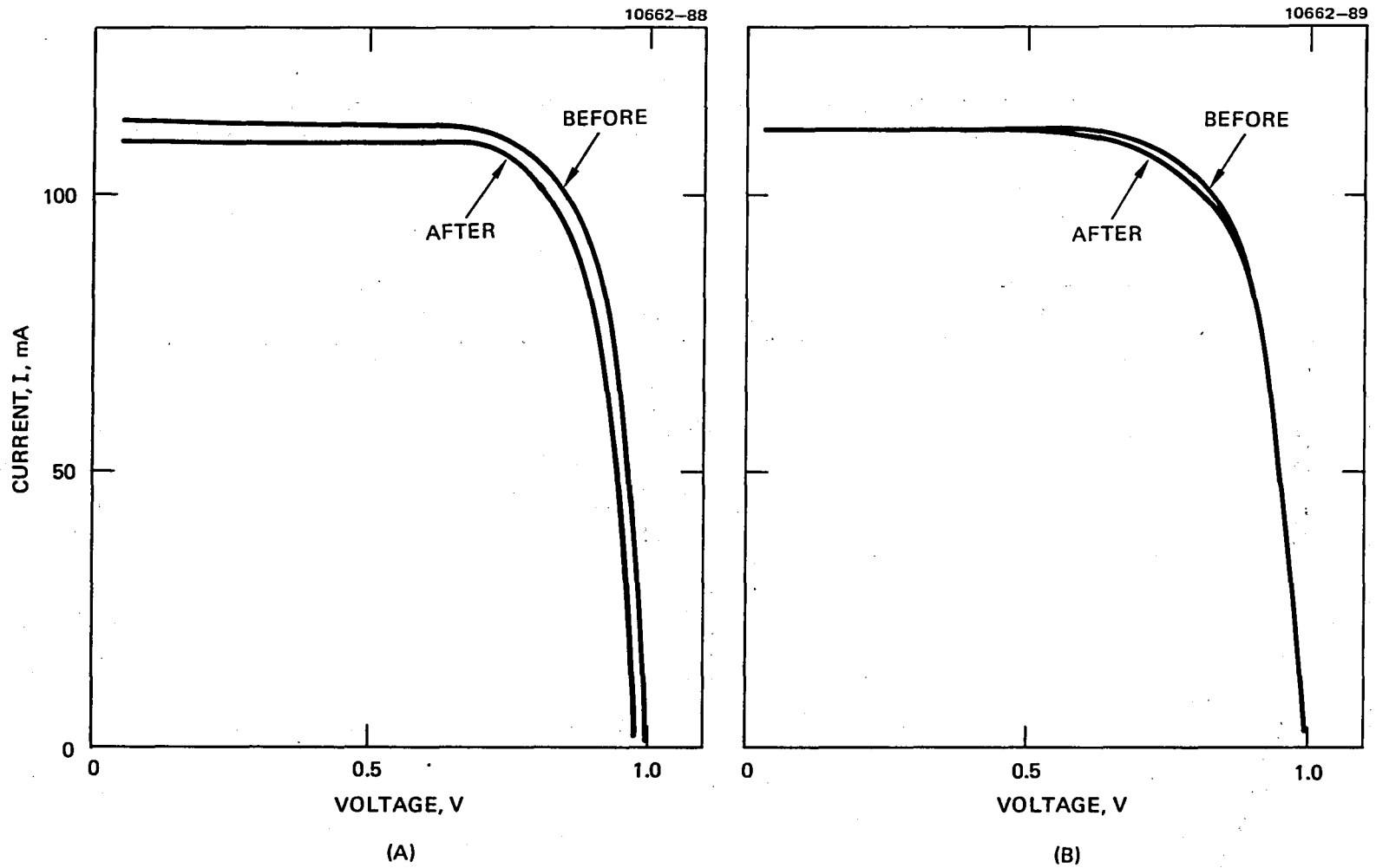
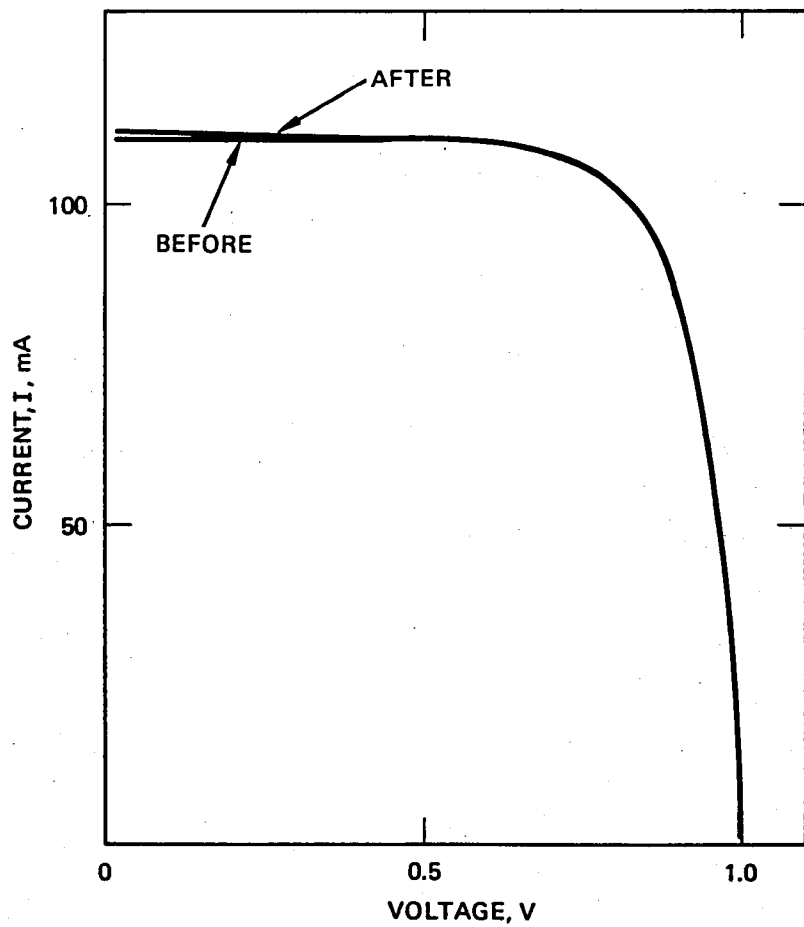


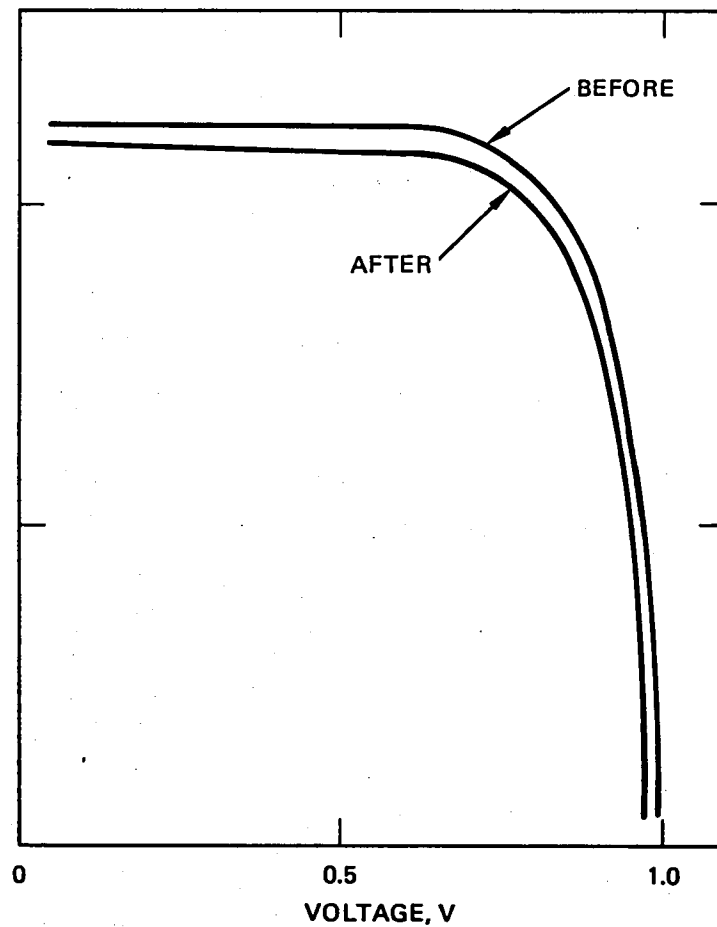
Figure B-15. Photo I-V characteristics before and after $10 \text{ MeV}; 1 \times 10^{10} \text{ p cm}^{-2}$ proton irradiation. (a) Cell 4064, without coverglass, (b) Cell 4068, without coverglass.

10662-90



(A)

10662-91



(B)

Figure B-16. Photo I-V characteristics before and after $10 \text{ MeV}; 1 \times 10^{10} \text{ p cm}^{-2}$ proton irradiation. (a) Cell 4063, without coverglass, (b) Cell 4062, without coverglass.

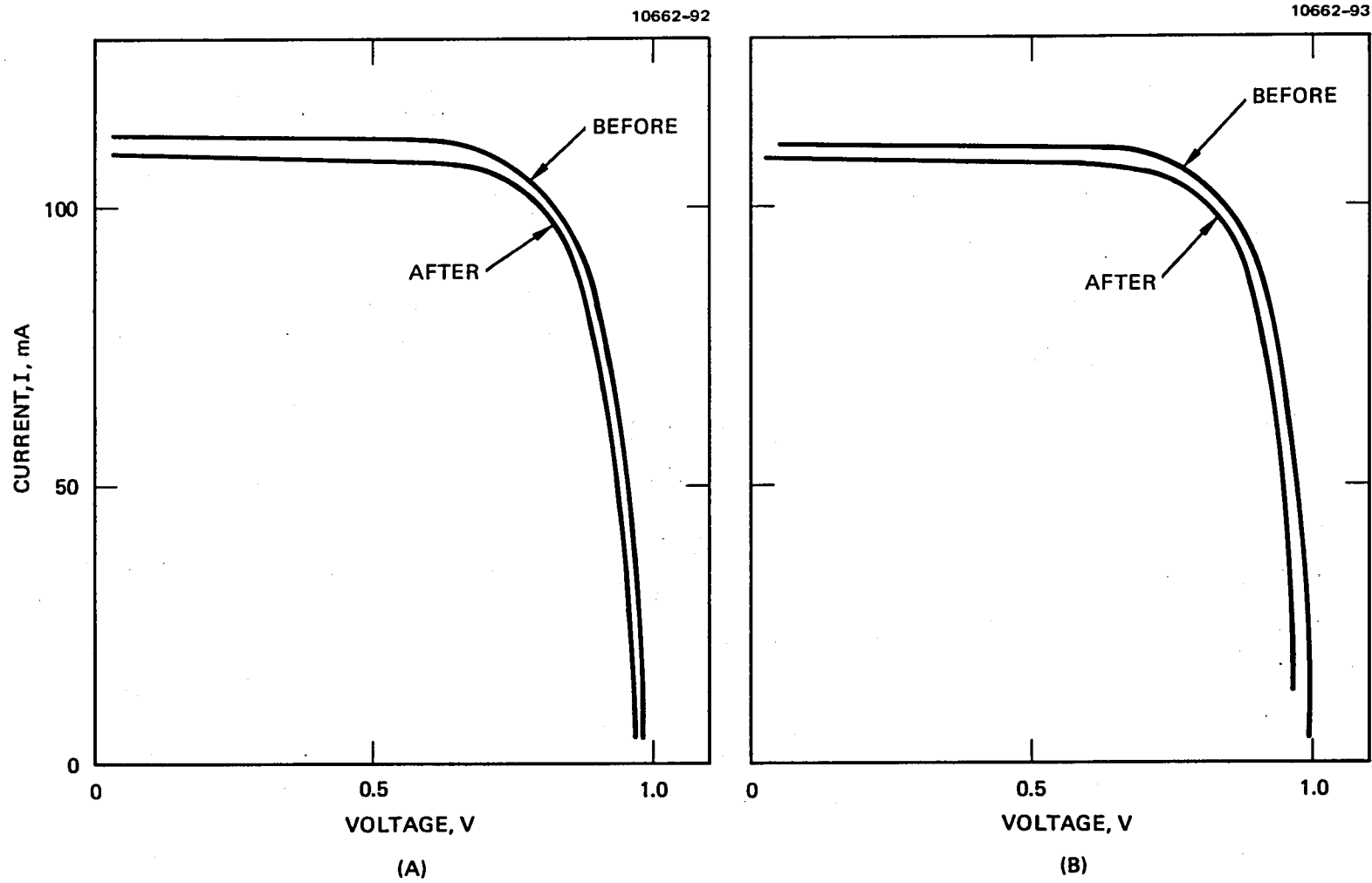


Figure B-17. Photo I-V characteristics before and after $10 \text{ MeV}; 1 \times 10^{11} \text{ p cm}^{-2}$ proton irradiation. (a) Cell 4109, without coverglass, (b) Cell 4113, without coverglass.

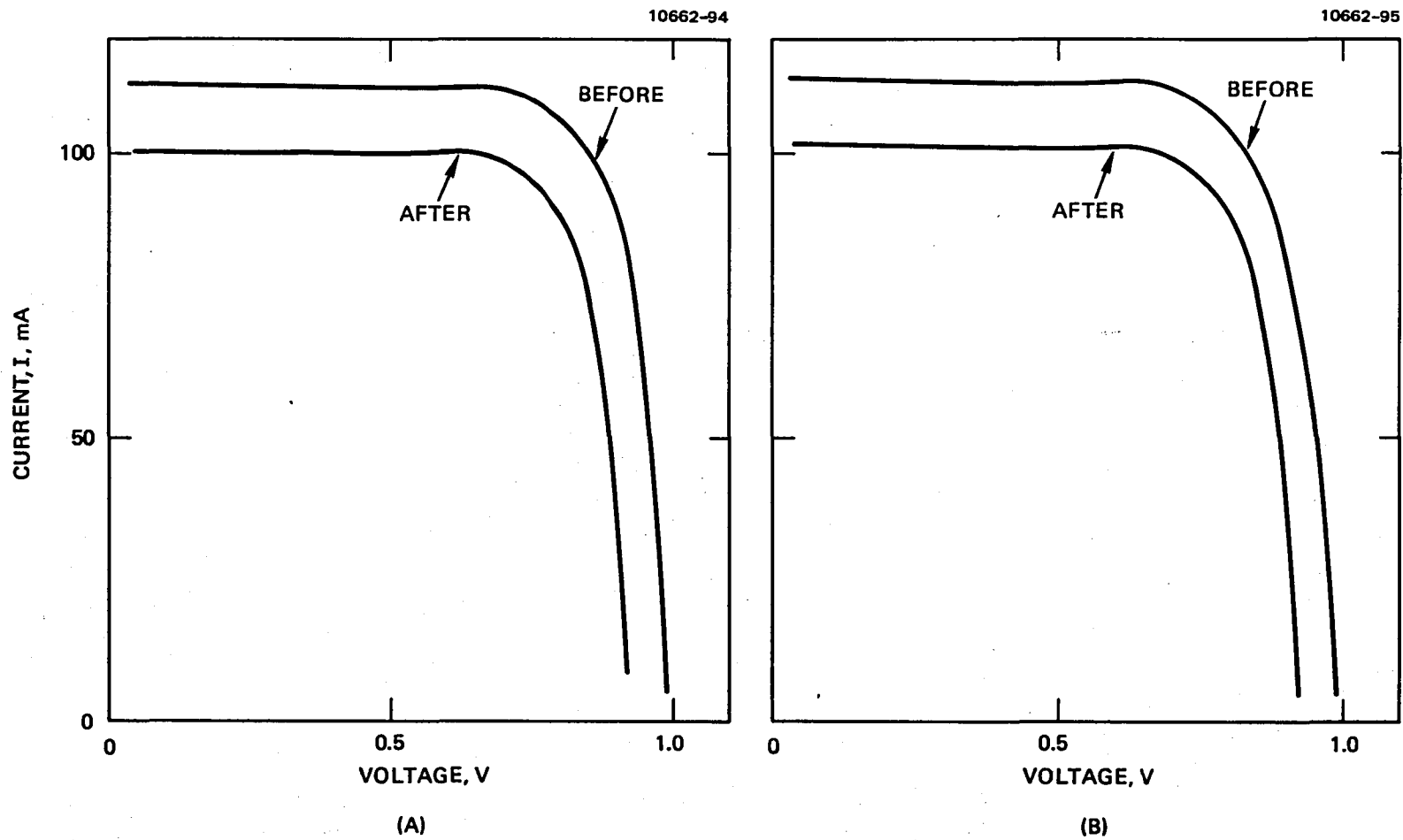


Figure B-18. Photo I-V characteristics before and after $10 \text{ MeV}; 1 \times 10^{12} \text{ p cm}^{-2}$ proton irradiation. (a) Cell 4105, without coverglass; (b) Cell 4106, without coverglass.

7662-96

10662-97

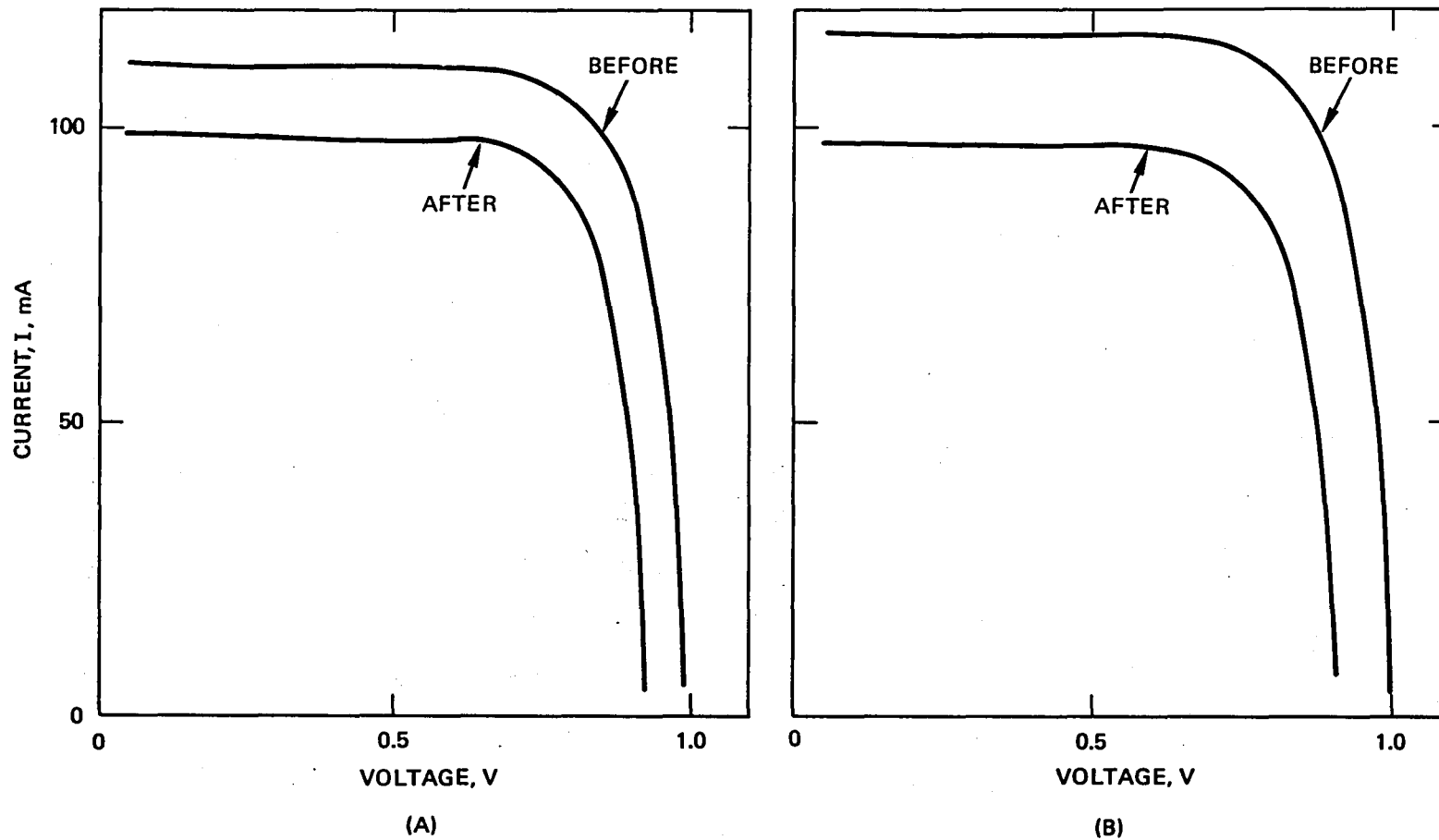


Figure B-19. Photo I-V characteristics before and after $10 \text{ MeV}; 1 \times 10^{12} \text{ p cm}^{-2}$ proton irradiation. (a) Cell 4107, without coverglass; (b) Cell 3988, with coverglass.

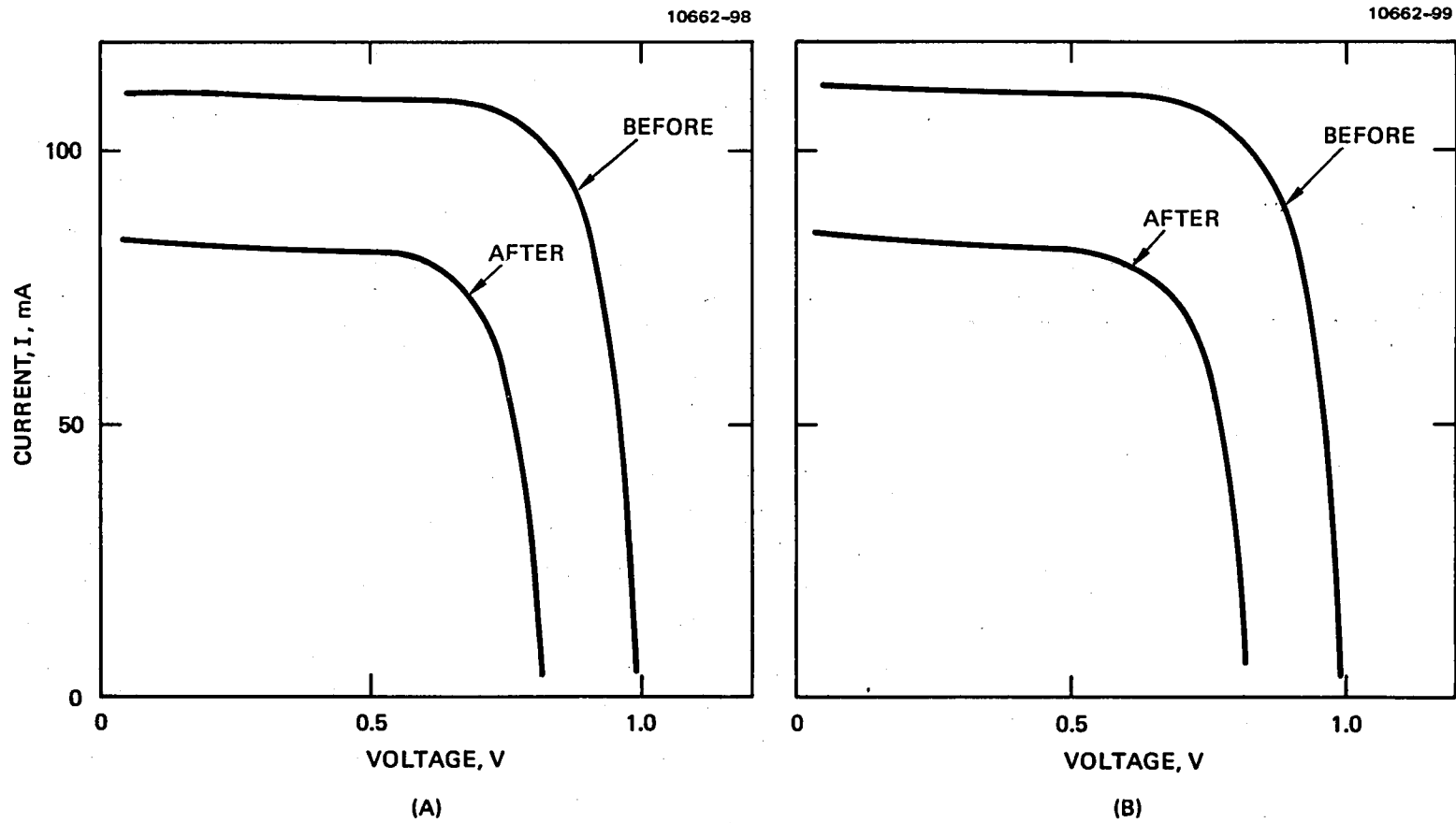


Figure B-20. Photo I-V characteristics before and after 10 MeV; 1×10^{13} p cm⁻² proton irradiation. (a) Cell 4104, without coverglass; (b) Cell 4102, without coverglass.

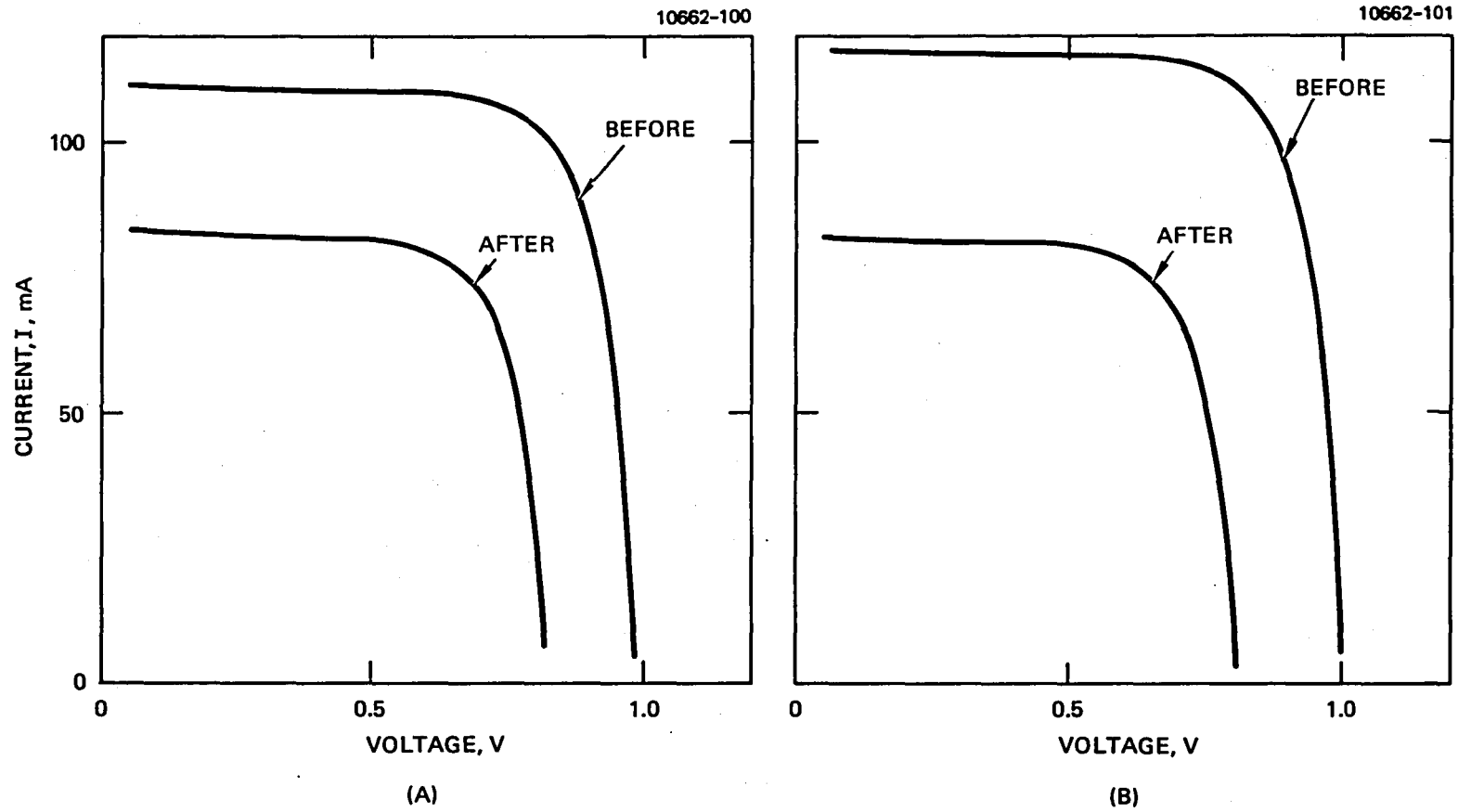


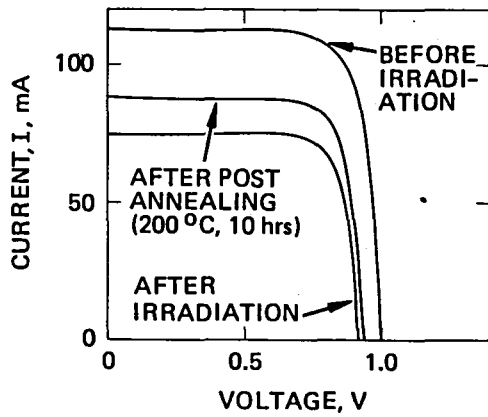
Figure B-21. Photo I-V characteristics before and after 10 MeV; 1×10^{13} p cm⁻² proton irradiation. (a) Cell 4103, without coverglass; (b) Cell 3992, with coverglass.

This Page Intentionally Left Blank

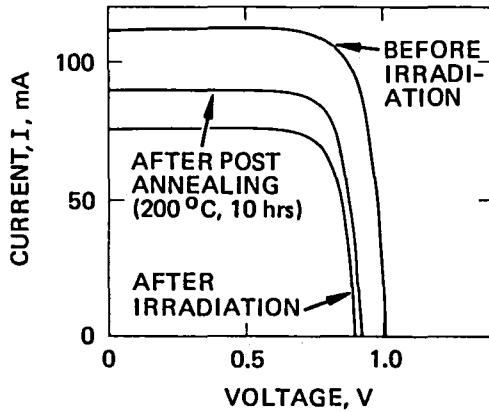
APPENDIX C

PHOTO I-V CHARACTERISTICS OF (AlGa)As GaAs SOLAR CELLS BEFORE AND AFTER A
CONTINUOUS ANNEALING EXPERIMENT AT 200°C

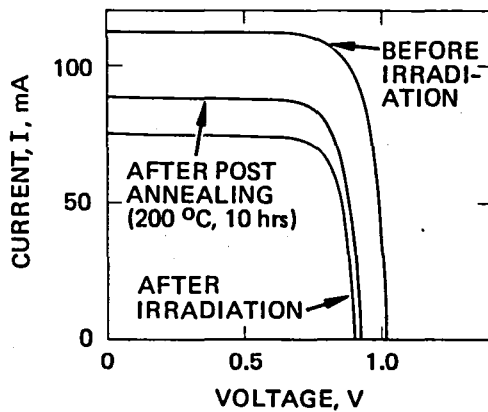
This Page Intentionally Left Blank



a. CELL NO. 7743



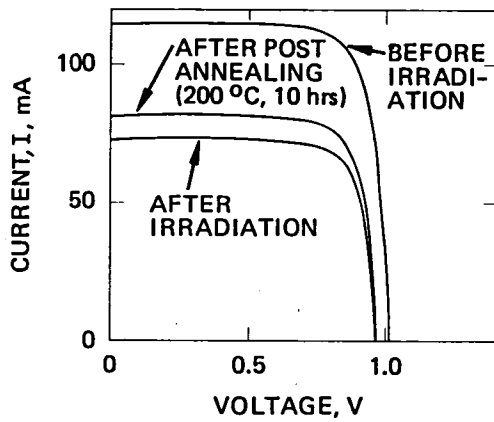
b. CELL NO. 7744



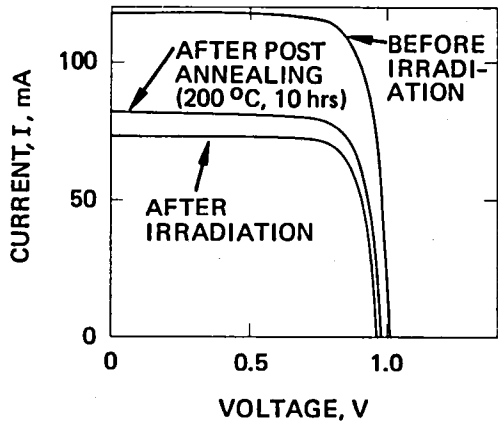
c. CELL NO. 7746

Figure C-1.

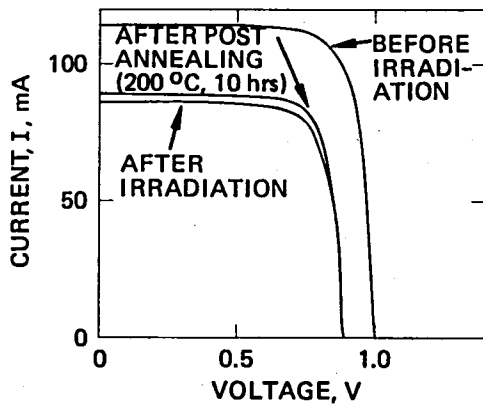
Photo I-V characteristics before and after 200 keV proton; $1 \times 10^{11} \text{ p cm}^{-2}$ at 25°C at a flux of $1 \times 10^{10} \text{ p cm}^{-2} \text{ hr}^{-1}$ (total irradiation time = 10 hrs), and after post annealing at 200°C for 10 hr. (cell Nos. 7743, 7744, 7746)).



a. CELL NO. 7755

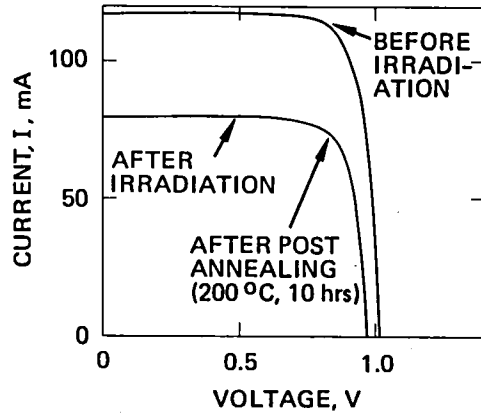


b. CELL NO. 7756

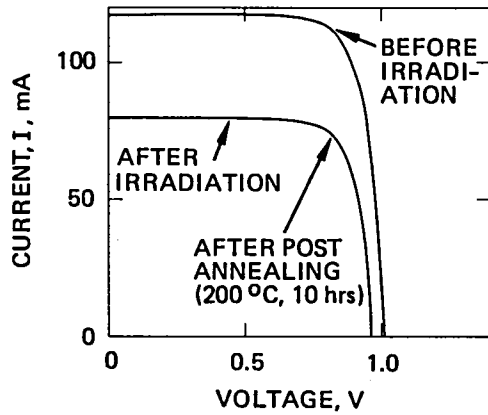


c. CELL NO. 7742

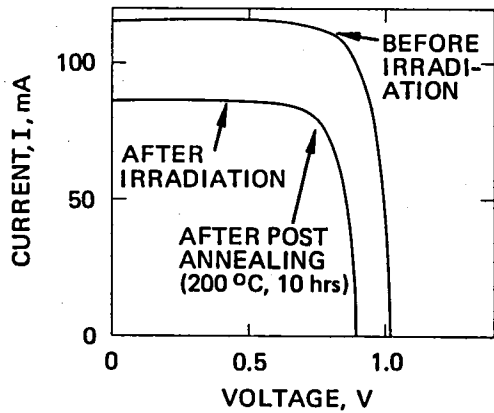
Figure C-2.
Photo I-V characteristics before and after 200 keV proton; $1 \times 10^{11} \text{ p cm}^{-2}$ 200°C at a flux of $1 \times 10^{11} \text{ p cm}^{-2} \text{ hr}^{-1}$ (total irradiation time = 1 hr), and after post annealing at 200°C for 10 hr. (Cell Nos. 7755, 7756, and 7742).



a. CELL NO. 7757



b. CELL NO. 7758



c. CELL NO. 7814

Figure C-3.

Photo I-V characteristics before and after 200 keV proton; $1 \times 10^{11} \text{ p cm}^{-2}$ at 200°C at a flux of $1 \times 10^{10} \text{ p cm}^{-2} \text{ hr}^{-1}$ (total irradiation time = 10 hr), and after post annealing at 200°C for 10 hr. (Cell Nos. 7757, 7758, and 7814).

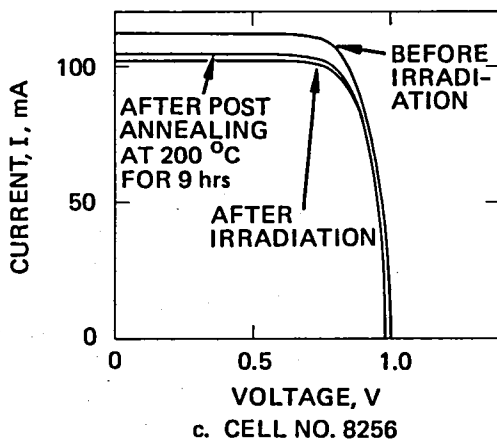
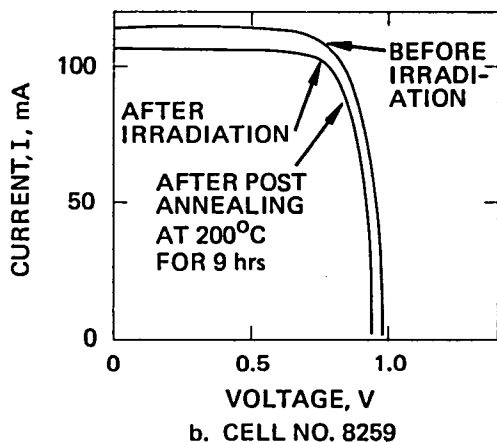
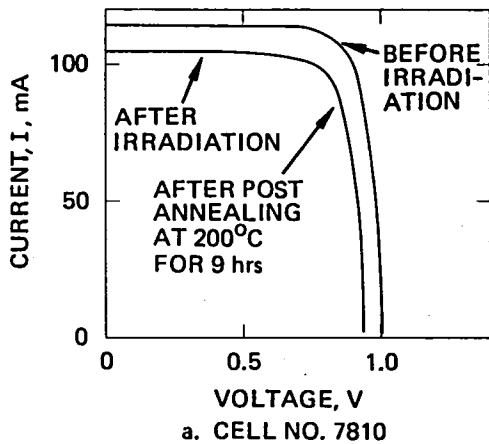
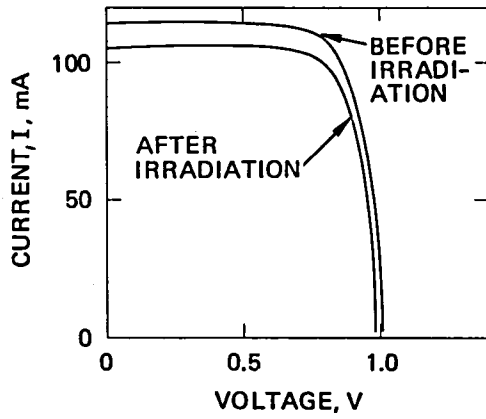
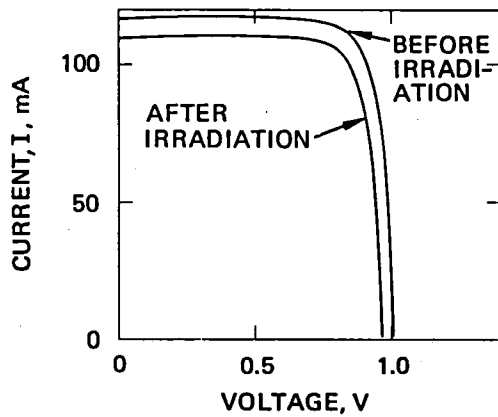


Figure C-4.

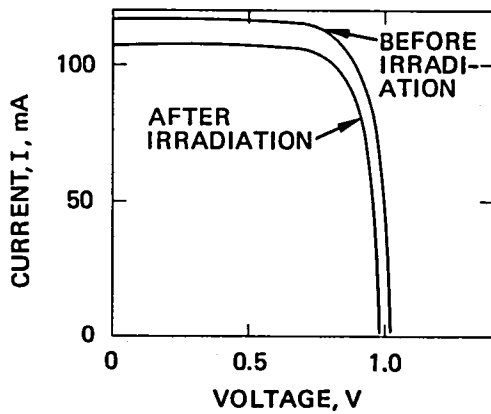
Photo I-V characteristics before and after 200 keV proton; $1 \times 10^{10} \text{ p cm}^{-2}$ continuous annealing experiment at 200°C at a flux of $1 \times 10^{10} \text{ p cm}^{-2} \text{ hr}^{-1}$, and after post annealing at 200°C for 10 hr. (Cell Nos. 7810, 8259, and 8256). (In this experiment, the cells were irradiated to a fluence of $1 \times 10^9 \text{ p cm}^{-2}$ and then subsequently annealed for an hour at 200°C . This process was repeated ten times until the final fluence was cumulated to $1 \times 10^{10} \text{ p cm}^{-2}$).



a. CELL NO. 8258



b. CELL NO. 7869



c. CELL NO. 7831

Figure C-5.

Photo I-V characteristics before and after 200 keV proton; $1 \times 10^{10} \text{ p cm}^{-2}$ at 200°C at a flux of $1 \times 10^{10} \text{ p cm}^{-2} \text{ hr}^{-1}$ (total irradiation time = 0.1 hr), and after post annealing at 200°C for 9 hr. (Cell Nos. 8258, 7869, and 7831).

This Page Intentionally Left Blank

NASA Contractor Report 165946
Distribution List
NASI-15926

	No. Copies
NASA Langley Research Center Hampton, VA 23665 Attn: Report and Manuscript Control Office, M/S 180A Gilbert H. Walker, M/S 160	1 25
NASA Ames Research Center Moffett Field, CA 94035 Attn: Library, Mail Stop 202-3	1
NASA Dryden Flight Research Center P. O. Box 273 Edwards, CA 93523 Attn: Library	1
NASA Goddard Space Flight Center Greenbelt, MD 20771 Attn: Library	1
NASA Lyndon B. Johnson Space Center 2101 Webster Seabrook Road Houston, TX 77058 Attn: JM6/Library	1
NASA Marshall Space Flight Center Marshall Space Flight Center, AL 35812 Attn: Library, AS24L	1
Jet Propulsion Laboratory 4800 Oak Grove Drive Pasadena, CA 91103 Attn: Library, Mail Code 111-113	1
NASA Lewis Research Center 21000 Brookpark Road Cleveland, OH 44135 Attn: Library, Mail Stop 60-3	1
NASA John F. Kennedy Space Center Kennedy Space Center, FL 32899 Attn: Library, NWSI-D	1
Scientific and Technical Information Facility 6571 Elkridge Landing Road Linthicum Heights, MD 21090	21 + original

Dr. John Goldsmith
Solarex Corporation
1335 Piccard Drive
Rockville, MD 20850

Dr. Leonard Magid
Department of Energy
600 E Street, NW
Washington, DC 20585

Dr. Harold J. Hovel
IBM Corporation
P.O. Box 218
Yorktown Heights, NY 10593

Dr. Andrew Meulenberg
COMSAT Laboratories
22300 Comsat Drive
Clarksburg, MD 20734

Dr. James A. Hutchby
RTI
P.O. Box 12194
Res Triangle Park, NC 27709

Dr. Arthur G. Milnes
Carnegie Mellon University
Schenley Park
Pittsburg, PA 15213

Mr. Peter A. Illes
Applied Solar Energy Corporation
15251 E. Don Julian Road
City of Industry, CA 91746

Dr. Morton B. Prince
Department of Energy
1000 Independence Avenue, SW
Washington, DC 20585

Mr. Gerald E. Jellison
Oak Ridge National Laboratory
Oak Ridge, TN 37830

Dr. David Redfield
RCA Laboratories
Princeton, NJ 08540

Dr. Sheng S. Li
227 Benton Hall
University of Florida
Gainesville, FL 32611

Dr. Ralph P. Ruth
Consultant
5242 Wendover Road
Yorba Linda, CA 92686

Dr. Fredrik A. Lindholm
216 Larsen Hall
University of Florida
Gainesville, FL 32611

Dr. C. T. Sah
University of Illinois
403 Pond Ridge Lane
Urbana, IL 61801

Dr. Joseph J. Loferski
Division of Engineering
Brown University
Providence, RI 02912

Mr. Eugene L. Ralph
Spectrolab, Inc.
12500 Gladstone Avenue
Sylmar, CA 91342

Dr. Bruce E. Anspaugh
Mail Stop 183B-167
Jet Propulsion Laboratory
4800 Oak Grove Drive
Pasadena, CA 91109

Dr. David E. Carlson
RCA Corporation
514 Nancy Road
Yardley, PA 19067

Dr. Charles E. Backus
College of Engineering and Applied
Science
Arizona State University
Tempe, AZ 85281

Mr. Larry D. Chidester
Mail Code 6216/151
Lockheed Missile and Space Company
1111 Lockheed Way
Sunnyvale, CA 94086

Dr. Richard Blieden
Tosco Corporation
10100 Santa Monica Boulevard
Los Angeles, CA 90067

Dr. Henry B. Curtis
Mail Stop 302-1
NASA Lewis Research Center
21000 Brookpark Road
Cleveland, OH 44135

Dr. Peter G. Borden
Varian Associates
Mail Stop K-115
611 Hansen Way
Palo Alto, CA 94303

Dr. Alan L. Fahrenbruch
Department of Materials Science and
Engineering
Stanford University
Stanford, CA 94305

Dr. Jose M. Borrego
Ecse Department JEC-7020
Rensselaer Polytechnic Institute
Troy, NY 12181

Dr. John C. Fan
MIT Lincoln Laboratory
244 Wood Street
Lexington, MA 02173

Dr. Henry W. Brandhorst, Jr.
Mail Stop 302-1
NASA Lewis Research Center
21000 Brookpark Road
Cleveland, OH 44135

Mr. Americo F. Forestieri
Mail Stop 302-1
NASA Lewis Research Center
21000 Brookpark Road
Cleveland, OH 44135

Mr. Donald Briggs
Mail Stop G31
Ford Aerospace Communications Corp.
3939 Fabian Way
Palo Alto, CA 94303

Dr. Donald L. Feucht
Solar Energy Research Institute
1617 Cole Boulevard
Golden, CO 80401

Dr. Richard H. Bube
Department of Materials Science and
Engineering
Stanford University
Stanford, CA 94305

Dr. Peter Glaser
Arthur D. Little, Inc.
Acorn Park
Cambridge, MA 02140

Dr. Lynwood P. Randolph
Code RTS-6
National Aeronautics and Space
Administration
Washington, DC 20546

Dr. Irving Weinberg
Mail Stop 302-1
NASA Lewis Research Center
21000 Brookpark Road
Cleveland, OH 44135

Mr. Richard L. Statler
Naval Research Laboratory
Code 6612
Washington, DC 20375

Mr. Joseph F. Wise
Air Force Aeropropulsion Laboratory
AFWAL/POOC
Wright-Patterson AFB, OH 45433

Dr. Elias K. Stefanakos
Electrical Engineering Department
North Carolina A&T State University
Greensboro, NC 27411

Dr. Martin Wolf
Dept. of Electrical Engineering
308 Moore Hall
University of Pennsylvania
Philadelphia, PA 19104

Dr. Richard J. Stirn
Mail Stop 512-103
Jet Propulsion Laboratory
4800 Oak Grove Drive
Pasadena, CA 91109

Dr. Stanley W. Zehr
Rockwell International
P.O. Box 1085
Thousand Oaks, CA 91360

Dr. George M. Storti
Solarex Corporation
1335 Piccard Drive
Rockville, MD 20850

Dr. Solomon Zwerdling
Mail Stop 512-103
Jet Propulsion Laboratory
4800 Oak Grove Drive
Pasadena, CA 91109

Dr. Thomas Surek
Solar Energy Research Institute
1617 Cole Boulevard
Golden, CO 80401

Mr. John A. Scott-Monck
Mail Stop 125-231
Jet Propulsion Laboratory
4800 Oak Grove Drive
Pasadena, CA 91109

Dr. D. K. Wagner
420 Phillips Hall
Cornell University
Ithaca, NY 14853

1. Report No. NASA-CR-165946		2. Government Accession No.		3. Recipient's Catalog No.	
4. Title and Subtitle MEDIUM ENERGY PROTON RADIATION DAMAGE TO (AlGa)As-GaAs SOLAR CELLS				5. Report Date JULY 1982	
				6. Performing Organization Code	
7. Author(s) R.Y. Loo, G.S. Kamath, and R.C. Knechtli				8. Performing Organization Report No.	
				10. Work Unit No.	
9. Performing Organization Name and Address Hughes Research Laboratories 3011 Malibu Canyon Road Malibu, California 90265				11. Contract or Grant No. NAS1-15926	
				13. Type of Report and Period Covered Contractor Report 8 Aug 1979 - 1 May 1982	
12. Sponsoring Agency Name and Address National Aeronautics and Space Administration Washington, DC 20546				14. Sponsoring Agency Code	
15. Supplementary Notes Langley Technical Monitor - Gilbert H. Walker Final Report					
16. Abstract <p>In the first phase of this contract we evaluated the performance of (AlGa)As-GaAs solar cells irradiated by medium energy 2, 5, and 10 MeV protons. This study, together with our previous work on low-energy (50 to 300 keV) and high-energy (15 to 40 MeV) proton irradiation, form a solid foundation for a thorough evaluation of the suitability of these cells for space missions. In all these studies, both the Si cells without coverglass and a number of GaAs solar cells with 12 mil coverglass were irradiated simultaneously with our bare GaAs cells. The key observation is that the cell degradation is directly related to the penetration of depth of protons with GaAs. The GaAs solar cells are superior in radiation hardness to Si solar cells at all proton energies higher than 5 MeV. The region below 5 MeV, is the only proton energy region where GaAs cells are more susceptible to damage. Conventional coverglass offers sufficient protection to virtually eliminate cell damages.</p> <p>In the second phase of this contract, we investigated the influence of periodic and continuous thermal annealing on the GaAs solar cells. It has been observed that the damage produced by low-energy protons in the GaAs cells may be substantially reduced by annealing at temperatures as low as 200°C. Although there is still damage that cannot be annealed at 200°C, we believe that these damages are caused by defect complexes that are formed by the high flux rate ($\sim 10^7$ p cm⁻² sec⁻¹) used in our laboratory experiments. In the space environment we have fluxes on the order of 1×10^3 p cm⁻² sec⁻¹, which should result in mainly simple annealable defects.</p>					
17. Key Words (Suggested by Author(s)) (AlGa)As-GaAs solar cell, Medium Energy Proton Irradiation Periodic Thermal Annealing			18. Distribution Statement Unclassified - Unlimited Subject Category 44		
19. Security Classif. (of this report) UNCLASSIFIED		20. Security Classif. (of this page) UNCLASSIFIED		21. No. of Pages 101	22. Price

End of Document